MORPHOLOGICAL EFFECTS ON COATED AEROSOL KINETICS

Elias Patrick Rosen

A dissertation submitted to the faculty of the University of North Carolina at Chapel Hill in partial fulfillment of the requirements for the degree of Doctor of Philosophy in the Department of Chemistry

Chapel Hill
2008

Approved by:

Tomas Baer

Christopher Fecko

Gary Glish

Richard Kamens

Sergei Sheiko

ABSTRACT

Elias P. Rosen: Morphological Effects on Coated Aerosol Kinetics
(Under the direction of Tomas Baer)

Single-particle kinetic studies of the reaction between oleic acid and O_3 have been conducted on two different types of core particles: polystyrene latex and silica. Oleic acid was found to adsorb to both particle types in multilayer islands that resulted in a surfactant layer of a total volume estimated to be less than one monolayer. The rate of the surface reaction between surface-adsorbed oleic acid and O_3 has been shown for the first time to be influenced by the composition of the aerosol substrate in a mixed organic/inorganic particle. The reaction on the hydrophobic polystyrene core proceeded more efficiently than on a silica core at lower [O_3], and the observed dependence of the observed pseudo-first order rate constant with [O_3] suggests that the reaction is more efficient on the silica surface, but proceeds faster on the less polar PSL core at lower [O_3] due to the increased residence time of O_3 on the PSL surface. Values for the uptake coefficient, γ_{oleic}, for reaction of oleic acid on polystyrene latex spheres decrease from 2.5×10^{-5} to 1×10^{-5} with increasing [O_3] from 4 to 25 ppm and overlap at high [O_3] with the estimated values for γ_{oleic} on silica, which decrease from 1.6×10^{-5} to 1.3×10^{-5}.

ACKNOWLEDGEMENTS

I first thank my mentor, Dr. Tomas Baer, for instilling in me the power of a simple question. As soon as I can come up with something insightful to say while cat napping during a talk, I'll know that I am a true scientist. I also thank Dr. Eva Garland, who served on the front lines with me in our (almost) daily struggles to wring data out of the ATOFMS. Her patience and insight were invaluable. Baer Lab members past and present have been an instrumental support network. I would not have embarked on this path without the experience I received at Los Alamos National Labs, and for that I owe a great deal of thanks to Dr. Maureen McGraw. Finally, I would like to thank my wife, Kim, for inspiring me, cajoling me, and generally giving me a kick in the pants when I needed it. I owe her everything.

TABLE OF CONTENTS

LIST OF TABLES

Table

LIST OF FIGURES

Figure

CHAPTER 1

INTRODUCTION

1.1 Aerosols in the atmosphere and their impacts on health, climate, and chemistry

1.1.1 Definition of aerosols and how they are formed

Particulate matter is pervasive throughout the atmosphere and comes from a host of sources with both biogenic origins, such as windborne dust and sea spray, and anthropogenic origins, such as combustion of fuels. Condensed-phase particulate matter suspended in the atmosphere can be either ejected or emitted into the air in a fully formed state at the time of entrainment (primary particulate matter), or formed *in situ* by gaseous molecules in the atmosphere through chemical reaction, nucleation, condensation, or some combination of these processes (secondary particulate matter).[1] The ensemble of these particles and the vapor they are entrained in is known as an aerosol. Though diminutive in size, aerosols can have a large influence on human health, the global energy budget, and the prevailing chemistry of the atmosphere. This chapter details the role that aerosols play in atmospheric chemistry, the prevalence of organic material in ambient aerosols, and the importance of understanding how this organic material is processed by our oxidizing atmosphere. A model case of the reaction between oleic acid and ozone will be considered.

1.1.2 Health effects of aerosols

Most aerosols are sufficiently small, typically having diameters between 10 nm and 10 μm,[2] that they can be respired by the human lungs, and aerosols below about 100 nm in diameter can "penetrate the membranes of the respiratory tract and enter the blood circulation or be transported along olfactory nerves into the brain."[3] Exposure to particulate matter has been linked worldwide to an increase in cardiac and respiratory morbidity and mortality. A recent study in the US showed a correlation between exposure to particulate matter smaller than 10 microns (PM_{10}) and mortality in 20 US cities as well as hospitalization in persons 65 years and older in 14 US cities. The effects of PM_{10} on mortality and hospitalization persisted and were not substantively changed with control for other pollutants.[4] These cases were most closely associated with cardiovascular and respiratory issues. Respired aerosols can inflame or obstruct the airways. While the exact toxicological response to different types of particles is still unclear, many aerosol characteristics including particle size, surface area, and chemical composition determine the health risk posed by PM.[5]

1.1.3 Climate effects of aerosols

Aerosols alter Earth's energy balance by interacting directly with extraterrestrial radiation or reflected radiation from the Earth's surface. Particles can scatter light impinging from the sun and reflect some portion of this light away from the Earth's surface, which results in a net loss of energy to the atmosphere and has a cooling effect. Particles can also absorb some of the impinging solar energy as well as reflected energy from the Earth, and the subsequent re-emission of a portion of the absorbed energy by the particles serves as a net gain in energy to the atmosphere, which has a warming effect. By serving as seeds, or cloud

condensation nuclei (CCN), for clouds which have an enormous effect on the Earth's albedo, aerosol particles can also have an indirect effect on climate. As an ensemble, these direct and indirect perturbations require equilibrium shifts in the Earth's climate on local, regional, and global scales. The net climate forcing of an individual particle depends sensitively on a particle's size, chemical composition, and mixing state, as well as its complex interaction with other atmospheric constituents such as water vapor. The chemical heterogeneity of aerosols render global assessments of climate forcing by aerosols incredibly challenging, and as a result these assessments remain "the dominant uncertainty in radiative forcing" according to the recently issued Fourth Assessment Report by the Intergovernmental Panel on Climate Change.[6]

1.1.4 Influence of aerosols on atmospheric chemistry

The presence of condensed phase materials in the atmosphere also influences its chemistry. Although current understanding of heterogeneous reactions is small relative to homogeneous gas phase reactions, the impacts on the chemistry of the atmosphere due to aerosols are significant. Incorporation of a species into the condensed phase may serve to sequester or scavenge a species from the atmosphere, limiting its ability to participate in homogeneous gas-phase reactions. Alternatively, the presence of a condensed-phase surface can catalyze chemical reactions that would otherwise proceed much more slowly in homogeneous gas-phase reactions. Even in regions of the atmosphere that are relatively devoid of particulates, such catalytic processes can have profound results. The stratospheric ozone hole, perhaps the most widely recognized discovery in the field of atmospheric chemistry, has been attributed to heterogeneous processes occurring on the sparse 1-10

particles cm^{-3} existing in the stratosphere based on evidence that the halogen-based chemistry governing ozone loss occurs more efficiently and at a higher rate in condensed environments.[7,8] Particle number densities increase substantially closer to the Earth's surface, with concentrations in excess of 10^5 particles cm^{-3} in an urban environment, suggesting that aerosols can play an even greater role in governing the chemistry of the troposphere.[2]

1.2 Composition of tropospheric aerosols

1.2.1 Prevalence of organics in aerosols

The impacts aerosols have on health, climate, and atmospheric chemistry are all dependent on the chemical composition of the particles. The sources of input for particulate matter in the troposphere are many and varied, as are the resulting particulate components. Tropospheric aerosols can take the form of water and ice, dust, sea salts, natural and anthropogenic sulfates, and organic matter.[9,10] Increasing attention has been paid to organic aerosols, which are common in the troposphere and have been measured in urban[11] and remote[12] environments. As field observations devoted to the measurement of organic aerosols have increased, it has become clear that organic matter is a major component of fine particulate matter in all regions of the atmosphere and can make up to 90% of the total particle mass under certain conditions.[11,13] Organic aerosols are directly emitted to the atmosphere (primary organic aerosol, POA) from sources including wax emission from plants, sea spray, combustion emissions, and biomass burning. Condensed phase organic carbon is also formed in the atmosphere from low-volatility products produced by the oxidation of gas-phase anthropogenic and/or biogenic precursors (secondary organic aerosols, SOA). Organic aerosols can include a variety of functional groups including linear

and cyclic alkanes, alkenes, aromatics, alcohols, and carboxylic acids.[14] The complexity of organic material in aerosols is evidenced by the fact that as many as 10,000 separate organic components have recently been identified from a single urban source through the use of a sensitive orthogonal gas chromatography/ mass spectrometry techniques.[15] Unfortunately, analytical methods employed in most field campaigns leave significant portions of organic material unresolved and unidentified.

1.2.2 Mixing state of organic aerosols

Part of the difficulty of component identification is that organics tend to be internally mixed in particles[9,16-18], limiting the amount of analyte for analysis. Internal mixing can occur at the point of particle formation, for example when wave action in regions of the ocean subject to biofilms creates ocean spray with an organic surfactant layer that has been modeled as an inverted micelle.[19] Mixing within an aerosol particle can also occur throughout the evolution of an aerosol as organic vapors adsorb onto/absorb into surfaces of existing organic and inorganic particulates[20] or as externally mixed particles agglomerate and coagulate[21]. Characterization of ambient particles has revealed that the heterogeneity within particles can be both compositional and morphological. A recent study cataloging the organic functional groups of almost 600 particles collected from different geographical locations and altitudes found that in addition to 14 distinct groupings of organic functionalities across all particles sampled, more than 80% of the particles exhibited chemical signatures indicating internal mixing with non-carbonaceous material.[22] The distribution of organic material within individual ambient particles is also highly heterogeneous. Soft X-ray spectromicroscopy two-dimensional mapping of organics on aerosols from a variety of sources (i.e. Asian mixed

combustion over the Sea of Japan, African mineral dust over the Carribean Sea, and U.S. combustion in New Jersey) reveals that the total organic material on the collected particles, shown in the left column of Figure 1.1, is not distributed uniformly over an entire particle.[23] When such organic matter is adsorbed to a solid core or is immiscible with a liquid seed particle, the result is an organic surfactant layer.

1.2.3 Impact of surface active organics

The presence of these organic films may alter the physical properties of the resulting internally mixed aerosol particle, as well as hinder some chemical reactions while promoting others. Films can serve as a barrier to mass transfer, limiting uptake of some gases as well as evaporation of the core. For example, non-reactive uptake of water by an aqueous core is decreased by an organic coating due to the layer's hydrophobicity[29,30], which has important consequences for the particle's ability to serve as CCN. The organic film can also inhibit chemical reaction. McNeill and coworkers observed a reduction in the uptake of N_2O_5 by aqueous NaCl aerosols by almost an order of magnitude due to the presence of an organic monolayer of sodium dodecyl sulfate.[31] Smoyzdin et al. performed numerical simulations of the impact that an oleic acid surfactant coating has on marine aerosols and found that the presence of the surface film reduced mass transfer from the sea salt water core to the atmosphere.[32] An organic coating may also alter the net optical properties of the particle. Importantly, all of these effects are perturbed as the organic coating reacts with gaseous oxidants in the atmosphere.

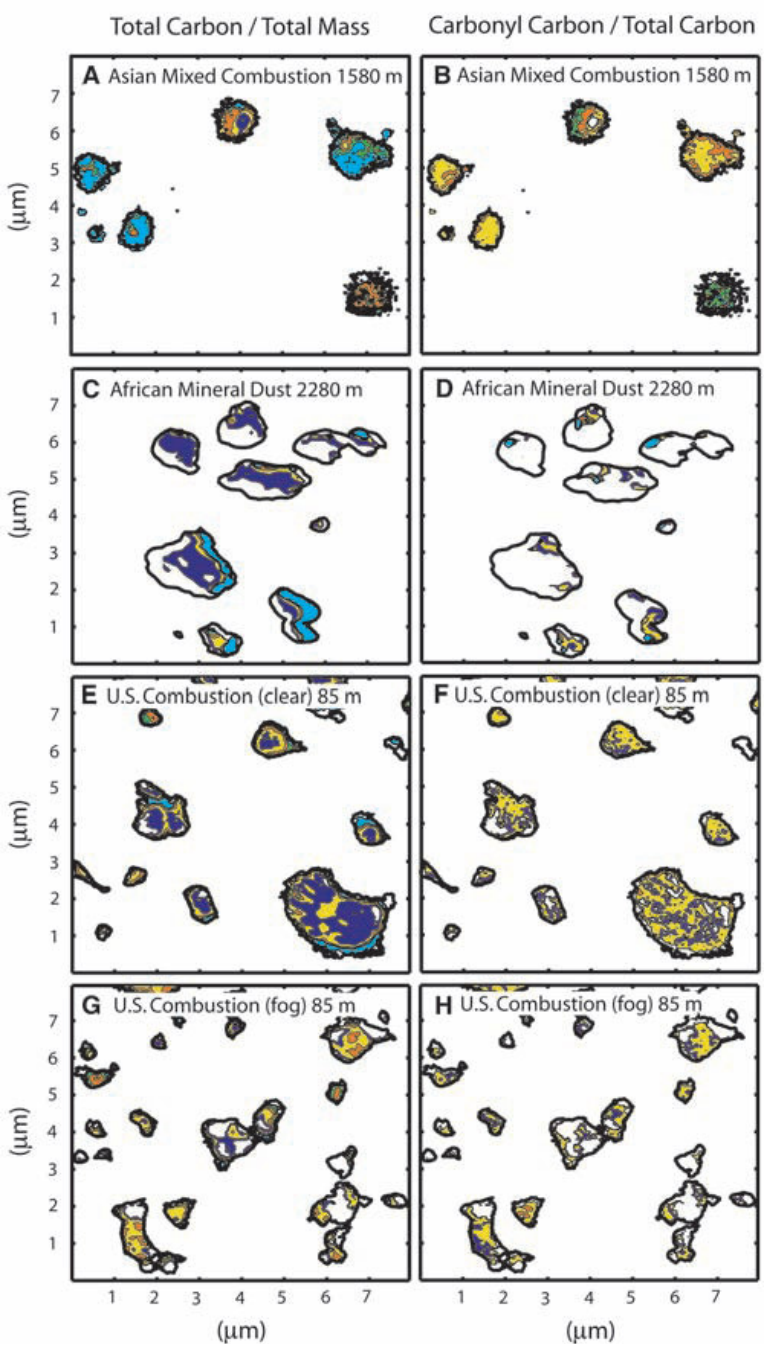

Figure 1.1. *Two-dimensional mapping of organic functional groups on ambient particles.* The left column of images (A, C, E, and G) reflect the ratio of total carbon to total mass measured on the particles. Legend: ratios 0.02 – 0.2 (dark blue), 0.2 – 0.4 (yellow), 0.4 – 0.6 (orange), 0.6 – 0.8 (green), >0.8 (light blue). The right column of images (B,D,F,and H) reflect the ratio of carbonyl carbon to total mass measured on the same particles. Legend: ratios 0.02 – 0.08 (dark blue), 0.08 – 0.16 (yellow), 0.16 – 0.24 (orange), 0.24 – 0.32(green), >0.32 (light blue). From Maria et al.[23] Reprinted with permission from AAAS.

1.3 Chemical aging of organic particles

1.3.1 Oxidation reactions, typical products, and prevalence

Once emitted to the atmosphere, the lifetime of organic compounds is determined by chemical removal pathways. These include direct photolysis by ambient radiation, or more frequently by photochemical oxidation due to a host of oxidizing species of the atmosphere including ·OH, O_3, NO_x, SO_x, and halogen radicals.[1,2,33] Oxidation reaction products are highly oxygenated, adding functional groups such as alcohols, aldehydes, carboxylic acids, and more complex peroxy acids to an organic molecule. The products of homogeneous reactions between gas phase oxidants and organics, as well as secondary chemistry among the primary products, can have sufficiently low vapor pressure to condense and form SOA.[14] Oxidation can also occur through heterogeneous reaction between gas phase oxidants and condensed phase organics. Chemical characterization of aerosols sampled around the world by aerosol mass spectrometry has shown that the presence of oxygenated organic matter is "ubiquitous" in the atmosphere and has been measured in both rural and urban environments.[34] Two-dimensional mapping of carbonyl carbon groups on particles collected by Maria et al.[23], pictured in the right column of Figure 1.1, shows that these groups are prevalent in organic aerosols of very different geographical and mechanical origin, and that they are distributed over a similar areal extent as the total carbon.

1.3.2 Ramifications of compositional changes

Oxidation alters the physical and chemical properties of an organic coating. For example, the addition of oxygen can decrease the hydrophobicity of a fatty acid layer of oleic acid allowing it to take up water vapor.[35] Many of the oleic acid oxidation products are water

soluble, which changes the surface composition as well as its structure.[36] Recently, Shilling et al. have shown that the conversion of an oleic acid film from CCN inactive to CCN active is associated with oligomerization of the products accompanied by a lowering of the interfacial surface tension of a particle[37], which has also been seen for other humic-like substances[38]. Water soluble organic compounds can be significant players in direct radiative forcing and also as CCN.[39] The influence of the hydrophobic to hydrophilic conversion of organic films on climate is currently being assessed. A recent Global Climate Model study found that the presence of marine organic aerosol was essential to predict correct CCN concentrations, and that the mixing state of the organic particles influenced the results.[40] Oxidation can also result in low molecular weight volatile products that can increase the atmospheric burden of oxygenated volatile organic products such as nonanal, and these volatile products may be an important source of gaseous organic carbon.[41]

1.3.3 Degree of oxidation as a tool for determining the age of organics

The amount of oxygenation of an organic species increases with time in the atmosphere, and as a result the carbon-normalized oxygen content of an aerosol can be used as a means of measuring the aging of the organic fraction in atmospheric particles.[42] Establishing the age of an aerosol is critical for source apportionment, as well as for determining its oxidation rate.

1.4 Physical chemistry of aging

1.4.1 Processes involved in heterogeneous reactions and the concept of γ

Accurately modeling the impact that oxygenated organic aerosols have on atmospheric chemistry and climate, as well as human health, requires understanding the mechanisms by which such reactions occur. Considerable experimental effort has been devoted to quantifying the rate of chemical transformation and aging of aerosol particles and the processes that control this transformation. Homogeneous reaction mechanisms, involving collision between two gaseous species, are generally well understood. Heterogeneous reactions are considerably more complicated, entailing some combination of the following processes:

- *Diffusion of the oxidant to the particle surface*
- *Accommodation of the oxidant at the particle surface*
- *Reaction between oxidant and organic at the particle surface, and/or*
- *Diffusion of the oxidant into the organic particle*
- *Reaction between the oxidant and organic within the bulk of the particle*

Figure 1.2 depicts these processes for the simplest system: an oxidant, X, attacking a particle comprised entirely of a single organic species, Y. Laboratory and field measurements of reaction between two species such as X and Y are typically reported in terms of an uptake coefficient, γ, which encapsulates all of the physics and chemistry shown in Figure 2 and reflects the probability that an encounter between a molecule of X and the surface of Y will result in a chemical reaction.

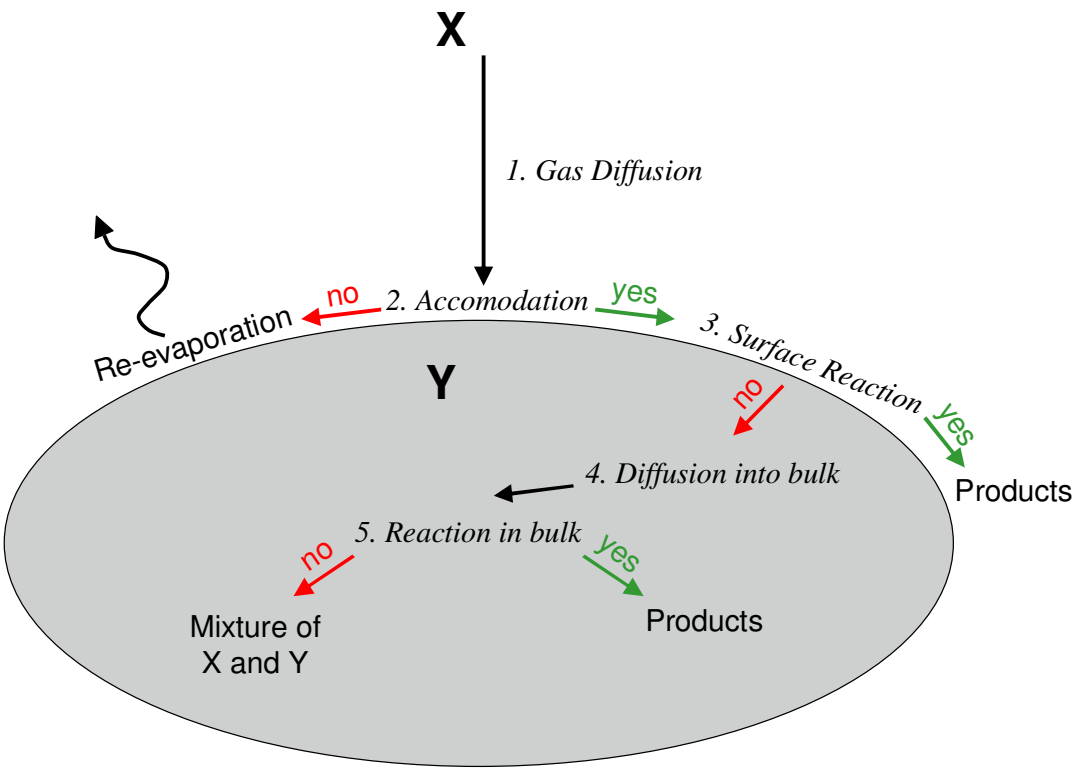

Figure 1.2. *Processes controlling heterogeneous reactions*. In this simplified reaction scheme, the two reactants are a gas phase oxidant, X, and a condensed phase organic species, Y.

1.4.2 Modeling the processes of γ with the Resistor Model

Deconvoluting the separate contributions of each of these processes from measurements of a net uptake coefficient is not straightforward, but necessary in order to incorporate into atmospheric chemistry models. Methods to parameterize each process as a separate, independent "resistance" have been developed into the aptly named Resistor Model describing heterogeneous reactions.[43] A generalization of this concept is shown in Figure 1.3. Solutions of this model can be found for certain limiting conditions, and laboratory based kinetics experiments involving simple particle morphologies have been designed to test this model. However, its applications are not universal, particularly when considering more realistic particle morphologies as will become evident in the work to be described.

1.4.3 Movement toward experiments of more complex morphologies

While the simplified heterogeneous systems that have been the focus of laboratory experiments to date have provided a useful framework for developing a means of understanding the processes that are controlling heterogeneous reactions in the atmosphere, it is clear that they have not yet been able to mimic the complexity of atmospheric processes. As the body of experimental work has grown, it has become clear that there is a significant "gap"[44] between the rates of chemical oxidation of organic aerosols measured in the laboratory and observed in field experiments. One of the primary differences between the two bodies of measurements is the morphology of the particles that are analyzed. Increasing the compositional complexity of model aerosols also increases the difficulty of the

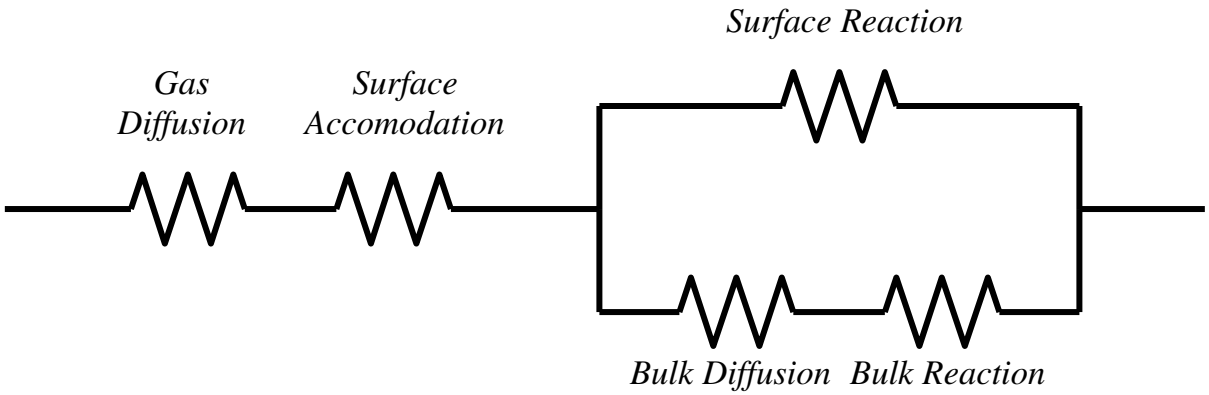

Figure 1.3. *Generalized Resistor Model.* The model is a representation of the physical and chemical processes controlling heterogeneous reaction as a circuit of separate resistances.

experiments and requires the development of new methods to interpret the oxidation of complex morphologies.

1.5 Oleic acid: A model system to investigate morphological effects on chemical reactivity

Particle morphology plays an important role in influencing the reactivity once an oxidant comes into contact with an aerosol particle, as has become evident in the case of the reaction between oleic acid ($C_{18}H_{34}O_2$) and ozone (O_3). Oleic acid is a monounsaturated carboxylic acid that is found in cooking oils, many types of meats, and is the primary unsaturated species in olive oil. It is released to the atmosphere during meat cooking and has been used as a chemical tracer for source apportionment of meat cooking aerosols.[45-47] Oleic acid is a common urban pollutant, and accounts for approximately 10% of organic aerosol measured in Pittsburgh in a recent study.[48] In addition to its individual contribution to the primary aerosol burden, oleic acid has also become a benchmark compound to study experimentally since it serves as a suitable proxy for larger lipid systems. Oleic acid's double bond is susceptible to attack by O_3, and considerable experimental attention has been paid to characterization of the products and kinetics of the reaction between oleic acid and O_3, which has been recently summarized in a comprehensive review.[49] Laboratory experiments measuring the rate of reaction of pure oleic acid and O_3 estimate a lifetime of oleic acid in the atmosphere on the order of seconds.[50-53] Yet, oleic acid persists in the atmosphere and has been collected in particulate form, suggesting a lifetime on the order of days.[12,45] This disparity is illustrated in Figure 1.4, which shows the particle size dependence of the estimated lifetime of a pure oleic acid particle reacting with 50 parts per billion (ppb) O_3, a

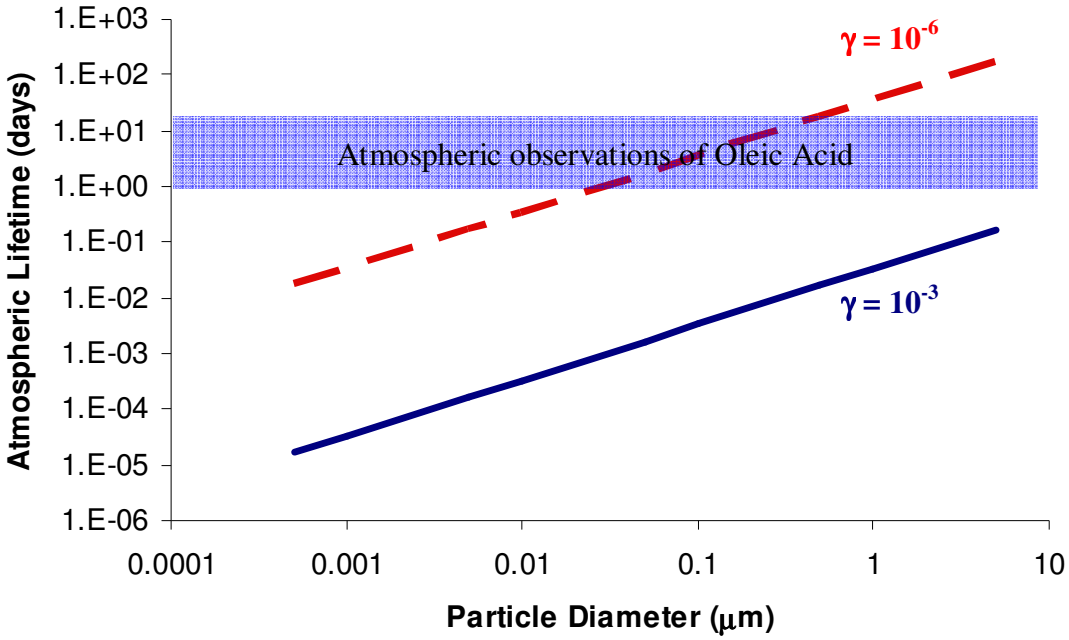

Figure 1.4. *Estimated lifetime of pure oleic acid particles based on measured uptake coefficients*. Estimates are shown based on values of g measured for condensed phase particles (blue line) and gas-phase oleic acid (red dashed line). Adapted from Robinson et al.[67]

typical concentration in the atmosphere. Lifetime estimates are based on an uptake coefficient of $\gamma = 10^{-3}$, which is the average value determined from laboratory experiments, and compared to the lifetime estimated by the measured uptake coefficient for the homogeneous reaction of oleic acid and O_3, $\gamma = 10^{-6}$. The estimated oleic acid lifetime in ambient particles is also shown in Figure 1.4 as a reference.

One obvious simplification in unary phase experiments is the homogeneity of pure oleic acid particles and films, and matrix effects within internally mixed ambient particles have long been hypothesized to be responsible for the difference in reactivity between unary phase and atmospheric oleic acid particles.[51,53] Subsequent laboratory studies have investigated the reactivity of oleic acid in internally mixed particles containing other organic acids expected to be released from meat cooking.[54-58] The phase and morphology of these mixed fatty acid systems vary widely, and are dependent on the relative amounts of the components. These studies have demonstrated the important role of morphology in the reactivity of oleic acid particles, as well as some of the inherent difficulties associated with even an incremental increase in morphological complexity in kinetic studies. The particle morphology of the internally mixed fatty acid systems is highly dependent on the preparation of particles, which can undergo supercooling[57], and the preparation of films, which can influence the resulting crystal structure[56]. When the resulting morphology involves oleic acid being encased or trapped by a diffusional barrier of a solid fatty acid, the reactive uptake coefficient of O_3 has been shown to decrease by more than an order of magnitude. However, a recent smog chamber study does not show a clear trend in reactivity even going up to a 12 component mixture of fatty acids.[59] While the reactivity of mixed fatty acid systems can be

decreased relative to pure oleic acid based on the morphology, there still remains a gulf between laboratory measurements and field observations that indicates the exploration of the reactivity involving different particle morphologies is warranted.

In addition to self-aggregating, organic species are frequently found to be internally mixed with inorganic particles of anthropogenic and biogenic origin that are prevalent in the atmosphere, as mentioned previously. Internal mixtures of organic material with sulfate, ammonium, sea salt, soot, and minerals have been measured.[9,11,18,24,26,28,60,61] Solid particles such as soot and dust represent a large fraction of the available surface area in the boundary layer on which low volatility organic species may condense. A recent report from the ACE-Asia campaign observed that 6-50% of organic carbon incorporated within super-micron particles was associated with dust particles.[26] Importantly, the chemical composition of an aerosol core has been shown to affect the reactivity of an organic surfactant layer.[62-66] One class of organic matter that is typically surface active is lower molecular weight (C_{14}-C_{19}) fatty acids (LFAs), of which oleic acid is a member. Prevalent in the cell walls of most organisms, LFAs generally derive from plant wax and microbes and have been found extensively to form hydrophobic surfactant films in marine[24,25] and continental aerosols[26-28].

Despite the potential atmospheric relevance, few studies have examined the kinetics of adsorbed oleic acid on solid inorganic particles. Katrib et al. coated oleic acid onto polystyrene latex spheres (PSLs), and monitored the change in aerodynamic diameter and density of the particle as it reacted with O_3, but did not report any kinetic information.[42] A

recent study by McNeill *et al.* is the first to report kinetic information for a surfactant layer of sodium oleate on an aqueous sea salt core.[66]

1.6 The Current Work

The goal of this work was to investigate the reaction between oleic acid and O_3 on two different core particles: silica, which serves as an analog to mineral dust; and polystyrene, which represents a hydrophobic surface like soot. The importance of size dependence and porosity of the core particles was also investigated. Chapter 2 details the development of techniques to deposit an adsorbed layer of oleic acid onto the core particles. Chapter 3 discusses the characterization of the resulting coated particles. Chapter 4 reports the results of flow tube studies employing single-particle mass spectrometry that were conducted to carefully measure the reaction kinetics of a surfactant layer of oleic acid on these two particle types.

References

1. Seinfeld, J. H.; Pandis, S. N. *Atmospheric Chemistry and Physics;* Wiley Interscience: New York, 1998.

2. Finlayson-Pitts, B. J.; Pitts, J. N. *Chemistry of the Upper and Lower Atmosphere: Theory, Experiments and Applications;* Academic Press: New York, 2000.

3. Poschl, U. Atmospheric aerosols: Composition, transformation, climate and health effects. *Angewandte Chemie-International Edition* **2005,** *44* (46), 7520-7540.

4. Samet, J. M.; Dominici, F.; Curriero, F. C.; Coursac, I.; Zeger, S. L. Fine particulate air pollution and mortality in 20 US Cities, 1987-1994. *New England Journal of Medicine* **2000,** *343* (24), 1742-1749.

5. Nel, A. Air pollution-related illness: effects of particles (vol 308, pg 804, 2005). *Science* **2005,** *309* (5739), 1326.

6. Solomon, S.; D.Qin; M.Manning; Z.Chen; M.Marquis; K.B.Averyt; M.Tignor; and H.L.Miller (eds.) *IPCC, 2007: Summary for Policymakers. In: Climate Change 2007: The Physical Science Basis. Contribution of Working Group I to the Fourth Assessment Report of the Intergovernmental Panel on Climate Change*; Cambridge University Press: 07.

7. Reid, P. J. Understanding the Phase-Dependent Reactivity of Chlorine Dioxide Using Resonance Raman Spectroscopy. 34 ed.; 2001; pp 691-698.

8. Molina, M. J.; Molina, L. T.; Kolb, C. E. Gas-phase and hetergeneous chemical kinetics of the troposphere and stratosphere. *Ann. Rev. Phys. Chem.* **1996,** *47*, 327-367.

9. Buseck, P. R.; Posfai, M. Airborne minerals and related aerosol particles: Effects on climate and the environment. *Proceedings of the National Academy of Sciences of the United States of America* **1999,** *96* (7), 3372-3379.

10. Ravishankara, A. R.; Longfellow, C. A. Reactions on tropospheric condensed matter. *Phys. Chem. Chem. Phys.* **1999,** *1*, 5433-5441.

11. Lee, S.-H.; Murphy, D. M.; Thompson, D. S.; Middlebrook, A. M. Chemical components of single particles measured with Particle Analysis by Laser Mass Spectrometry (PALMS) during the Atlanta SuperSite Project: Focus on organic/sulfate, lead, soot, and mineral particles. *J. Geophys. Res.* **2002,** *107*, AAC 1-1.

12. Limbeck, A.; Puxbaum, H. Organic acids in continental background aerosols. *Atmos. Environ.* **1999,** *33* (12), 1847-1852.

13. Lim, H. J.; Turpin, B. J. Origins of primary and secondary organic aerosol in Atlanta: Results' of time-resolved measurements during the Atlanta supersite experiment. *Environmental Science & Technology* **2002,** *36* (21), 4489-4496.

14. Seinfeld, J. H.; Pankow, J. F. Organic Atmospheric Particulate Material. *Ann. Rev. Phys. Chem.* **2003,** *54*, 121-140.

15. Hamilton, J. F.; Webb, P. J.; Lewis, A. C.; Hopkins, J. R.; Smith, S.; Davy, P. Partially oxidised organic components in urban aerosol using GCXGC-TOF/MS. *Atmospheric Chemistry and Physics* **2004,** *4*, 1279-1290.

16. Vester, B. P.; Ebert, M.; Barnert, E. B.; Schneider, J.; Kandler, K.; Schutz, L.; Weinbruch, S. Composition and mixing state of the urban background aerosol in the Rhein-Main area (Germany). *Atmos. Environ.* **2007,** *41* (29), 6102-6115.

17. Worobiec, A.; Szaloki, I.; Osan, J.; Maenhaut, W.; Stefaniak, E. A.; Van Grieken, R. Characterisation of Amazon Basin aerosols at the individual particle level by X-ray microanalytical techniques. *Atmos. Environ.* **2007,** *41* (39), 9217-9230.

18. Russell, L. M.; Maria, S. F.; Myneni, S. C. B. Mapping organic coatings on atmospheric particles. *Geophys. Res. Lett.* **2002,** *29* (16).

19. Ellison, G. B.; Tuck, A. F.; Vaida, V. Atmospheric processing of organic aerosols. *J. Geophys. Res.* **1999,** *104*, 11633-11641.

20. Goss, K. U. The air/surface adsorption equilibrium of organic compounds under ambient conditions. *Critical Reviews in Environmental Science and Technology* **2004,** *34* (4), 339-389.

21. Hinds, W. C. *Aerosol Technology: Properties, Behavior, and Measurement of Airborne Particles;* 2nd ed.; Wiley-Interscience: New York, 1999.

22. Takahama, S.; Gilardoni, S.; Russell, L. M.; Kilcoyne, A. L. D. Classification of multiple types of organic carbon composition in atmospheric particles by scanning transmission X-ray microscopy analysis. *Atmos. Environ.* **2007,** *41* (40), 9435-9451.

23. Maria, S. F.; Russell, L. M.; Gilles, M. K.; Myneni, S. C. B. Organic Aerosol Growth Mechanisms and Their Climate-Forcing Implications. *Science* **2004,** *306* (5703), 1921-1924.

24. Tervahattu, H.; Juhanoja, J.; Kupiainen, K. Identification of an organic coating on marine aerosol particles by TOF-SIMS. *Journal of Geophysical Research-Atmospheres* **2002,** *107* (D16).

25. Mochida, M.; Kitamori, Y.; Kawamura, K.; Nojiri, Y.; Suzuki, K. Fatty acids in the marine atmosphere: Factors governing their concentrations and evaluation of

organic films on sea-salt particles. *Journal of Geophysical Research-Atmospheres* **2002,** *107* (D17).

26. Mochida, M.; Umemoto, N.; Kawamura, K.; Lim, H. J.; Turpin, B. J. Bimodal size distributions of various organic acids and fatty acids in the marine atmosphere: Influence of anthropogenic aerosols, Asian dusts, and sea spray off the coast of East Asia. *Journal of Geophysical Research-Atmospheres* **2007,** *112* (D15).

27. Graham, B.; Guyon, P.; Taylor, P. E.; Artaxo, P.; Maenhaut, W.; Glovsky, M. M.; Flagan, R. C.; Andreae, M. O. Organic compounds present in the natural Amazonian aerosol: Characterization by gas chromatography-mass spectrometry. *Journal of Geophysical Research-Atmospheres* **2003,** *108* (D24).

28. Tervahattu, H.; Juhanoja, J.; Vaida, V.; Tuck, A. F.; Niemi, J. V.; Kupiainen, K.; Kulmala, M.; Vehkamaki, H. Fatty acids on continental sulfate aerosol particles. *Journal of Geophysical Research-Atmospheres* **2005,** *110* (D6).

29. Rudich, Y.; Benjamin, I.; Naaman, R.; Thomas, E.; Trakhtenberg, S.; Ussyshkin, R. Wetting of hydrophobic organic surfaces and its implications to organic aerosols in the atmosphere. *J. Phys. Chem. A* **2000,** *104* (22), 5238-5245.

30. Donaldson, D. J.; Vaida, V. The influence of organic films at the air-aqueous boundary on atmospheric processes. *Chem. Rev.* **2006,** *106* (4), 1445-1461.

31. McNeill, V. F.; Patterson, J.; Wolfe, G. M.; Thornton, J. A. The effect of varying levels of surfactant on the reactive uptake of N2O5 to aqueous aerosol. *Atmospheric Chemistry and Physics* **2006,** *6*, 1635-1644.

32. Smoydzin, L.; von Glasow, R. Do organic surface films on sea salt aerosols influence atmospheric chemistry? a model study. *Atmospheric Chemistry and Physics* **2007,** *7* (21), 5555-5567.

33. Williams, J. Organic Trace Gases in the Atmosphere: An Overview. *Environmental Chemistry* **2004,** *1*, 125-136.

34. Zhang, Q.; Jimenez, J. L.; Canagaratna, M. R.; Allan, J. D.; Coe, H.; Ulbrich, I.; Alfarra, M. R.; Takami, A.; Middlebrook, A. M.; Sun, Y. L.; Dzepina, K.; Dunlea, E.; Docherty, K.; DeCarlo, P. F.; Salcedo, D.; Onasch, T.; Jayne, J. T.; Miyoshi, T.; Shimono, A.; Hatakeyama, S.; Takegawa, N.; Kondo, Y.; Schneider, J.; Drewnick, F.; Borrmann, S.; Weimer, S.; Demerjian, K.; Williams, P.; Bower, K.; Bahreini, R.; Cottrell, L.; Griffin, R. J.; Rautiainen, J.; Sun, J. Y.; Zhang, Y. M.; Worsnop, D. R. Ubiquity and dominance of oxygenated species in organic aerosols in anthropogenically-influenced Northern Hemisphere midlatitudes. *Geophys. Res. Lett.* **2007,** *34* (13).

35. Asad, A.; Mmereki, B. T.; Donaldson, D. J. Enhanced uptake of water by oxidatively processed oleic acid. *Atmospheric Chemistry and Physics* **2004,** *4*, 2083-2089.

36. Voss, L. F.; Bazerbashi, M. F.; Beekman, C. P.; Hadad, C. M.; Allen, H. C. Oxidation of oleic acid at air/liquid interfaces. *Journal of Geophysical Research-Atmospheres* **2007,** *112* (D6).

37. Shilling, J. E.; King, S. M.; Mochida, M.; Martin, S. T. Mass spectral evidence that small changes in composition caused by oxidative aging processes alter aerosol CCN properties. *J. Phys. Chem. A* **2007,** *111* (17), 3358-3368.

38. Taraniuk, I.; Graber, E. R.; Kostinski, A.; Rudich, Y. Surfactant properties of atmospheric and model humic-like substances (HULIS). *Geophys. Res. Lett.* **2007,** *34* (16).

39. Kanakidou, M.; Seinfeld, J. H.; Pandis, S. N.; Barnes, I.; Dentener, F. J.; Facchini, M. C.; van Dingenen, R.; Ervens, B.; Nenes, A.; Nielsen, C. J.; Swietlicki, E.; Putaud, J. P.; Balkanski, Y.; Fuzzi, S.; Horth, J.; Moortgat, G. K.; Winterhalter, R.; Myrhe, C. E. L.; Tsigaridis, K.; Vignati, E.; Stephanou, E. G.; Wilson, J. Organic aerosol and global climate modeling: A review. *Atmos. Chem. Phys.* **2005,** *5*, 1053-1123.

40. Roelofs, G. J. A GCM study of organic matter in marine aerosol and its potential contribution to cloud drop activation. *Atmospheric Chemistry and Physics* **2008,** *8* (3), 709-719.

41. Kwan, A. J.; Crounse, J. D.; Clarke, A. D.; Shinozuka, Y.; Anderson, B. E.; Crawford, J. H.; Avery, M. A.; McNaughton, C. S.; Brune, W. H.; Singh, H. B.; Wennberg, P. O. On the flux of oxygenated volatile organic compounds from organic aerosol oxidation. *Geophys. Res. Lett.* **2006,** *33* (15).

42. Katrib, Y.; Martin, S. T.; Hung, H. M.; Rudich, Y.; Zhang, H.; Slowik, J. G.; Davidovits, P.; Jayne, J. T.; Worsnop, D. R. Products and Mechanisms of Ozone Reactions with Oleic Acid for Aerosol Particles Having Core-Shell Morphologies. *J. Phys. Chem. A* **2004,** *108*, 6686-6695.

43. Hanson, D. R.; Ravishankara, A. R.; Solomon, S. Heterogeneous reactions in sulfuric acid aerosols: A framework for model calculations. *J. Geophys. Res.* **1994,** *99* (D2), 3615-3629.

44. Rudich, Y.; Donahue, N. M.; Mentel, T. F. Aging of organic aerosol: Bridging the gap between laboratory and field studies. *Ann. Rev. Phys. Chem.* **2007,** *58*, 321-352.

45. Rogge, W. F.; Hildemann, L. M.; Mazurek, M. A.; Cass, G. R.; Simoneit, B. R. T. Sources of fine organic aerosol 1. Charbroiler and meat cooking operations. *Environ. Sci. Technol.* **1991,** *25*, 1112-1119.

46. Schauer, J. J.; Rogge, W. F.; Hildemann, L. M.; Mazurek, M. A.; Cass, G. R.; Simoneit, B. R. T. Source Apportionment of Airborne Particulate Matter Using Organic Compounds as Tracers. *Atmos. Environ.* **1995,** *30* (22), 3837-3855.

47. He, L. Y.; Hu, M.; Huang, X. F.; Yu, B. D.; Zhang, Y. H.; Liu, D. Q. Measurement of emissions of fine particulate organic matter from Chinese cooking. *Atmos. Environ.* **2004,** *38* (38), 6557-6564.

48. Robinson, A. L.; Subramanian, R.; Donahue, N. M.; Bernardo-Bricker, A.; Rogge, W. F. Source apportionment of molecular markers and organic aerosol. 3. Food cooking emissions. *Environmental Science & Technology* **2006,** *40* (24), 7820-7827.

49. Zahardis, J.; Petrucci, G. A. The oleic acid-ozone heterogeneous reaction system: products, kinetics, secondary chemistry, and atmospheric implications of a model system - a review. *Atmospheric Chemistry and Physics* **2007,** *7*, 1237-1274.

50. Moise, T.; Rudich, Y. Reactive Uptake of Ozone by Aerosol-Associated Unsaturated Fatty Acids: Kinetics, Mechanism, and Products. *J. Phys. Chem. A* **2002,** *106*, 6469-6476.

51. Thornberry, T. D.; Abbatt, J. P. D. Heterogeneous reaction of ozone with liquid unsaturated fatty acids: detailed kinetics and gas-phase product studies. *Phys. Chem. Chem. Phys.* **2004,** *6*, 84-93.

52. Smith, G. D.; Woods III, E.; Hauser, C.; Miller, R. E.; Baer, T. Reactive uptake of ozone by oleic acid aerosol particles: Application of single particle mass spectrometry to heterogeneous reaction kinetics. *J. Phys. Chem. A* **2002,** *106*, 8085-8095.

53. Morris, J. W.; Davidovits, P.; Jayne, J. T.; Shi, Q.; Kolb, C. E.; Worsnop, D. R.; Barney, W. S.; Jimenez, J.; Cass, G. R. Kinetics of submicron oleic acid aerosols with ozone; a novel aerosol mass spectrometric technique. *Geophys. Res. Lett.* **2002,** *29*, 71-1-71/4.

54. Nash, D. G.; Tolocka, M. P.; Baer, T. The uptake of O_3 by myristic acid-oleic acid mixed particles: evidence for solid surface layers. *Phys. Chem. Chem. Phys.* **2006,** *8*, 4468-4475.

55. Katrib, Y.; Biskos, G.; Buseck, P. R.; Davidovits, P.; Jayne, J. T.; Mochida, M.; Wise, M. E.; Worsnop, D. R.; Martin, S. T. Ozonolysis of Mixed Oleic-Acid/Stearic-Acid Particles: Reaction Kinetics and Chemical Morphology. *J. Phys. Chem. A* **2005,** *109* (48), 10910-10919.

56. Knopf, D. A.; Anthony, L. M.; Bertram, A. K. Reactive Uptake of O_3 by Multicomponent and Multiphase Mixtures Containing Oleic Acid. *J. Phys. Chem. A* **2006,** *109* (25), 5579-5589.

57. Hearn, J. D.; Smith, G. D. Measuring Rates of Reaction in Supercooled Organic Particles with Implications for Atmospheric Aerosol. *Phys. Chem. Chem. Phys.* **2005,** *7* (13), 2549-2551.

58. Hearn, J. D.; Smith, G. A. Ozonolysis of mixed oleic acid/n-docosane particles: The roles of phase, morphology, and metastable states. *J. Phys. Chem. A* **2007,** *111* (43), 11059-11065.

59. Hartz, K. E. H.; Weitkamp, E. A.; Sage, A. M.; Donahue, N. M.; Robinson, A. L. Laboratory measurements of the oxidation kinetics of organic aerosol mixtures using a relative rate constants approach. *Journal of Geophysical Research-Atmospheres* **2007,** *112* (D4).

60. Hinz, K.-P.; Trimborn, A.; Weingartner, E.; Henning, S.; Baltensperger, U.; Spengler, B. Aerosol single particle composition at the Jungfraujoch. *J. Aerosol Sci.* **2005,** *36*, 123-145.

61. Falkovich, A. H.; Schkolnik, G.; Ganor, E.; Rudich, Y. Adsorption of organic compounds pertinent to urban environments onto mineral dust particles. *Journal of Geophysical Research-Atmospheres* **2004,** *109* (D2).

62. Poschl, U.; Letzel, T.; Schauer, C.; Niessner, R. Interaction of ozone and water vapor with spark discharge soot aerosol particles coated with benzo[a]pyrene: O_3 and H_2O adsorption, benzo[a]pyrene degradation, and atmospheric implications. *J. Phys. Chem. A* **2001,** *105* (16), 4029-4041.

63. Mmereki, B. T.; Donaldson, D. J. Direct observation of the kinetics of an atmospherically important reaction at the air-aqueous interface. *J. Phys. Chem. A* **2003,** *107*, 11038-11042.

64. Kwamena, N. O. A.; Thornton, J. A.; Abbatt, J. P. D. Kinetics of surface-bound benzo[a]pyrene and ozone on solid organic and salt aerosols. *J. Phys. Chem. A* **2004,** *108* (52), 11626-11634.

65. Kwamena, N. O. A.; Staikova, M. G.; Donaldson, D. J.; George, I. J.; Abbatt, J. P. D. Role of the aerosol substrate in the heterogeneous ozonation reactions of surface-bound PAHs. *J. Phys. Chem. A* **2007,** *111* (43), 11050-11058.

66. McNeill, V. F.; Wolfe, G. M.; Thornton, J. A. The Oxidation of Oleate in Submicron Aqueous Salt Aerosols: Evidence of a Surface Process. *J. Phys. Chem. A* **2007,** *111(6),* 1073-1083.

67. Robinson, A. L.; Donahue, N. M.; Rogge, W. F. Photochemical oxidation and changes in molecular composition of organic aerosol in the regional context. *Journal of Geophysical Research-Atmospheres* **2006,** *111* (D3).

CHAPTER 2

DESIGN AND THEORY OF A NEW CONDENSATION OVEN

2.1 Introduction

This chapter focuses on the development of methods to adsorb oleic acid onto two different types of solid particles: silica, and polystyrene latex. First, the nature of these two particle types will be discussed. The design and development of a new condensation oven will be detailed. Finally, the theory of condensation of a gas onto a condensed phase particle will be addressed.

2.2 Core types and properties

2.2.1 Silica as a proxy for mineral dust

Mineral dust comprises a significant portion of the atmospheric aerosol burden, as mentioned in Chapter 1. The mineral structure, or mineralogy, of the dust particles is highly variable, and influences ability of a particle to take up gases such as water vapor.[1] The chemical composition of mineral dust is similarly variable depending on source[2], but its primary component is silica (SiO_2).[3] Silica has been selected as a proxy for mineral dust in these studies, and it has been used in a similar capacity in several studies investigating

heterogeneous chemistry on mineral dust.[4-11]

Silica surfaces possess terminal silanol OH groups that are mildly acidic and can promote chemistry, creating a hydrophilic surface for the uptake of gases. Silanol groups serve as adsorption sites for organic vapors[12], and in the case of carboxylic acid head groups, such as the one possessed by oleic acid, this adsorption is due to hydrogen bonding with the silanol groups.[13,14]

Dust aerosols entrained in air by wind-driven soil range in size across the standard aerosol classes of nuclei (0.005-0.1 μm), accumulation (0.1-2.5 μm), and coarse (>2.5 μm) modes. Supermicron silica particles have been used in this work since particles of this size represent most of the mass in the atmosphere and are more readily investigated with the UNC Aerosol Time-of-Flight Mass Spectrometer (ATOFMS). In addition to solid silica spheres, porous silica particles have also been investigated to mimic the voids created on certain types of mineral particles due to wind erosion.[3]

2.2.2 Polystyrene latex as a proxy for hydrophobic soot-like particles

Soot is the result of incomplete hydrocarbon combustion and, like mineral dust, is ubiquitous in the atmosphere. Soot is comprised of agglomerated graphene carbon sheets. Adsorption of organic molecules on soot has been known to be driven by hydrogen bonding

and van der Waals forces involving π-π bonds between unsaturated organics and the soot surface.[15] The uptake of small dicarboxylic acids on soot surfaces has been shown to be on the same order as monocarboxylic acids, indicating that carboxylic acid groups can also bind directly to soot surfaces.[16]

Soot particles are highly fractal, which makes their passage through a fluid such as air highly non-ideal. This non-ideality serves to severely reduce the transmission of soot particles into high vacuum instruments like the ATOFMS. As a result, polystyrene latex spheres (PSLs) have been used in this study as a proxy for the hydrophobic surface of soot particles. PSLs are highly ordered like soot, and are made of interlocking styrene monomer units. They can be fabricated in a large range of sizes and serve as standardized spherical aerosols used for testing. PSL particles matching the silica particle diameters used have been selected to provide a direct comparison between the two types of surfaces.

2.2.3 Properties of the core particles

The core particles investigated were 1.6 and 3 μm diameter PSL spheres (Duke Scientific), 1.6 μm diameter silica spheres (Duke Scientific), and 3 μm diameter highly porous silica spheres (Supelcosil, Supelco). The physical properties of the core particles are summarized in Table 2.1. As is evident from Table 2.1, the porosity of the 3 μm diameter silica spheres represents a 50 fold increase in surface area over the surface area of a solid 3

μm diameter silica sphere.

Table 2.1 - Relevant parameters of core particles

Core type	d_p	Pore Size	Density	Pore Volume	Surface Area	$SA_{porous}:SA_{solid}$[a]
	μm	*nm*	*g/mL*	*μm^3*	*μm^2*	
Silica	1.6	NA	2.07	NA	8	NA
	3.0	12	0.58	5	1400	50
PSL	1.6	NA	1.05	NA	8	NA
	3.0	NA	1.05	NA	28	NA

[a] SA = Surface Area

2.3 Design and development of the coating oven

Techniques to create internally mixed, coated particles include direct atomization of a mixed solution or controlled condensation of a vapor onto a particle surface. Although the latter method is more experimentally demanding, it also more closely mimics mechanisms by which internally mixed particles are created in the atmosphere and for this reason was selected as the method of creating an adsorbed layer of oleic acid onto the core particles. Previous experimental efforts by the Baer group generated internally mixed ethylene glycol/oleic acid aerosols using a "pick-up" cell.[17] Mixed particles were created by introducing liquid glycerol droplets into a glass bulb containing a saturated vapor of oleic acid, which condensed into a film on the surface of the ethylene glycol. The motivation for this earlier study was to assess the ability of a two-step laser desorption/ionization process to surficially probe an aerosol particle and, as such, precise knowledge of the coating

thicknesses was not essential. However, analyzing the kinetics of an adsorbed layer requires accurate estimates of the amount of material in the adsorbed layer. Early attempts to adopt the pick-up cell methodology to the present work were not successful. Turbulence in the pick-up cell resulted in varied residence times for the silica particles, and coating thicknesses were impossible to control. As a result, it became necessary to design and build a new, well-characterized oven that could create internally mixed particles in a repeatable manner.

The design of the oven was inspired by the work of Han et al.[18] and consisted of a 1.9 cm o.d., 33 cm long stainless steel tube encased in a solid aluminum block. Four cartridge heaters (Watlow, Model C2A4) powered by a temperature controller (Watlow, Series 989) regulated the temperature of the oven. This design is similar to several others that have emerged recently with increasing awareness of the need to characterize properties of internally mixed particles.[19-21] Adsorption of oleic acid onto the core particles occurs as a flow of atomized core particles passes through the coating oven, containing a pool of liquid oleic acid along the length of the tube. The amount of adsorption onto the core particles was controlled by two key parameters:

1. *Oven Temperature* – The oven temperature controlled the saturated vapor pressure, and the resulting concentration, of oleic acid within the tube. This dependence is shown in Figure 2.1, based on the work of Tang et al.[22] An upper bound of 75°C was used for the oven temperature set point due to the formation

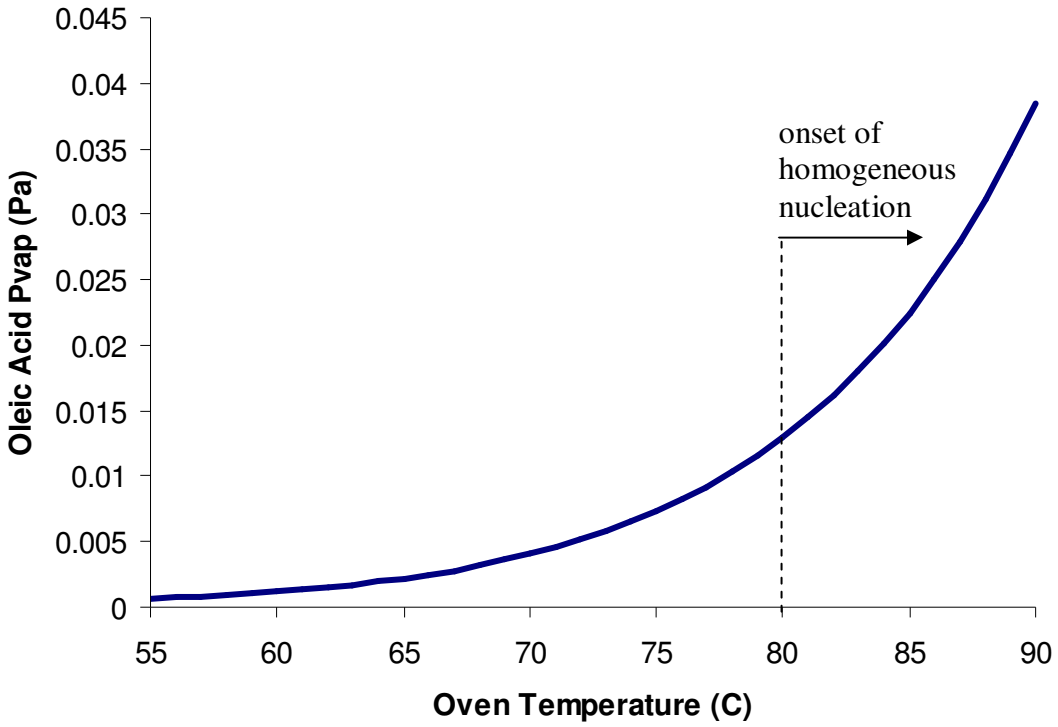

Figure 2.1. *Vapor pressure of oleic acid as a function of oven temperature*. Velocimetry indicates that detectable homogeneously nucleated oleic acid particles begin to form at approximately 80°C.

of homogeneously nucleated oleic acid particles.

2. *Aerosol Flow Rate* – The residence time of the core particles in the oven is controlled by the flow rate through the oven. In order to ensure predictable residence times for all particles through the coating oven, the aerosol flow rate was kept sufficiently low that the flow was laminar. The velocity profile of a well-developed laminar flow is parabolic:

$$v = v_o\left[1-\left(\frac{r}{R}\right)^2\right] \tag{2.1}$$

where v_o is the maximum velocity determined by the set aerosol flow rate, r is the radial distance from the centerline, and R is the radius of the tube. The average flow rate is $\bar{v} = v_o/2$, and the resulting average residence time in the oven, of length L, is then $\tau_{avg} = L/\bar{v}$.[23] Determining the flow conditions requires the calculation of the Reynolds number (Re) for the flow conditions:

$$\mathrm{Re} = \frac{\rho V d}{\mu} \tag{2.2}$$

where ρ is the density of the carrier gas, V is the velocity of the gas, d is the tube diameter, and μ is the gas viscosity which is temperature dependent. The condition for laminar flow requires Re < 1500. As shown in Figure 2.2 these conditions are met for an aerosol flow of 1.3 liters per minute (lpm) over the entire range of oven temperatures investigated.

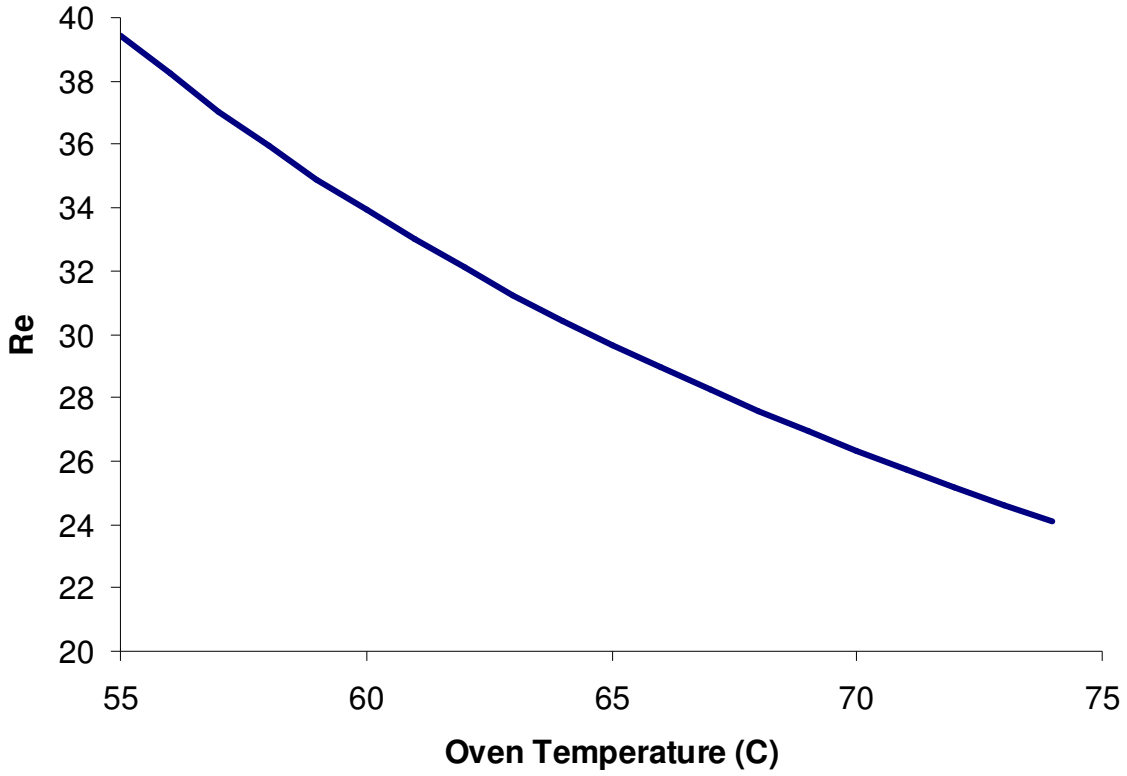

Figure 2.2. *Reynolds number in the coating oven as a function of temperature*.

Operationally, it was much more convenient to alter the oven temperature than to alter the flow rate. The Constant Output Atomizer (TSI Inc., Model 3076) used to aerosolize the core particles required at least a 1.0 lpm flow rate of air to atomize particles, and efforts to reduce this flow rate by pumping off part of the flow prior to the coating oven invariably reduced the particle concentration and were unworkable. As such, a flow rate of approximately 1.3 lpm was used throughout these experiments, corresponding to an average aerosol residence time of approximately 20 seconds in the oven. At this flow rate, no additional dilution flow was necessary in order to operate the ATOFMS, which draws 0.3 lpm through its inlet, and an external particle sizer, requiring a simultaneous flow of 1.0 lpm.

A computational fluid dynamics model of the coating oven and the associated inlet connections was created using the FLUENT software package. Figure 2.3 shows the velocity profile of the flow through the coating oven. The flow is clearly laminar, with well-defined streamlines. Figure 2.4 shows the temperature profile of the oven.

2.4 Prediction of coating mass by condensation theory

2.4.1 Condensation to a solid sphere: Evaluating the mass transfer regime

The phenomena controlling mass transfer of a gas to a particle surface depend on the size of the particle relative to the mean free path of the gas. For small particles, mass transfer is controlled kinetically by collision of a gas molecule with the particle surface. Mass transfer

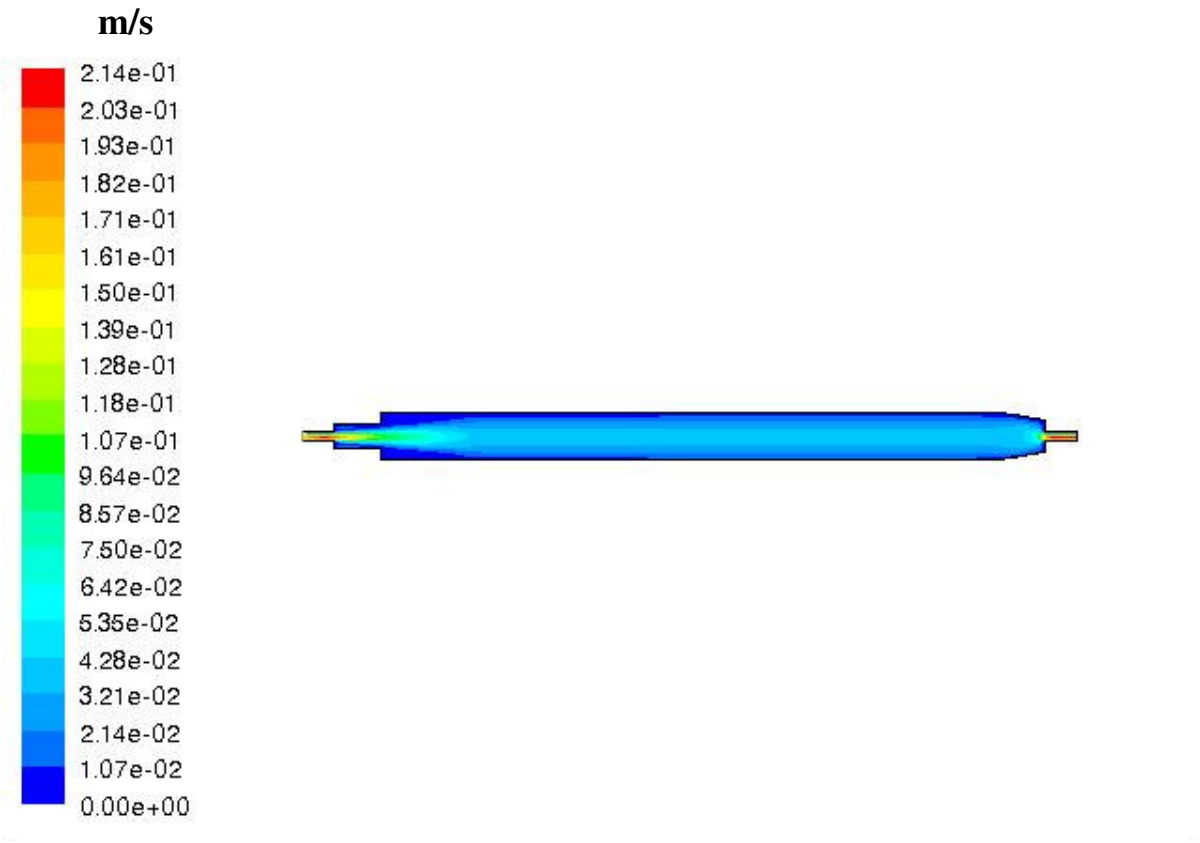

Figure 2.3. *Velocity contours in the coating oven calculated by FLUENT*. Units are meters per second. Conditions are based on a flow rate of 1.3 lpm and an oven wall temperature of 68°C.

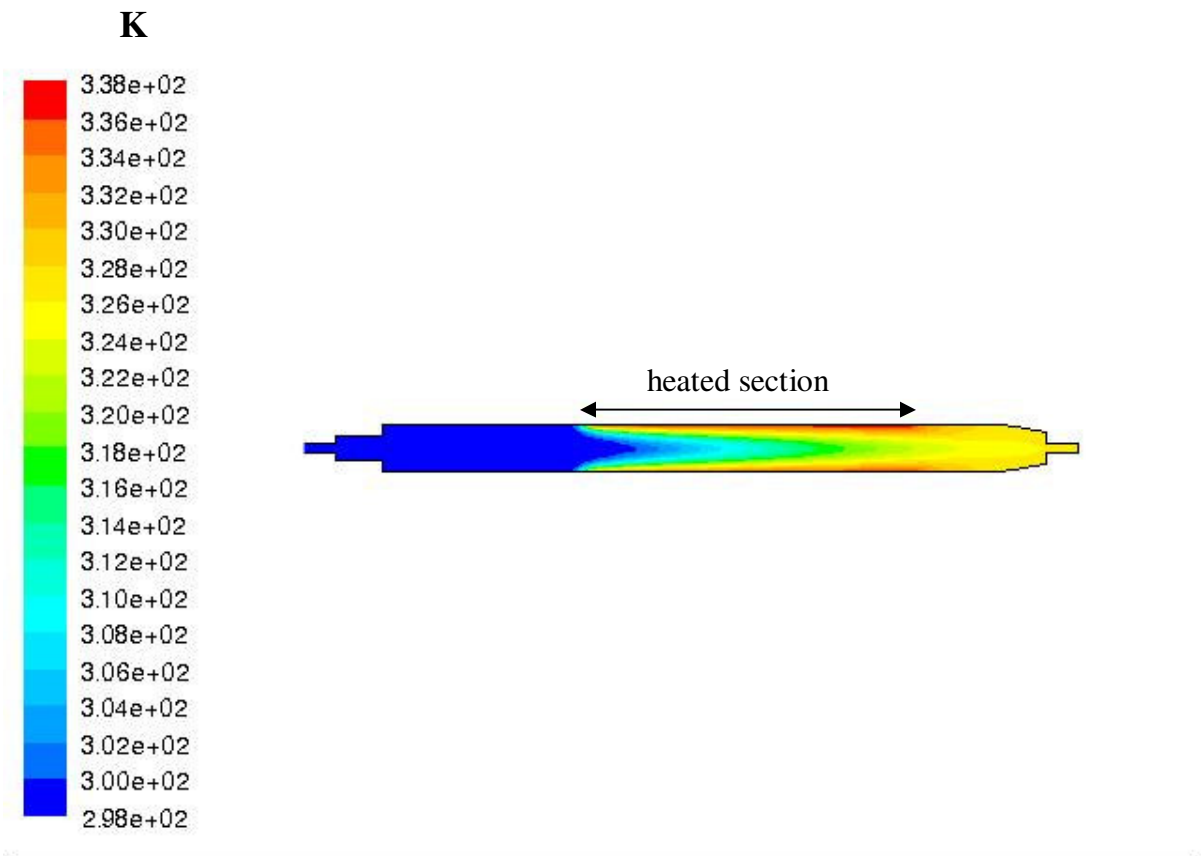

Figure 2.4. *Temperature contours in the coating oven calculated by FLUENT*. Units are degrees Kelvin. Conditions are based on a flow rate of 1.3 lpm and an oven wall temperature of 341 K. The computational fluid dynamics model included the heated section of the oven, as well as associated tubing. The location of the heated section of the coating oven is noted.

to particles sufficiently larger than the mean free path of the condensing gas is controlled by diffusion. The mass transfer regime is evaluated by the Knudsen number[24]:

$$Kn = \frac{2\lambda}{d} \tag{2.3}$$

where λ is the gas mean free path and d is the particle diameter. The mean free path is defined as the quotient of the binary diffusion coefficient of the condensing vapor in air, D_{AB}, and the molecular speed of the gas, $\bar{c}$, allowing the Knudsen number to be re-expressed as:

$$Kn = \frac{2D_{AB}}{d\bar{c}} \tag{2.4}$$

The diffusion coefficient for the binary mixture of oleic acid vapor and nitrogen, as a proxy for air, has been calculated here using Chapman-Enskog theory[25]. For an ideal gas mixture, the binary diffusion coefficient can be expressed in units of $cm^2\ s^{-1}$ according to:

$$D_{AB} = \frac{0.00266T^{3/2}}{PM_{AB}^{1/2}\sigma_{AB}^2\Omega_{AB}} \tag{2.5}$$

where P represents the total pressure of the system, M_{AB} represents the reduced mass of the system, and σ_{AB} represents the mean collision diameter of the two species. The collision integral, encapsulating intermolecular interactions, is represented by Ω_{AB} and is dependent on the binary Lennard-Jones energy ε_{AB}. These parameters can be derived from literature values reported for nitrogen and oleic acid acid according to:

$$M_{AB} = 2\left(\frac{1}{M_A} + \frac{1}{M_B}\right)^{-1} \tag{2.6}$$

$$\varepsilon_{AB} = (\varepsilon_A \varepsilon_B)^{1/2} \tag{2.7}$$

$$\sigma_{AB} = \frac{\sigma_A + \sigma_B}{2} \tag{2.8}$$

An analytical approximation for Ω_{AB}, based on the 12-6 Lennard-Jones potential, has been used here[25]:

$$\Omega_{AB} = \frac{1.06036}{\left(\frac{kT}{\varepsilon_{AB}}\right)^{0.15610}} + \frac{0.19300}{\exp\left(\frac{kT}{\varepsilon_{AB}}\right)} + \frac{1.03587}{\exp\left(1.52996\frac{kT}{\varepsilon_{AB}}\right)} + \frac{1.76474}{\exp\left(3.89411\frac{kT}{\varepsilon_{AB}}\right)} \tag{2.9}$$

The binary parameters derived for this work based on the expressions above and tabulated values for homogeneous parameters[25,26] are shown in Table 2.2. The calculated binary parameter have been used to evaluate D_{AB}.

Table 2.2 – Derived parameters used to calculate D_{AB}

	Nitrogen	Oleic Acid	Calculated Binary Value for Nitrogen/Oleic Acid
M (g/mol)	28.01	282.46	**50.97**
ε (K)	71.4 [25]	729.0 [26]	**228.1**
σ (Å)	3.798 [25]	9.551 [26]	**6.675**

Based on the values for D_{AB}, the Knudsen number for each core particle size was calculated over the range of oven temperatures used. The resulting values for the Knudsen number (*Kn* = 0.05 - 0.1) indicate that the mass transport of oleic acid to the core particles is on the cusp of the continuum regime and the transition regime, wherein corrective factors are applied to the continuum solution to capture the change in transport from diffusion to kinetic molecular

motion.

2.4.2 Condensation to a solid sphere: Estimating the rate of collisions

In the continuum regime the flux of gaseous molecules to a surface is determined by the diffusion, and the rate of collisions of vapor molecules with a particle surface is expressed as[27]:

$$n_z = 2\pi D_{AB} d_p N_{oleic} = \frac{2\pi D_{AB} d_p}{k}\left(\frac{p_\infty}{T_\infty} - \frac{p_d}{T_d}\right)_{oleic} \tag{2.10}$$

where the net concentration of oleic acid vapor, N, is expressed in terms of the partial pressure p_∞ and temperature T_∞ of oleic acid away from the particle surface and the partial pressure p_d and temperature T_d at the particle surface. The pressure over a curved surface is given by the Kelvin equation but is dependent on the particle surface temperature, which can be elevated due to the release of latent heat of vaporization during the condensation process. The uncertainty of the particle temperature makes calculation of the p_∞/T_∞ term difficult, but given the extremely low volatility of oleic acid this term is likely to be small and has been neglected, effectively assuming that oleic acid adsorbed to the surface does not re-evaporate. The suitability of this assumption will be addressed later. Neglecting the p_∞/T_∞ term of Equation 2.6, the reformulated expression for the flux of oleic acid to the particle surface is:

$$n_z = \frac{2\pi D_{AB} d_p p_{oleic}}{kT_{oven}} \tag{2.11}$$

Because the values for *Kn* indicate that mass transfer to the core particles is in the transition

regime, a corrective term ϕ has been used to account for deviations to the continuum regime solution. The formulation for ϕ proposed by Fuchs and Sutugin is[28]:

$$\phi = \frac{1 + Kn}{1 + 0.773Kn + 1.33Kn(1 + Kn)/\alpha} \tag{2.11}$$

where α is the accommodation coefficient representing the likelihood that a gas phase molecule sticks to the surface upon collision. The final estimate for the total number of adsorbed oleic acid molecules on a solid core particle surface is then:

$$N_{adsorbed} = n_z \phi \tau_{avg} \tag{2.12}$$

Predictions of the amount of oleic acid adsorbed to a spherical 3μm sphere based on Equation 2.12 are shown in Figure 2.5. Evident from these predictions is the influence that the "stickiness" of the interaction between oleic acid and the surface, encapsulated by α, has on determining the volume of oleic acid adsorbed. The magnitude of α has not been measured before for oleic acid adsorbing on either silica or soot surfaces, so α has been used as a fitting parameter in the characterization of the coated particles as will be discussed in Chapter 3.

2.4.3 Condensation to a porous sphere: Capillary condensation and confinement

The presence of a porous network was expected to increase the total amount of adsorbed oleic acid on the core silica particles. In addition to the increase in surface area

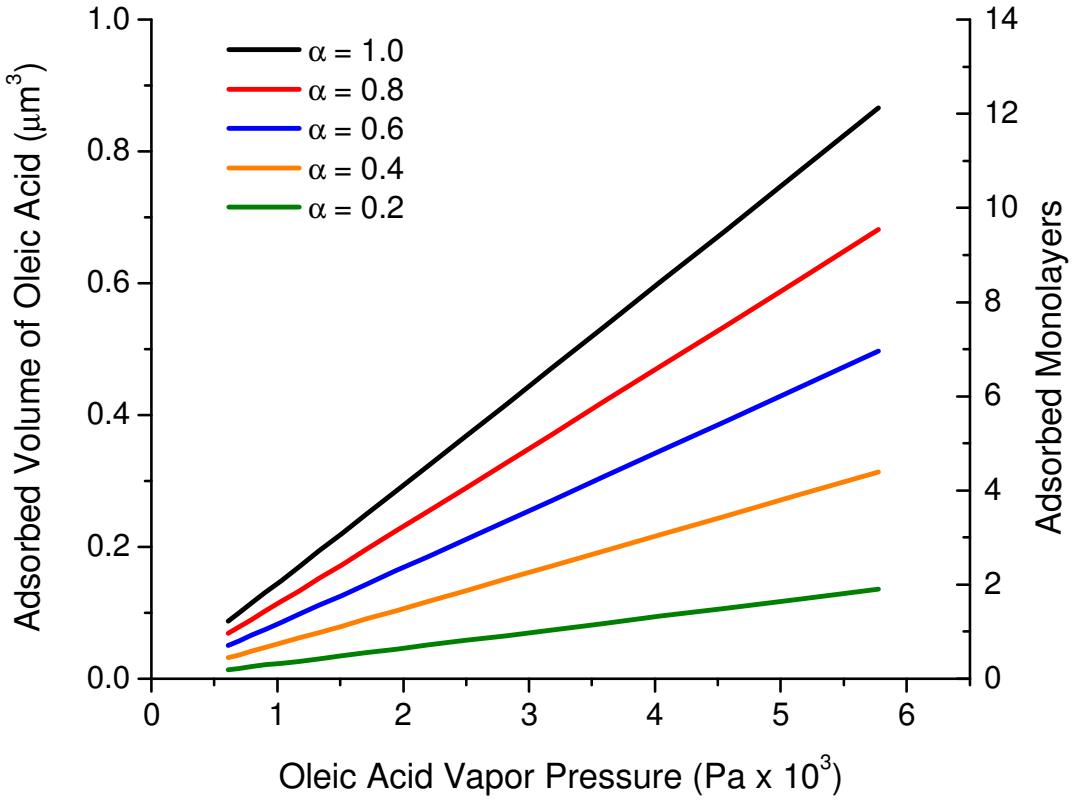

Figure 2.5. *Predictions of adsorbed oleic acid volume based on condensation theory*. The influence of the mass accommodation coefficient, α, is also shown.

available for adsorption of a gas on a porous particle, as highlighted in Table 1, the presence of pores also provides an enthalpic advantage to condensation. The negative radius of the meniscus that forms in the constriction of a pore allows condensation to occur at a vapor pressure lower than on a surface, as defined by the Kelvin equation:

$$\ln\left(\frac{p}{p^o}\right) = -\frac{4\sigma M}{d_{pore}\rho RT} \tag{2.11}$$

where σ is the surface tension within the pore, M is the molar mass of the condensing gas, ρ is the density, and d_{pore} is the pore diameter. Hence, as the pore diameter decreases, the vapor pressure required to initiate condensation decreases. The dependence of condensation on the pore diameter and shape has been demonstrated theoretically[29,30] and experimentally[31,32]. An example of the enhancement in condensation afforded by a porous network relative to a non-porous substrate is pictured in Figure 2.6 for the case of *n*-hexane condensation on mesoporous (3-10 nm) siliceous particles.[31]

Confinement of oleic acid within the pores of a silica particle was also hypothesized to alter the adsorption energetics and orientation of oleic acid, which was believed to be capable of changing the reactivity of O_3 with oleic acid in the pore space. Confinement effects within the pores have been shown to influence the enthalpies of adsorption[32] and the contact angle[33] of the adsorbate.

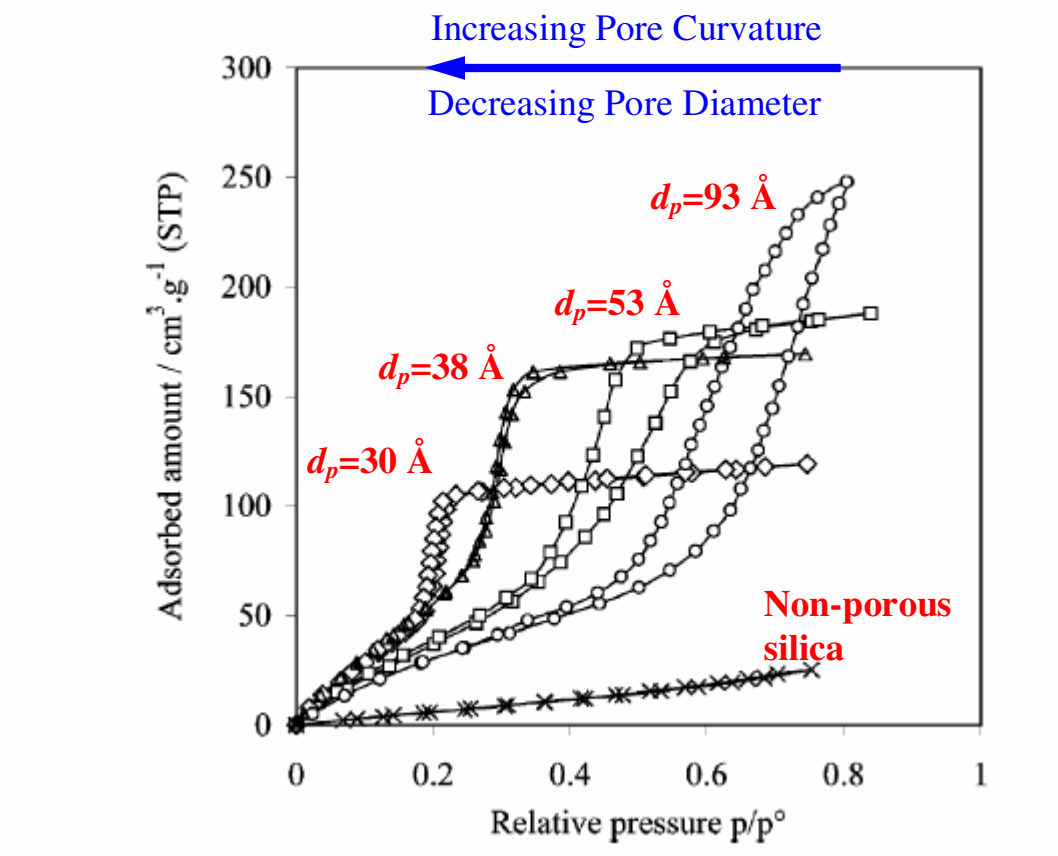

Figure 2.6. *Adsorption isotherms of n-hexane onto porous silica substrates of different pore diameters and non-porous silica*. Adsorption in the pores occurs at lower vapor pressures with decreasing pore diameter, as evidenced by the break points in the isotherms. For all pore sizes, the enhancement in the amount of *n*-hexane adsorbed to the porous substrates relative to non-porous silica is evident. From Trens et al.[31] Reproduced by permission of The Royal Society of Chemistry on behalf of the Centre National de la Recherche Scientifique.

2.5 Conclusion

A new coating oven has been designed and built to control condensational growth of oleic acid onto solid core particles. Key design parameters of the oven such as flow rate and oven temperature have been modeled using a computational fluid dynamics to fully characterize the performance of the oven. Condensation theory was used to develop predictions for the amount of oleic acid deposited onto core particle surfaces during passage through the oven. Comparison between these predictions and analytical measurements of the adsorbed oleic acid will be discussed in the next chapter.

References

1. Schuttlefield, J. D.; Cox, D.; Grassian, V. H. An investigation of water uptake on clays minerals using ATR-FTIR spectroscopy coupled with quartz crystal microbalance measurements. *Journal of Geophysical Research-Atmospheres* **2007,** *112* (D21).

2. Krueger, B. J.; Grassian, V. H.; Cowin, J. P.; Laskin, A. Heterogeneous chemistry of individual mineral dust particles from different dust source regions: the importance of particle mineralogy. *Atmos. Environ.* **2004,** *38* (36), 6253-6261.

3. Usher, C. R.; Michel, A. E.; Grassian, V. H. Reactions on mineral dust. *Chem. Rev.* **2003,** *103* (12), 4883-4939.

4. Usher, C. R.; Michel, A. E.; Stec, D.; Grassian, V. H. Laboratory studies of ozone uptake on processed mineral dust. *Atmos. Environ.* **2003,** *37* (38), 5337-5347.

5. Goss, K. U.; Schwarzenbach, R. P. Adsorption of a diverse set of organic vapors on quartz, $CaCO_3$, and α-Al_2O_3 at different relative humidities. *J. Colloid Interface Sci.* **2002,** *252* (1), 31-41.

6. Alebic-Juretic; A.; Cvitas, T.; Klasinc, L. Kinetics of heterogeneous ozone reactions. *Chemosphere* **2000,** *41* (5), 667-670.

7. Perraudin, E.; Budzinski, H.; Villenave, E. Kinetic study of the reactions of ozone with polycyclic aromatic hydrocarbons adsorbed on atmospheric model particles. *Journal of Atmospheric Chemistry* **2007,** *56* (1), 57-82.

8. Perraudin, E.; Budzinski, H.; Villenave, E. Kinetic study of the reactions of NO_2 with polycyclic aromatic hydrocarbons adsorbed on silica particles. *Atmos. Environ.* **2005,** *39* (35), 6557-6567.

9. Perraudin, E.; Budzinski, H.; Villenave, E. Identification and quantification of ozonation products of anthracene and phenanthrene adsorbed on silica particles. *Atmos. Environ.* **2007,** *41* (28), 6005-6017.

10. Alebic-Juretic, A.; Cvitas, T.; Klasinc, L. Heterogeneous polycyclic aromatic hydrocarbon degradation with ozone on silica gel carrier. *Environ. Sci. Technol.* **1990,** *24* (1), 62-66.

11. Wu, C. H.; Salmeen, I.; Niki, H. Fluorescence Spectroscopic Study of Reactions Between Gaseous Ozone and Surface-Adsorbed Polycyclic Aromatic-Hydrocarbons. *Environmental Science & Technology* **1984,** *18* (8), 603-607.

12. Thomas, J. K. Physical aspects of radiation-induced processes on SiO_2, γ-Al_2O_3, zeolites, and clays. *Chem. Rev.* **2005,** *105* (5), 1683-1734.

13. Blyholder, G.; Adhikar, C.; Proctor, A. Structure and Orientation of Oleic-Acid Adsorbed Onto Silica-Gel. *Colloids and Surfaces A-Physicochemical and Engineering Aspects* **1995,** *105* (1), 151-158.

14. Lee, D. H.; Condrate, R. A. FTIR spectral characterization of thin film coatings of oleic acid on glasses: I. Coatings on glasses from ethyl alcohol. *J. Mater. Sci.* **1999,** *34* (1), 139-146.

15. Kubicki, J. D. Molecular simulations of benzene and PAH interactions with soot. *Environmental Science & Technology* **2006,** *40* (7), 2298-2303.

16. Levitt, N. P.; Zhang, R. Y.; Xue, H. X.; Chen, J. M. Heterogeneous chemistry of organic acids on soot surfaces. *J. Phys. Chem. A* **2007,** *111* (22), 4804-4814.

17. Woods III, E.; Smith, G. D.; Miller, R. E.; Baer, T. Depth-profiling of heterogeneously mixed aerosol particles using single particle mass spectrometry. *Anal. Chem.* **2002,** *74*, 1642-1649.

18. Han, J. H.; Martin, S. T. An Aerosol Chemical Reactor for Coating Metal Oxide Particles with $(NH_4)_2SO_4$-H_2SO_4-H_2O. 1. New Particle Formation. *Aerosol Sci. Technol.* **2001,** *34*, 363-372.

19. Katrib, Y.; Martin, S. T.; Hung, H. M.; Rudich, Y.; Zhang, H.; Slowik, J. G.; Davidovits, P.; Jayne, J. T.; Worsnop, D. R. Products and Mechanisms of Ozone Reactions with Oleic Acid for Aerosol Particles Having Core-Shell Morphologies. *J. Phys. Chem. A* **2004,** *108*, 6686-6695.

20. Garland, R. M.; Wise, M. E.; Beaver, M. R.; Dewitt, H. L.; Aiken, A. C.; Jimenez, J. L.; Tolbert, M. A. Impact of palmitic acid coating on the water uptake and loss of ammonium sulfate particles. *Atmospheric Chemistry and Physics* **2005,** *5*, 1951-1961.

21. Abbatt, J. P. D.; Broekhuizen, K.; Kumal, P. P. Cloud condensation nucleus activity of internally mixed ammonium sulfate/organic acid aerosol particles. *Atmos. Environ.* **2005,** *39* (26), 4767-4778.

22. Tang, I. N.; Munkelwitz, H. R. Determination of Vapor Pressure from Droplet Evaporation Kinetics. *J. Colloid Interface Sci.* **1990,** *141* (1), 109-118.

23. Bird, R. B.; Stewart, W. E.; Lightfoot, E. N. *Transport Phenomena;* 2nd ed.; John Wiley & Sons, Inc.: New York, 2002.

24. Seinfeld, J. H.; Pandis, S. N. *Atmospheric Chemistry and Physics;* Wiley Interscience: New York, 1998.

25. Poling, B. E.; Prausnitz, J. M.; O'Connell, J. P. *The Properties of Gases and Liquids;* 5 ed.; McGraw-Hill: 2001.

26. Rader, D. J.; McMurry, P. H.; Smith, S. Evaporation Rates of Monodisperse Organic Aerosols in the 0.02- to 0.2-um-Diameter Range. *Aerosol Sci. Technol.* **1987,** *6*, 247-260.

27. Hinds, W. C. *Aerosol Technology: Properties, Behavior, and Measurement of Airborne Particles;* 2nd ed.; Wiley-Interscience: New York, 1999.

28. Fuchs, N. A.; Sutugin, A. G. High-dispersed aerosols. In *Topics in Current Aerosol Research*, Pergamon Press: 1971.

29. Wallacher, D.; Kunzner, N.; Kovalev, D.; Knorr, N.; Knorr, K. Capillary condensation in linear mesopores of different shape. *Phys. Rev. Lett.* **2004,** *92* (19).

30. Oh, J. S.; Shim, W. G.; Lee, J. W.; Kim, J. H.; Moon, H.; Seo, G. Adsorption equilibrium of water vapor on mesoporous materials. *Journal of Chemical and Engineering Data* **2003,** *48* (6), 1458-1462.

31. Trens, P.; Tanchoux, N.; Maldonado, D.; Galarneau, A.; Di Renzo, F.; Fajula, F. Study of *n*-hexane adsorption in MCM-41 mesoporous materials: a scaling effect approach of capillary condensation processes. *New J. Chem.* **2004,** *7*, 874-879.

32. Trens, P.; Tanchoux, N.; Papineschi, P. M.; Maldonado, D.; Di Renzo, F.; Fajula, F. Confinements effects in MCM-41-type materials: Comparison of the energetics of n-hexane and 1-hexene adsorption. *Microporous and Mesoporous Materials* **2005,** *86* (1-3), 354-363.

33. Aharoni, C. Effect of the energy of adsorption at the pore wall surface on capillary condensation. *Langmuir* **2002,** *18* (20), 7441-7446.

CHAPTER 3

CHARACTERIZATION OF SURFACE-ADSORBED OLEIC ACID ON SOLID CORE PARTICLES

3.1 Introduction

This chapter discusses the characterization of adsorbed oleic acid on the two types of core particles by multiple analytical techniques. These observations will be compared to predictions of adsorbed volume based on condensation theory. The morphology of the resulting adsorbed layer will also be addressed.

3.2 Experimental methods for particle characterization

3.2.1 Generation of coated aerosols

Figure 3.1 shows the experimental set-up used for particle generation and analysis. Equal concentrations of the 1.6 and 3 μm PSLs, 1.6 μm silica spheres, and 3 μm highly porous silica spheres of core particles were each suspended in a 50:50 water/methanol solution and aerosolized with filtered air using a Constant Output Atomizer. The atomized particles passed through a heated tube followed by a diffusion dryer (TSI Inc., Model 3062) to remove the solvent, and the possibility of incomplete removal of adsorbed water on the core particle surface will be discussed later. The denuded core particles then entered the

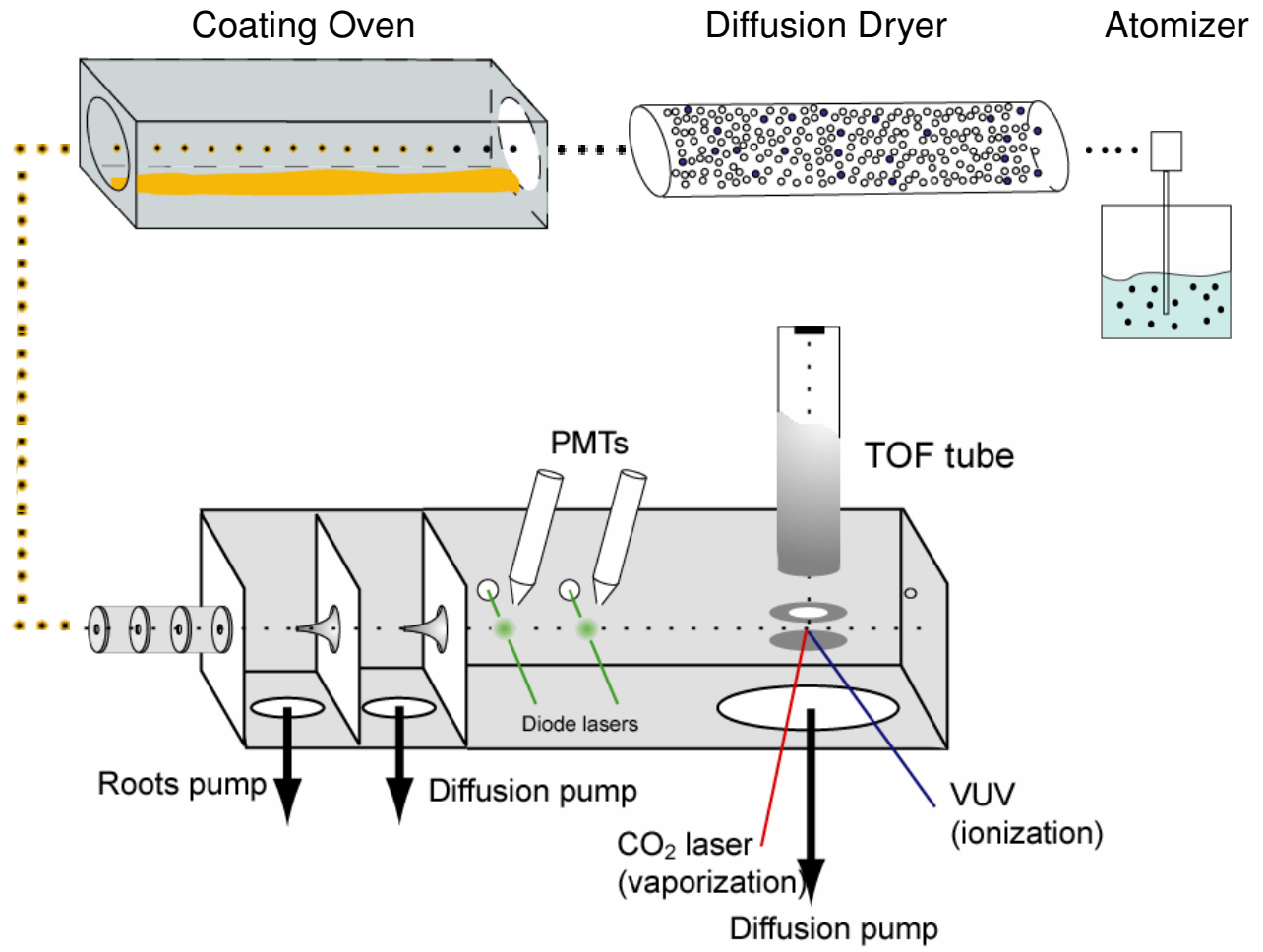

Figure 3.1. *Experimental Set-up: Particle generation, coating, and particle characterization by ATOFMS.*

home-built oven for vapor deposition. Composition and morphology of the coated particles were evaluated with the ATOFMS, a Scanning Electron Microscopy (SEM), and an Atomic Force Microscope (AFM). The composition of the coated particles was also explored by a series of filter studies using GC-MS. Particle sizing was performed by the ATOFMS and an Aerodynamic Particle Sizer (APS) (TSI Inc., Model 3321).

3.2.2 On-line characterization with ATOFMS and APS

Real-time quantitative analysis of organic species in aerosols has required the development of a host of new analytical methods.[1,2] Organic compounds generally possess low ionization energies and tend to fragment readily as a result. Hence, unambiguous mass peak assignments are greatly facilitated by a low-energy particle desorption/ionization scheme. The UNC-built ATOFMS has been designed specifically for this purpose. The instrument has two separate methods for particle desorption, and employs low-fluence vacuum UV light to gently ionize the resulting vapor.

The first method of particle desorption uses a cartridge heater to thermally desorb non-refractory aerosol components. By tuning the temperature of the probe tip, very little excess energy is imparted to the vapor molecules. As a result, thermal desorption has been incorporated into several real-time aerosol mass spectrometers.[3-5] Thermal desorption was not an effective method for analysis of adsorbed oleic acid, however. The refractory core particles to which the oleic acid was adsorbed likely had a very brief contact time with the

heater tip before bouncing off, and the core particle may have served to screen oleic acid not in direct contact with the heater from desorbing.

The second method of particle vaporization available with the UNC ATOFMS involves irradiation of the aerosol particle with infrared light from a CO_2 laser. Even at low laser fluence the CO_2 laser can transfer excess energy to the desorbed gas-phase molecules.[6] Although this two-laser desorption/ionization scheme has been shown to result in a greater degree of analyte fragmentation for liquid organic aerosols relative to desorption by a cartridge heater [7], it proved to be much more successful in analysis of the adsorbed surfactant layer and was used in all of the analysis reported in this work.

As depicted in Figure 3.1, after traversing the coating oven the particles entered the ATOFMS through an aerodynamic lens, which focused the particles into a narrow beam. The particles were accelerated proportionally to their size by the supersonic expansion of gases as the aerosol moved from the ambient conditions of the flow tube to the evacuated main chamber (10^{-7} Torr) of the ATOFMS. Particle trajectory through the chamber intersected the incident beams of two 532 nm green diode lasers separated by 10 cm. Light that was sequentially scattered by the particle as it passed through each beam was collected by separate photomultiplier tubes (PMTs) and translated into an electronic signal. A digital timing circuit used this signal to calculate each particle's velocity, and coordinated the charging and firing of a two-step laser desorption/ionization process. Upon arrival in the

center of the instrument, a particle was first volatilized by radiation from a CO_2 laser (λ = 9.3-10.6 μm) and subsequently ionized by 118 nm (10.5 eV) vacuum UV light produced by frequency tripling the 355 nm output of a Nd:YAG laser in a Xe/Ar gas cell. Prior to data collection, laser powers and temporal separation between IR and VUV firing were adjusted to maximize the intensity of the oleic acid molecular ion ($M^{+\cdot}$, m/z=282). A continuous 200 V cm^{-1} electric field applied between two plates bounding the ionization region accelerated the created ions into the 1 m long drift tube where the ions were detected by a multichannel electron multiplier. One hundred single particle mass spectra were averaged for each measurement.

3.2.3 Off-line characterization by SEM, AFM, and filter extraction

Two off-line techniques were employed to better understand the morphology of adsorbed oleic acid. First, particles were collected on carbon tape attached to a stainless steel stub, and imaged using a Hitachi S-4700 scanning electron microprobe (SEM) with a field emission source. Collected particles were sputter-coated with 2 nm of an Au/Pd alloy (60/40) prior to analysis to enhance conductivity and improve image quality. Post-processing of SEM images was performed using ImageJ.[8] Second, particles were also imaged using a multimode atomic force microscope (AFM) from Veeco Metrology group equipped with a Nanoscope IIIA control station in Tapping-mode. The AFM was operated with silicon cantilevers having spring constants of 5.0 N m^{-1} at resonance frequencies of about 200 kHz (MikroMasch). Topographical and phase images were created by scanning the tip over a portion of the core

particle surface.

Filter extraction was employed as an off-line method to investigate the amount of oleic acid adsorbed to the core particles. Coated particles were impacted on a filter over a period of several hours to accumulate a sufficient mass for analysis. Following the method of Jaoui and Kamens, oleic acid was removed from the filters by repeated reflux of methylene chloride ($MeCl_2$) in a Soxhlet extractor over the course of 6-12 hours.[9] After concentrating the remaining liquid down to ~10-20 µl by volatilization of the $MeCl_2$ using a dry N_2 flow, the samples were derivatized by bis-(trimethylsilyl) trifluoroacetamide (BSTFA) to facilitate sample passage through the GC column.

3.3. Results of coated particle characterization by on-line methods

3.3.1 Compositional analysis with the ATOFMS

In order to characterize the amount of oleic acid adsorbed onto the core particles, the mass spectrometry signal intensity for oleic acid was correlated to sample volume using pure oleic acid particles of known size. Oleic acid particles were either size-selected with a Scanning Mobility Particle Sizer (TSI Inc., Model 3080) or introduced into the ATOFMS as a polydisperse aerosol with the mass spectral response sorted by particle size. Laser powers and temporal separation between IR and VUV firing were tuned to maximize the intensity of the $M^{+\cdot}$ peak while minimizing the amount of excess thermal energy imparted to the resulting vapor which can lead to molecular fragmentation. The signal intensity of the $M^{+\cdot}$ peak and

the total integrated signal intensity at all masses both scale linearly with laser fluence before reaching an asymptotic limit. This upper limit in total signal intensity is suggestive of complete particle volatilization, as has been previously argued.[10] However, the assumption of complete vaporization has not been experimentally verified. The mechanism of particle evaporation is highly sensitive to the amount of energy imparted by the CO_2 laser. At laser fluences typical for this work, evaporation of liquid organic droplets of similar size has been shown to proceed by thermal ablation whereby the molecules evaporate layer-by-layer.[11] Under these conditions, the measured signal intensity of pure oleic acid aerosol varied linearly with particle volume over the range from 0.3 – 25 μm^3. The calibration of oleic acid droplet size to signal intensity is shown in Figure 3.2.

Similarly to the analysis of pure oleic acid particles, the $M^{+\cdot}$ peak intensity for oleic acid adsorbed on the core particles was maximized by adjusting the CO_2 laser fluence. Aerosol core composition strongly influenced the optimal CO_2 laser energy for particle volatilization: 22.9±1.4 mJ/pulse for both sizes of PSL spheres, 10.5±2.0 mJ/pulse for 1.6 μm silica particles, and 4.7±0.4 mJ/pulse for 3 μm porous silica particles. The difference in laser fluences by core type and the size dependence for the silica particles is attributed to enhanced absorption of the CO_2 laser radiation by the amorphous silica particle. Figure 3.3 shows the overlap between the two primary emission lines of the CO_2 laser and the IR transmittance spectrum of amorphous silica.[12] Energy absorbed by the silica particle may be transferred to the oleic acid on the particle surface. Despite the differences in absolute CO_2 fluence employed for desorption of adsorbed oleic acid, optimized conditions appeared

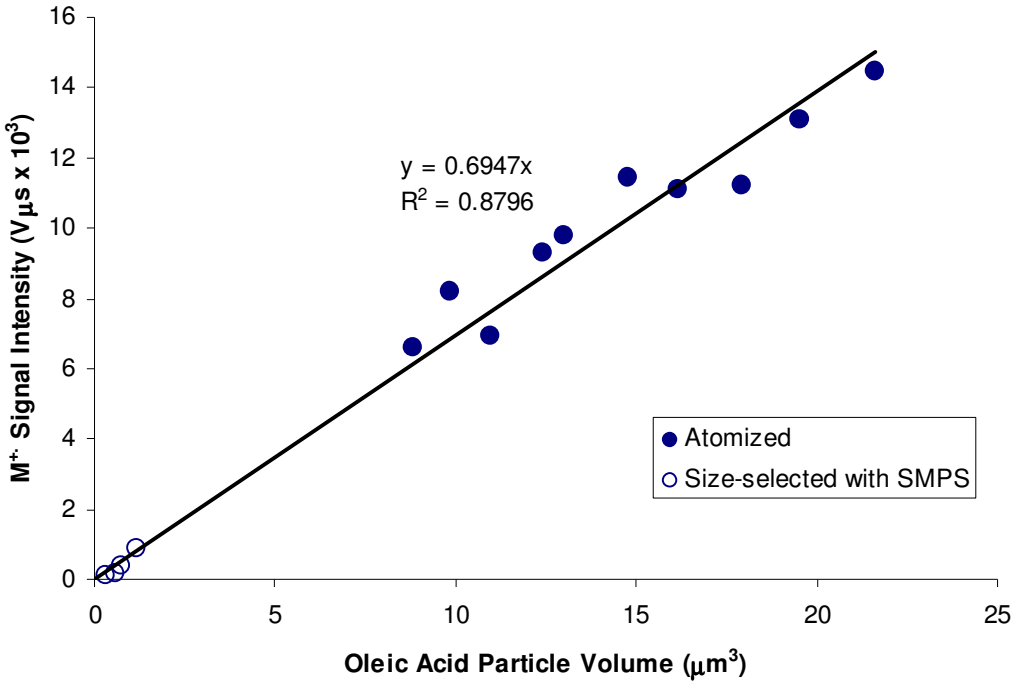

Figure 3.2. *Calibration of pure oleic acid particle volume to $M^{+\cdot}$ (m/z = 282) intensity measured by two-laser desorption/ionization using the ATOFMS.*

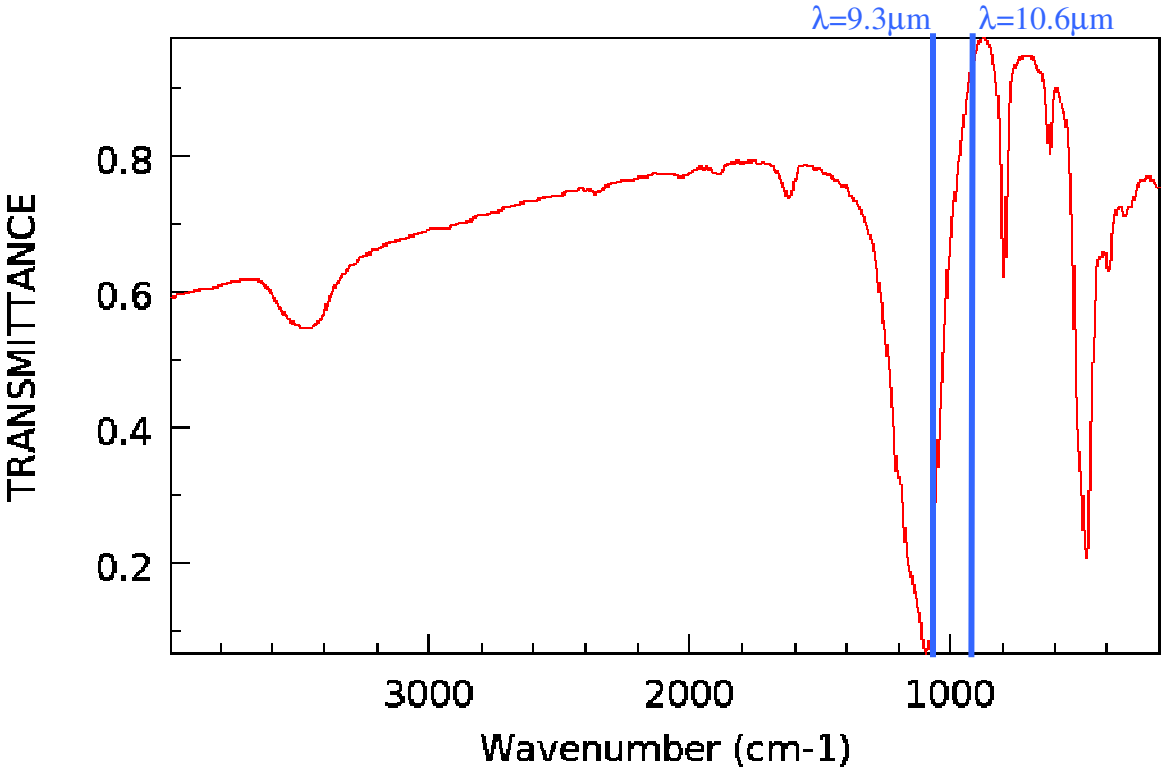

Figure 3.3. *Transmittance spectrum for amorphous silica*. The large absorption by silica at approximately 1100 cm^{-1} overlaps considerably with one of the two primary wavelengths of light emitted by the CO_2 laser denoted by the blue lines. Transmittance spectrum courtesy of NIST Chemistry WebBook.[12]

to ultimately impart similar amounts of energy to oleic acid on each core type, as evidenced by the similarity in fragmentation patterns of pure and adsorbed oleic acid shown in Figure 3.4.

Raising the oven temperature, and consequently the vapor pressure of oleic acid in the coating oven, increased the amount of oleic acid adsorbed to the core particles. Figure 3.5 shows the positive correlation between the oven vapor pressure of oleic acid and the $M^{+\cdot}$ signal intensity. Between 3 – 7 measurements were performed at each vapor pressure, and each data point and error bar represents the mean and standard deviation ($\pm 1\sigma$) of the measurements. Based on the calibration of pure oleic acid, the signal intensity of oleic acid on each core particle was correlated to an adsorbed volume. These values suggested multilayer coverage for all core types, with coating thicknesses increasing from 5 – 30 nm over $P_{vap} = 1 - 6.5 \times 10^{-3}$ Pa assuming uniform distribution over the surface. The estimates for the oleic acid adsorbed volume also agreed with predictions for the volume of adsorbed oleic acid using condensation theory, based on Equation 2.12. Condensation theory predictions for a non-porous sphere with diameters of (dashed line) 1.6 μm and (solid line) 3 μm, using the value $\alpha = 1$, are also shown in Figure 3.5.

No enhancement in the $M^{+\cdot}$ signal intensity was evident for oleic acid adsorbed to porous silica particles despite expectations that these particles would have more adsorbed oleic acid due to the effects discussed in Section 2.4.1. In order to account for the possibility

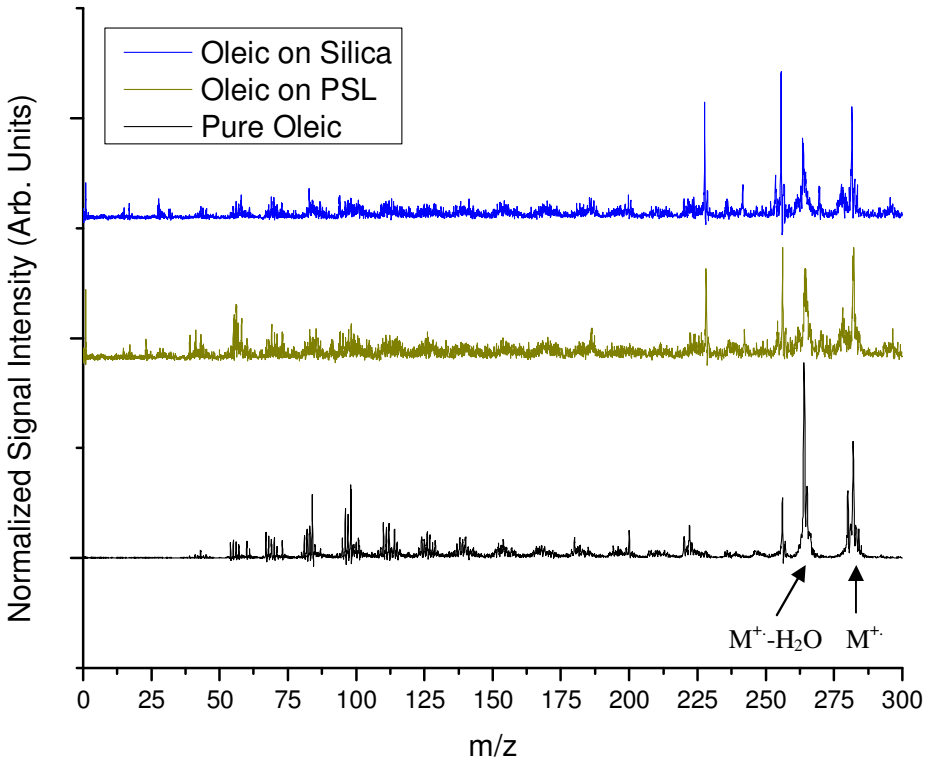

Figure 3.4. *Comparison of mass spectra of oleic acid adsorbed to silica and PSL particles and as pure droplets*. Two prominent peaks are pointed out: the molecular ion, and the water-loss fragment. The similarity of the fragmentation patterns indicates that similar energy is imparted to the oleic acid under all conditions.

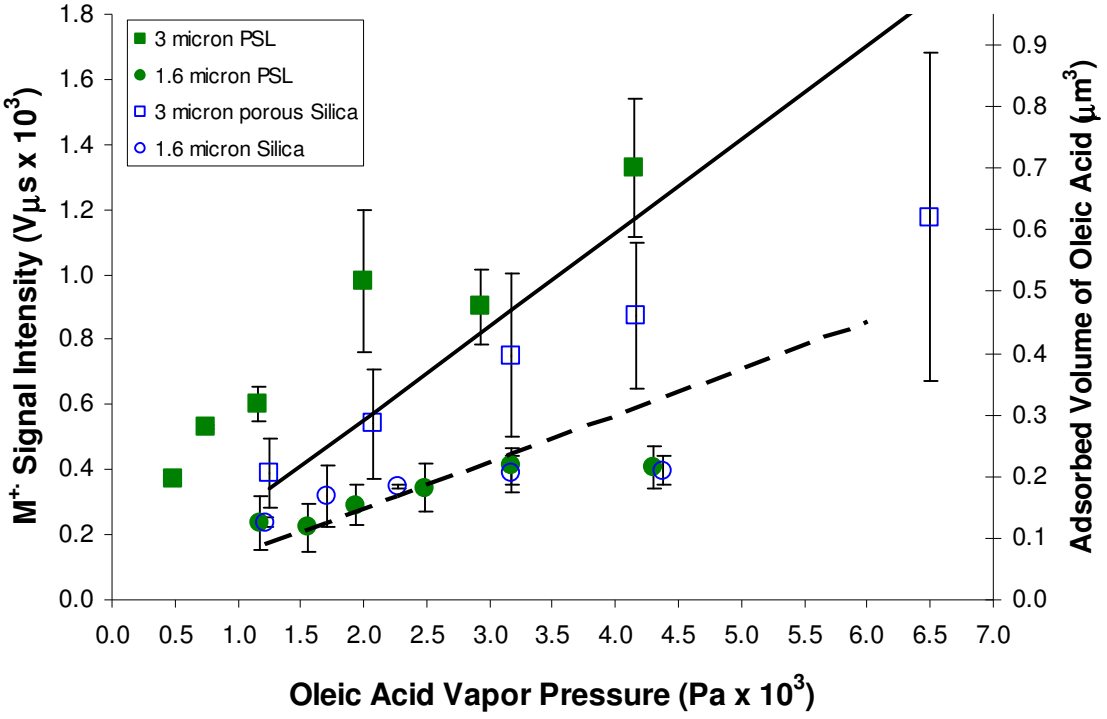

Figure 3.5. *Optimized $M^{+\cdot}$ (m/z = 282) signal intensity of adsorbed oleic acid as a function of oleic acid vapor pressure in the coating oven for each core type and size*. Error bars represent ±1σ. Using the pure oleic acid signal-to-volume calibration, the observed signal intensity was correlated with an adsorbed volume shown on the right axis. Predictions for the volume of adsorbed oleic acid using condensation theory, based on Eq. 2.9 with $\alpha = 1$, are also shown for a non-porous sphere with diameters of (dashed line) 1.6 μm and (solid line) 3μm.

of increased fragmentation of the molecular ion of oleic acid desorbed from the porous silica particles, the behavior of the total signal intensity over the entire mass spectrum was calculated as a function of oleic acid vapor pressure. This dependence is shown in Figure 3.6. The total signal intensity of oleic acid on the porous silica is slightly higher than that observed on its 3µm PSL counterpart, indicating that there may have been more fragmentation of the adsorbed oleic acid, but this analysis ultimately suggests that that the amount of oleic acid accommodated by the two types of inorganic cores prior to reaction is comparable.

3.3.2 Particle sizing analysis with the ATOFMS and APS

Contrary to the ATOFMS coverage estimates, velocimetry measurements of the vacuum aerodynamic diameter (d_{va}) by light-scattering in the ATOFMS, and measurements of the aerodynamic diameter (d_a) by the APS did not indicate a growth in particle size between the uncoated and coated particles. The aerodynamic diameter standardizes the shape and density of a real particle of diameter d_e to that of a sphere of unit density, ρ_0 = 1 g cm^{-3}. Figure 3.7 shows a comparison of gaussian approximations of APS measurements for the size distribution of uncoated 3µm PSLs and 3µm PSLs passing through a 70°C oven. Rather than observing a positive shift in the size distribution to larger diameters as was predicted, and as has been observed before for oleic acid deposition on much smaller core particles[13], the size distribution shifted in the opposite direction. This shift was systematic for all core types investigated as shown in Figure 3.8. The ATOFMS and APS are capable of detecting a change in particle diameter of 6 and 16 nm, respectively, which is less than the 10 – 60 nm

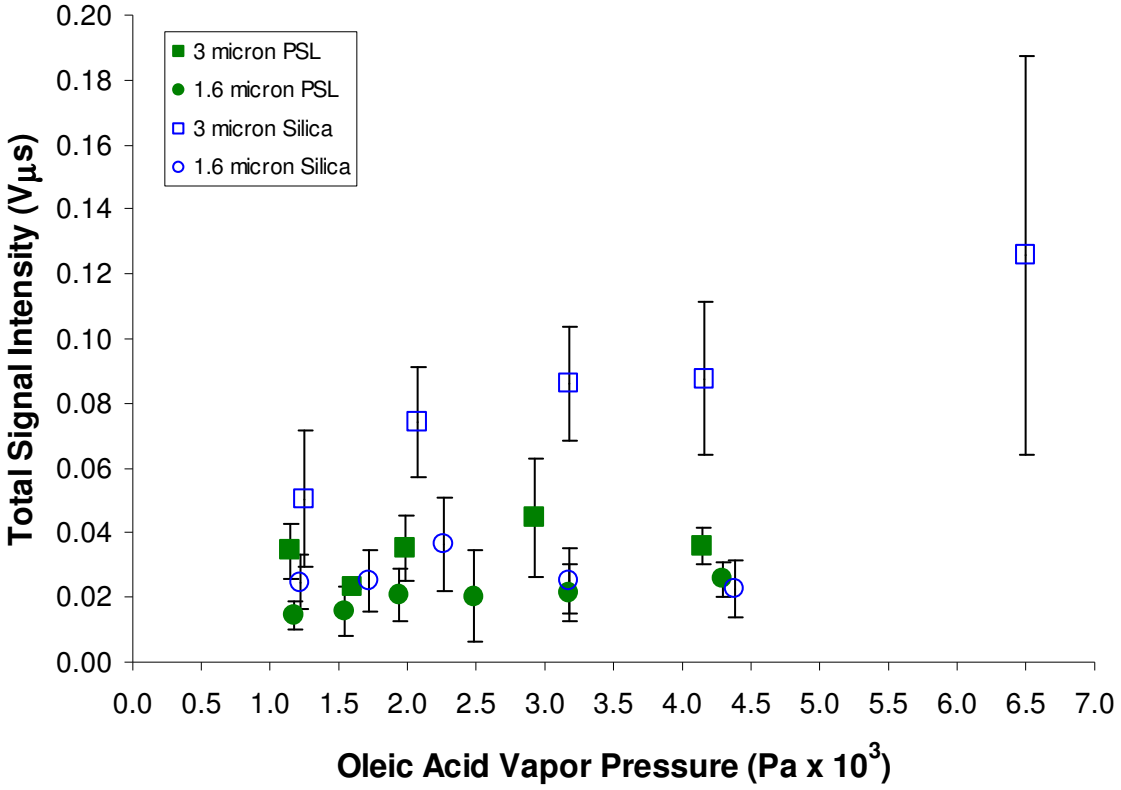

Figure 3.6. *Optimized total signal intensity of adsorbed oleic acid as a function of oleic acid vapor pressure in the coating oven for each core type and size*. Error bars represent ±1σ.

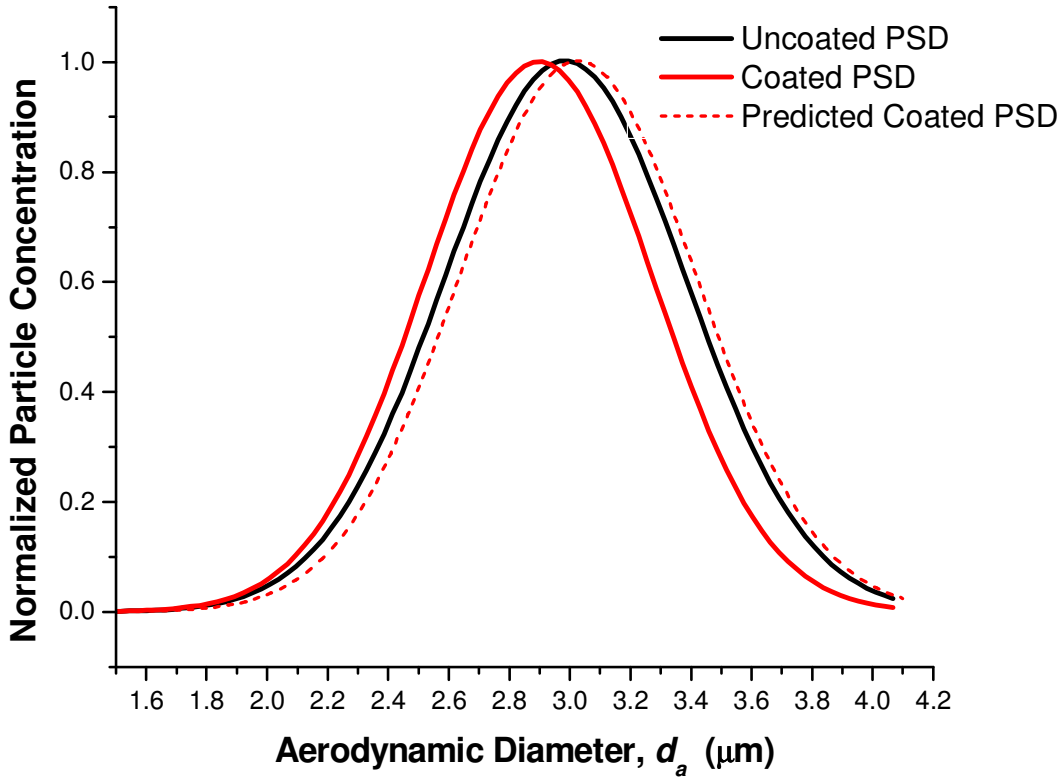

Figure 3.7. *Particle size distributions of 3 μm PSL particles (black line) before and (red line) after coating in a 70°C oven*. The predicted shift in aerodynamic diameter based on a uniform distribution of the estimated volume of oleic acid adsorbed to the core particle is also shown (red dashed line) for comparison.

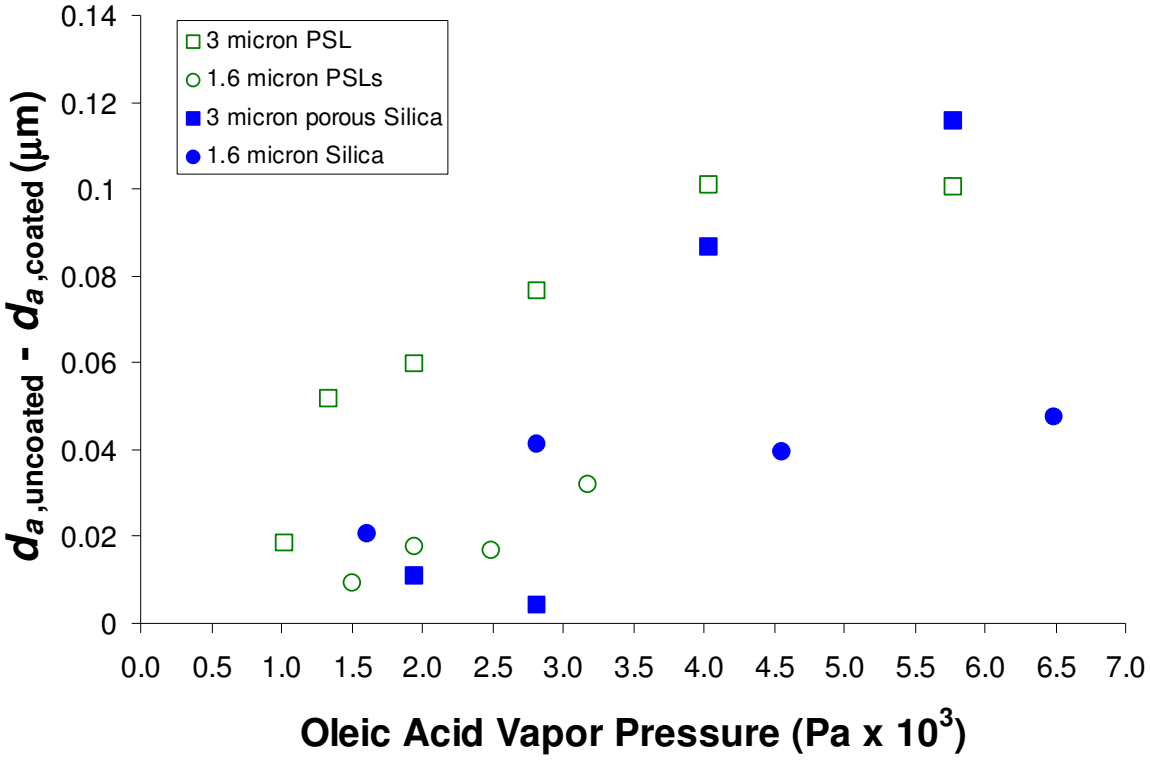

Figure 3.8. *Shift in measured aerodynamic diameter of coated core particles as a function of oleic acid vapor pressure in the coating oven.*

increase suggested by the ATOFMS calibration. As will be discussed below, there is both kinetic and imaging evidence that the morphology of the adsorbed oleic acid is not uniform, which changes the shape factor, χ, of the particle. Both d_{va} and d_a are inversely related to χ, which represents the ratio of resistance drag of the particle to that of a sphere having the same volume. For example, the aerodynamic diameter is defined as:[14]

$$d_a = d_e \left(\frac{\rho_p}{\rho_0 \chi} \right)^{1/2} \tag{3.1}$$

The density of a coated particle of the particle, ρ_p, can be expressed in terms of the amount of oleic acid coating on the core particle, approximating the surface as a sphere:

$$\rho_p = \frac{\left(\rho_{core} r_{core}^{\ 3} + \rho_{oleic} \left[(r_{core} + r_{oleic})^3 - r_{core}^{\ 3} \right] \right)}{(r_{core} + r_{oleic})^3} \tag{3.2}$$

The variation of d_a with changes in ρ_p and χ is shown in Figure 3.9. Unfortunately, the shape factor and density are coupled in some manner which cannot be resolved by the current measurements. Experimental determination of χ requires simultaneous measurement of d_{va} and the mobility diameter (d_m), and as such is not possible for this system because supermicron particles can not be accurately sized by commercial mobility particle sizers.[15,16] However, the current measurements lie somewhere on the surface depicted in Figure 3.9, which indicates that adsorption of oleic acid and increasing χ result in a decrease in the observed value for d_a and d_{va} relative to a uniform coating.

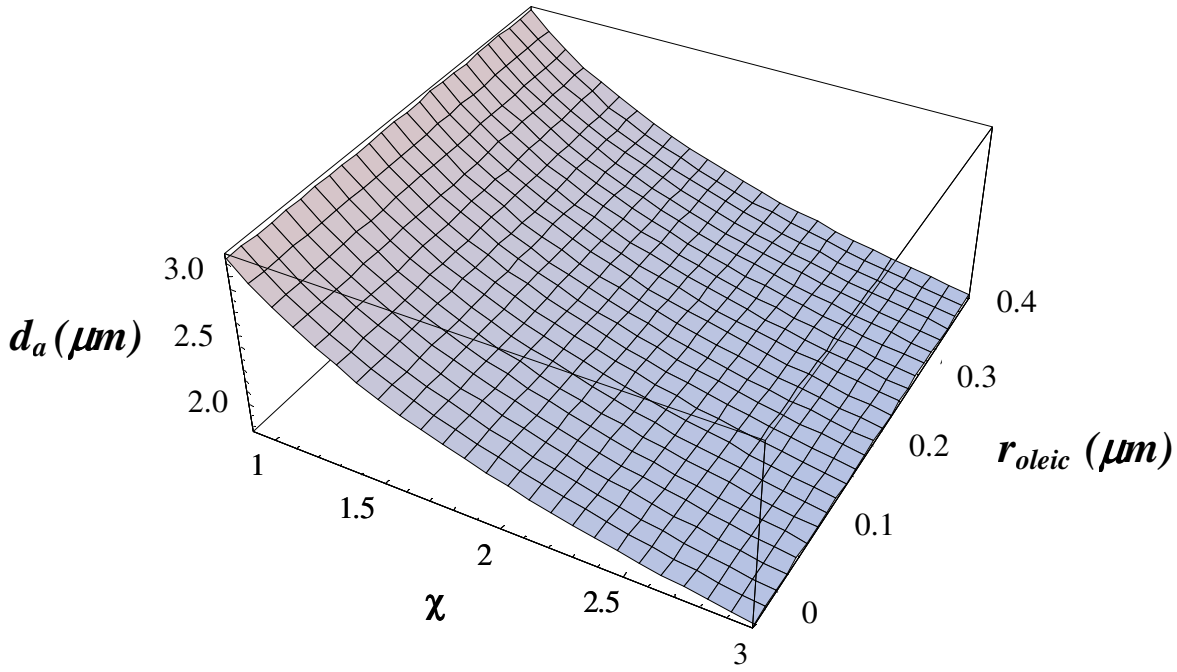

Figure 3.9. *Estimated effect of changes in ρ_p and χ on d_a based on Equations 3.1 and 3.2.*

3.4. Results of coated particle characterization by off-line methods

To reconcile the discrepancy between mass spectral and velocimetry measurements, coated particles were collected for analysis by two different microscopy techniques to image the particles and for compositional analysis using GC-MS.

3.4.1 SEM analysis

SEM images were collected for 1.6 μm silica and 1.6 μm PSL particles before coating and after exposure to oleic acid vapor pressures of P_{vap} = 1.2 and 4.3 x 10^{-3} Pa. The imaging results under these conditions are shown in Figure 3.10. These images revealed important information about both the uncoated and coated particles. First, images of the core particles that do not pass through the coating oven indicated the presence of some very small surface features (3.10 a,d). Mass analysis of uncoated particles showed no signature of oleic acid or methanol indicating that these surface features are likely to be adsorbed water, which has an ionization energy (12.62 eV) that is too high to be detectable by the ATOFMS. Second, the images of the core particles passing through the coating oven (3.10 b-c,e-f) indicated that rather than creating a uniform surfactant film on the core particle surface, adsorbed oleic acid formed distinct regions, or islands. Table 3.1 summarizes the average island geometry and coating characteristics based on analysis of the collected SEM images using ImageJ. The oleic acid islands on both core types are 30 – 35 nm in height, which indicates a localized multilayer of oleic acid molecules. The geometry of the average island on both core types does not change upon increasing the oleic acid P_{vap} from 1.2 to 4.3 x 10^{-3} Pa, suggesting that the adsorbed oleic acid has formed a stable, thermodynamically favorable

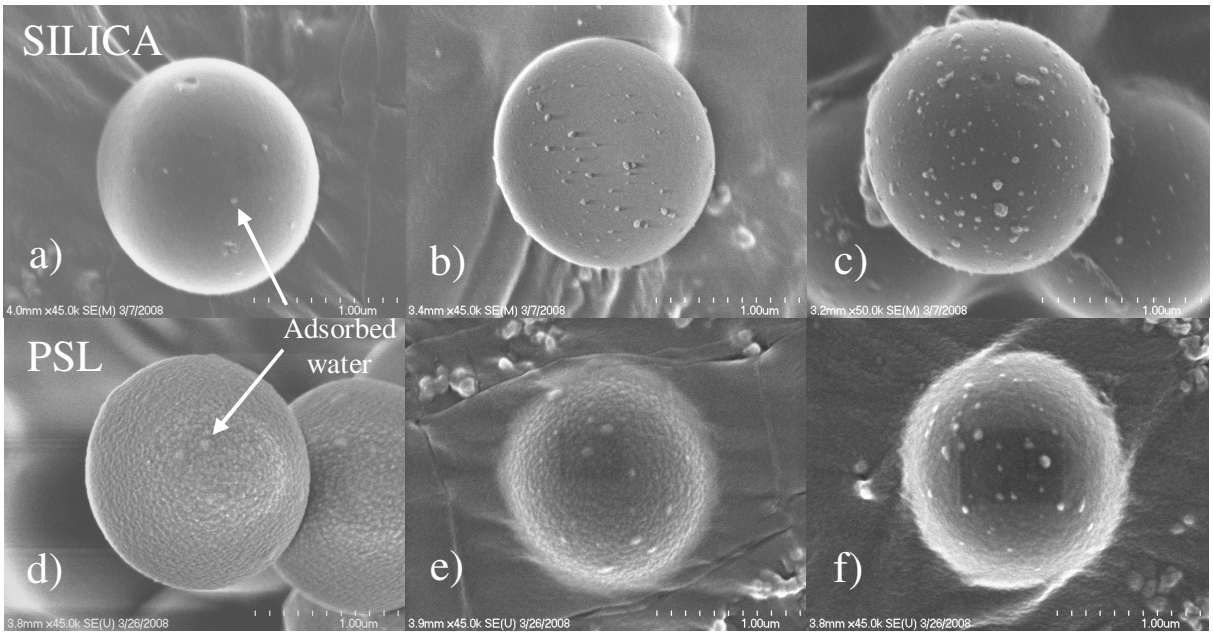

Figure 3.10. *SEM images of core particles before and after exposure to oleic acid vapor.* Surface features visible on (a) 1.6 μm silica and (d) 1.6 μm PSL particles before exposure are likely to be adsorbed water. Oleic acid vapor adsorbs to core particles in islands that increase in number on both (b,c) silica and (e,f) PSL upon exposure to oleic acid vapor pressures of 1.2 and 4.3 x 10^{-3} Pa, respectively.

size.

While the oleic acid island geometry does not change, the total number of islands increases with increasing oleic acid vapor pressure resulting in a higher surface coverage of the core particle. Based on the average geometry of an adsorbed island and the proportion of the total core surface area that the islands covered, an estimate for the total volume of oleic acid on each particle surface was determined, correcting for adsorbed water. The effective surface layer thickness reported in Table 3.1 represents the ratio of the estimated volume of adsorbed oleic acid to the volume of oleic acid comprising a uniform monolayer coverage of the surface as determined from the molecular cross-section, σ, of an oleic acid molecule in a monolayer (48 $Å^2$).[17] Effective surface layer thicknesses for both core types remain sub-monolayer over the range of oven conditions examined in this study, much lower than the estimates based on ATOFMS analysis.

Table 3.1 – Summary of image processing

Substrate	Oleic P_{vap} *Pa x 10^{-3}*	Height *nm*	Width *nm*	SA/V *μm^{-1}*	Island Coverage	Oleic Acid Monolayers
PSL	no coating	20±5	54±13	99±20	1.2±0.4%	
	1.2	35±10	75±27	69±30	2.3±1.0%	0.20±0.15
	4.3	34±13	60±24	85±53	3.4±0.8%	0.26±0.2
Silica	no coating	10±3	23±7	230±83	1.1±0.6%	
	1.2	30±15	45±18	123±86	2.5±1.1%	0.14±0.13
	4.3	33±8	44±20	111±63	4.3±1.8%	0.32±0.23

3.4.2 AFM analysis

The surface of uncoated and coated 1.6 μm particles was also characterized by AFM, which proved to be a considerable experimental challenge. Particles had to be impacted onto an adhesive surface that would limit the mobility of the particles upon contact with the AFM cantilever tip. Additionally, the curvature of the aerosol particles made quantitative measurement of surface island height difficult. The working parameters of the cantilever tip could only be optimized for a small working area of the surface. Even employing algorithms to flatten the resulting image, the island height measurements were inconsistent. Phase imaging, however, was able to differentiate the interaction of the AFM cantilever tip between surface islands and the core particle. Phase measurements made on the surface of each core particle coated at $P_{vap} = 4.3 \times 10^{-3}$ Pa are shown in Figure 3.11. The bright regions apparent on the surface of both core types correspond to the oleic acid islands and are of similar size to those observed by SEM. Some distortion of the islands due to motion of the tapping tip is evident, but there remains a clear distinction between the interaction phase of the island and the core surface. Supporting the SEM island geometry estimates, this distinction suggests that the islands are adsorbed directly to the core particle surface rather than above a mono/multilayer of oleic acid.

Experimental efforts by the Baer group associated with this project also investigated oleic acid adsorption onto flat substrates of spin-coated polystyrene and silicon with an oxidized surface layer.[18] The two substrates were exposed to oleic acid within a heated oven. AFM analysis of the coated substrates also revealed the formation of oleic acid islands on the

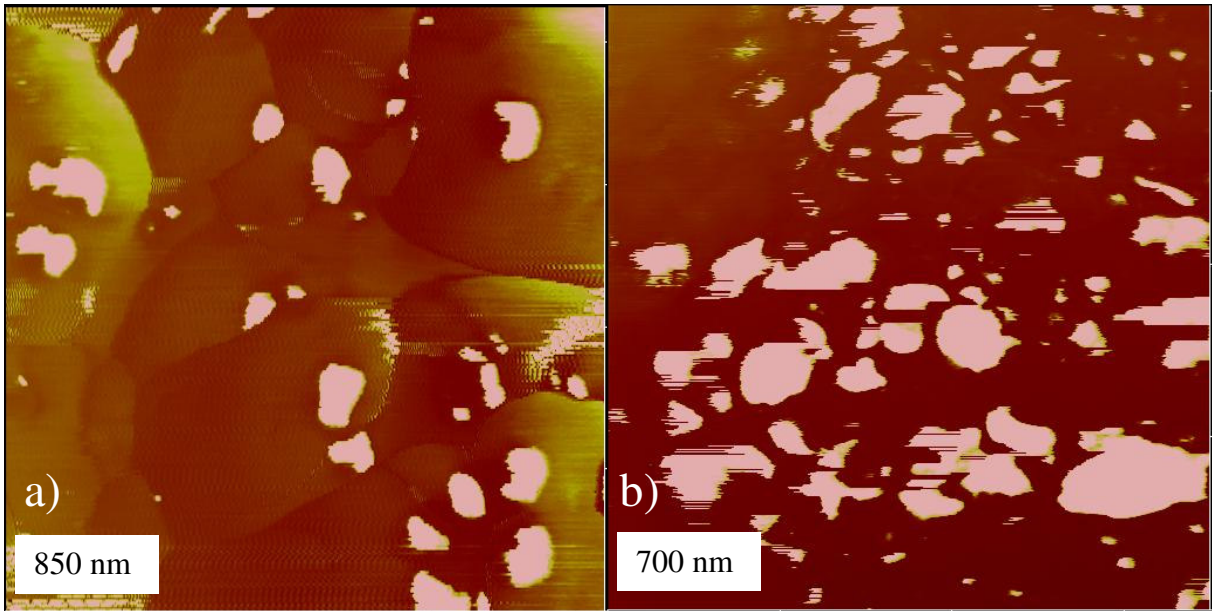

Figure 3.11. *AFM phase images of (a) 1.6 μm silica and (b) 1.6 μm PSL particles exposed to an oleic acid vapor pressure of 4.3 x 10^{-3} Pa*. Bright regions correspond to multilayer islands of adsorbed oleic acid. The length of the window mapped by the AFM tip for each image is noted in the inset.

substrate surfaces, as was observed by SEM and AFM analysis of coated particles. Figure 3.12 shows the growth of oleic acid islands onto the substrate in a 70°C oven as monitored by AFM. Similarly to the coated particles, the number of adsorbed islands increased as the substrate was exposed to oleic acid for longer times and the geometry of the islands remained stable. Contact angle measurements for water on the coated silica substrate also decreased with deposition, indicating that the area not associated with the islands was likely to be devoid of any oleic acid as was concluded based on AFM phase measurements on the core particles.[18]

At roughly 28 Å, the island heights reported by Garland et al. are on the order of a single oleic acid molecule in height, which is significantly smaller than the multilayer adsorbed oleic acid islands observed on the core particles.[18] However, recent measurements indicate that these islands on the substrate likely represent a metastable equilibrium between the condensation of oleic acid onto the substrate and evaporation from the substrate that is overcome at exposure times on the order of hours, where the islands have been observed to grow rapidly. The difference in the geometry of the particles with respect to the flat substrate and the different coating conditions likely accounts for the difference in island growth rates observed between the two systems.

3.4.3 Off-line Filter Analysis

Filter studies were conducted in an effort to employ the parameterization of gas to surface partitioning first developed by Pankow[19] and further developed for partitioning of

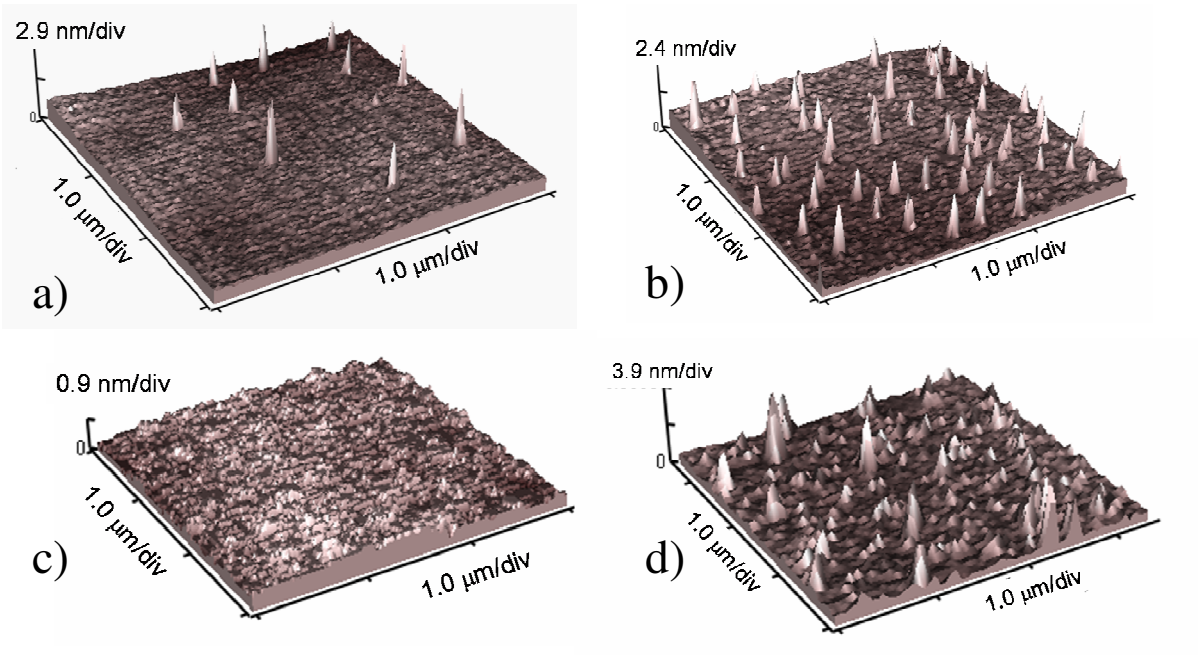

Figure 3.12. *AFM images of oleic acid on flat substrates.* Adsorbed oleic acid on a silica surface at a (a) short deposition time and at a (b) longer deposition time. The (c) bare spin-coated polystyrene surface also shows island formation (d) upon exposure to oleic acid vapor. The number of islands on both surfaces increases with deposition time, but the peak heights remain similar. From Garland et al.[18] Reproduced by permission of the PCCP Owner Societies.

vapors to inorganic dust by Jang and Kamens.[20] Unfortunately, the results of the filter analyses for collected coated particles of each type were inconsistent and irreconcilable. Due to the intensive time required to collect and process the filters, efforts to resolve the analytical issues associated with the filter analysis methodology were abandoned.

3.5 Discussion of morphology

3.5.1 Amount of adsorbed oleic acid

Except for the ATOFMS results, all methods to characterize particle morphology indicated that the total amount of oleic acid adsorbed to the core particles was less than a monolayer. An explanation for this discrepancy may be associated with the calibration of the mass spectrometry signal. Applying a signal-to-volume calibration for pure oleic acid to the coated particles may have resulted in an overestimation of adsorbed mass due to a difference in the extent of evaporation by the CO_2 laser. The net surface area to volume ratio of the adsorbed oleic acid is much greater than that of a comparably sized pure oleic acid droplet. Under layer-by-layer thermal desorption, enhancement in the surface area to volume ratio may have lead to greater evaporation efficiency. Additionally, matrix effects of the core particle were also likely to be contributing. The difference in optimized laser fluences for analysis demonstrates the fact that the core particle can absorb IR from the CO_2 laser and transfer energy to the adsorbed oleic acid.

The fact that the true adsorbed volume of oleic acid on the core particle was

overestimated based on the mass spectral data also suggests that the mass accommodation of oleic acid at the surface was much less efficient than initially predicted in Figure 3.5. Using estimates for the adsorbed volume of oleic acid based on the SEM image analysis summarized in Table 3.1, the value of the mass accommodation coefficient was re-evaluated to be $\alpha \approx 0.04$ for both polystyrene and silica surfaces, as shown in Figure 3.13. The time intensiveness of the off-line SEM particle analysis process limited the collection of coating information to only two oven conditions, which precludes evaluation of any temperature dependence of α as well as determination of adsorption thermodynamics. Although measurements of mass accommodation of fatty acids onto solid aerosol particles have not been reported, the estimate of the accommodation coefficient is similar to systems that have been studied. For example, Davidovits et al. measured a value of $\alpha = 0.067$ for the accommodation of formic acid onto a water droplet, and Maxwell-Meier et al. reported values of $\alpha<0.1$ for accommodation of trace gases onto mineral particles.[21,22]

3.5.2 Island formation and orientation of adsorbed oleic acid on the core surface

Consistent with the velocimetry measurements of the coated particles, particle microscopy showed the formation of discrete multilayer islands of oleic acid on the particle surface that have a similar geometry and appear to be thermodynamically stable. The formation of oleic acid islands was likely influenced by properties of both the oleic acid itself and the surfaces to which it is adsorbed. The structure of oleic acid within these islands may also have been influenced by the surface properties.

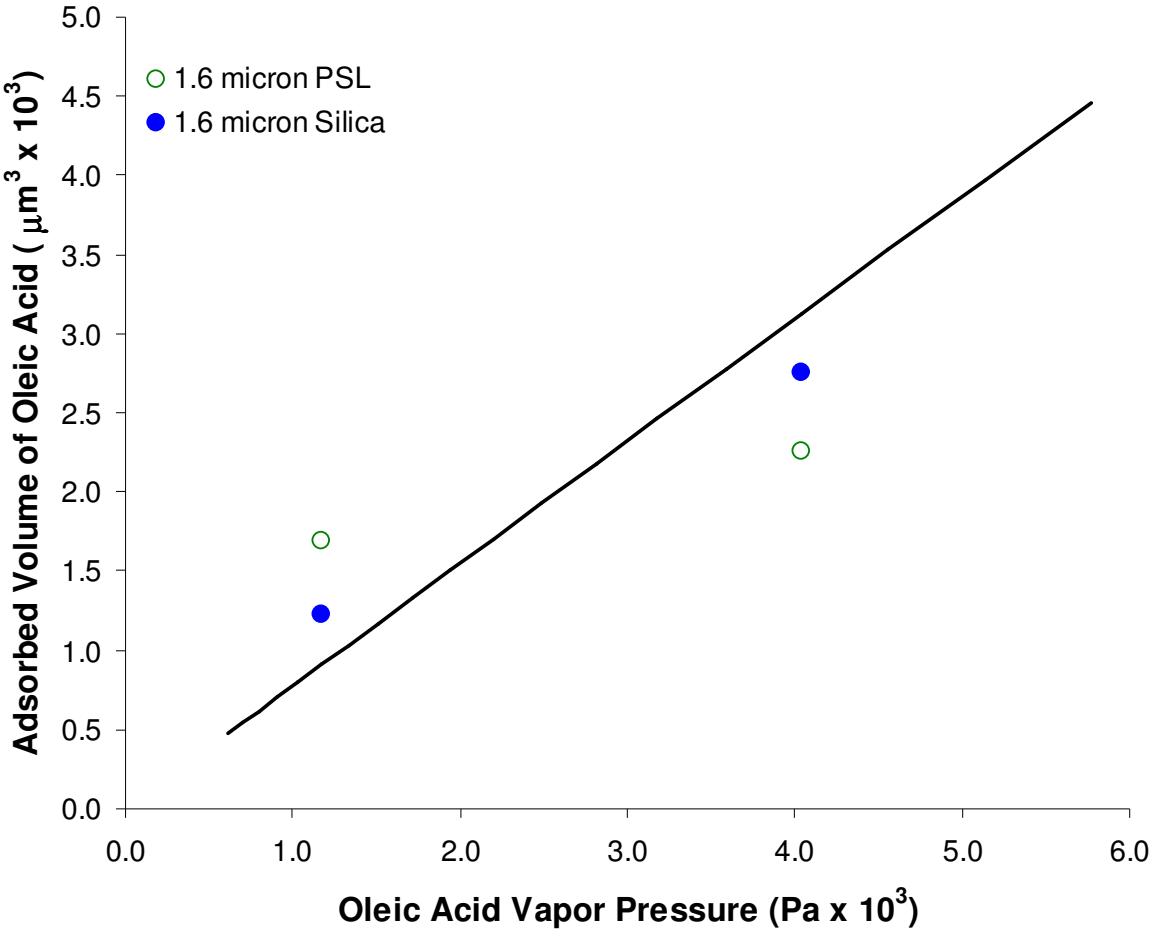

Figure 3.13. *Revised estimated adsorbed volume of oleic acid on 1.6 μm PSL and 1.6 μm silica particles based on collected SEM images*. Also shown is the prediction for the volume of adsorbed oleic acid on a 1.6 μm sphere using condensation theory, based on Eq. 2.9 with $\alpha = 0.04$.

Oleic acid has a considerable self-affinity and is known to form dimers by hydrogen bonding between acid head groups even at elevated temperatures. As a *cis*- unsaturated alkene with its double bond centered in its 18-carbon chain, oleic acid represents a sterically bulky molecule. However, its self-affinity leads to a close-packed "quasi-smectic" arrangement in bulk liquid, as pictured in Figure 3.14.[23] This arrangement creates a high density of double bonds that is believed to enhance the ability of O_3 to attack a double bond, catalyzing the reaction between O_3 and oleic acid in the condensed phase.[24] Formation of islands of oleic acid on the particle surface suggests that oleic acid may prefer to self-associate as dimers than to wet the surface uniformly. Interaction between the adsorbed oleic acid and the surface is also expected to influence the formation of the islands. On silica, the carboxylic acid head group of oleic acid can participate in hydrogen bonding with surface silanol groups.[25,26] The similarity between island geometries on the two core types suggests that even if the coordination of oleic acid to the PSL surface is different from the coordination to the silica surface, its orientation and packing may be similar. If the oleic acid preferentially adsorbs onto certain surface sites, localized films may be created that quickly reach their collapse pressure resulting in multilayer islands. Both oleic acid's self-affinity and the influence of surface adsorption site effects may have given rise to thermodynamically stable island sizes.

The arrangement and orientation of oleic acid molecules within the adsorbed islands may also be influenced by the core particle surface. While oleic acid in bulk liquid has a molecular footprint of approximately 21 $Å^2$, oleic acid molecules in monolayers have been measured to have molecular footprint closer to 50 $Å^2$.[17,23,27] Coordination of oleic acid to the

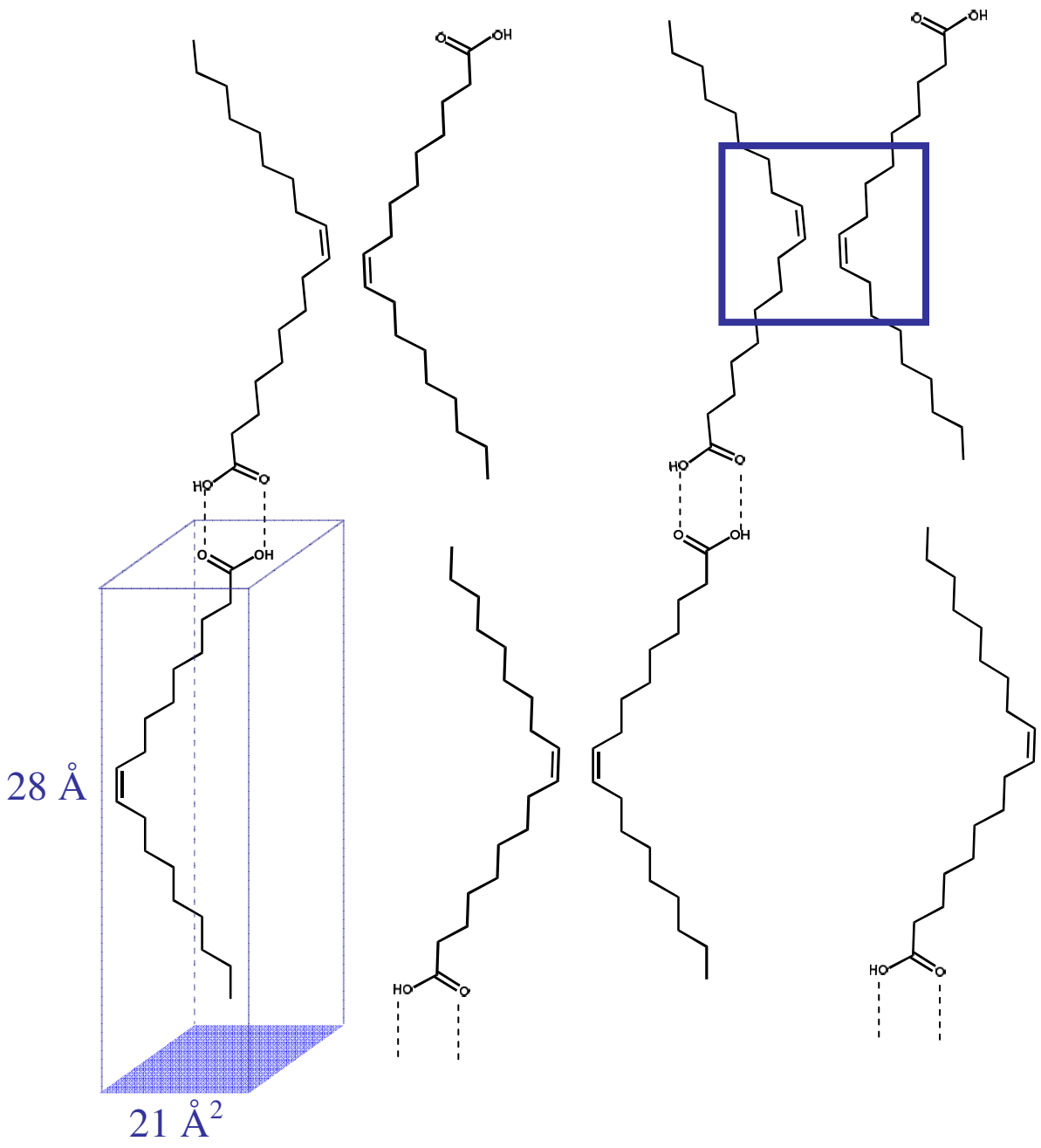

Figure 3.14. *"Quasi-smectic" packing of oleic acid in a bulk liquid*. The packing geometry results in high-density regions of double bonds as highlighted by the dark box. The physical dimensions of oleic acid molecules in this arrangement are shown, based on X-ray diffraction measurements by Iwahashi et al. Adapted from Iwahashi et al.[23]

core particle surface is likely to influence how closely oleic acid molecules can associate. The orientation of oleic acid adsorbed to flat silica and polystyrene substrates has been shown to be nearly vertical with respect to the surface for islands that are a single molecule tall[18] and multilayer adsorption may be similar or some hybrid between this orientation and bulk "quasi-smectic" packing, although it is beyond the scope of the current work to evaluate this.

3.5.3 Lack of evidence for pore condensation

Three possibilities exist as to why no effect of the pores was observed. These will be addressed in order of increasing likelihood. First, it is possible that oleic acid adsorbed within the pores was not efficiently desorbed by the CO_2 laser. Since the enthalpy of adsorption can be influenced by the presence of the pore, the oleic acid confined in the pore may have required more energy to desorb than surface bound oleic acid. However, optimization of the desorption conditions should account for this and the silica substrate provides an enhanced matrix for desorption as has already been discussed.

Second, oleic acid could block pore openings due to its self-affinity, which gives rise to its "quasi-smectic" structure in bulk liquid and is likely responsible for the multi-layer island formation. Levitt et al., measuring the uptake of oleic acid on various soot surfaces observed that this self-affinity of organic acids made diffusion into internal layers difficult. According to Levitt et al., oleic acid may inhibit access to pores due to "size issues or site

favorability limiting organic acid uptake area to the geometric surface."[28] A related phenomenon was observed by Kwon and Pignatello when studying benzene adsorption by charred maple wood shaving. They found benzene adsorption was depressed after char was exposed to vegetable oil and the resulting BET surface area of the lipid coated char was found to decrease significantly, which they attributed to micropore blockage.[29] At 12 nm, the reported pore size of the porous silica particles is a factor of 5 larger than the length of an individual oleic acid molecule, which has been measured to be between 21.2 Å[18] and 23.8 Å[23]. Under these conditions, access to the pores should not be blocked unless oleic acid adsorbed close to the throat of pores quickly dimerizes and agglomerates. However, the oleic acid island geometry observed is much larger than the pore apertures.

Finally, surface adsorbed water may have prevented enhanced adsorption of oleic acid. SEM images suggest that water could be present on the surface, and kinetic information to be presented in the next chapter also indicates the presence of water. Silanol groups readily bind water, and partial or complete filling of the pore space with water would serve to exclude oleic acid condensation. Adsorption coefficients of organic vapors have been shown to decrease with increasing relative humidity.[30]

3.6 Conclusions

The new coating oven was employed to adsorb oleic acid to two distinct types of core particles: silica, and polystyrene latex. These coated particles were analyzed by several

techniques in order to characterize the composition and morphology of the core particles after passing through the coating oven. Two key findings emerged from this analysis:

Conclusion 1: Under the coating conditions studied, oleic acid adsorbed to the core particles in multi-layer islands with a total adsorbed volume that was sub-monolayer.

Conclusion 2: There was no evidence of enhanced absorption of oleic acid into the pore network of porous silica particles.

References

1. Nash, D. G.; Baer, T.; Johnston, M. V. Aerosol mass spectrometry: An introductory review. *Int. J. Mass Spectrom.* **2006,** *258*, 2-12.

2. Sullivan, R. C.; Prather, K. A. Recent Advances in Our Understanding of Atmospheric Chemistry and Climate Made Possible by On-Line Aerosol Analysis Instrumentation. *Anal. Chem.* **2005,** *77* (12), 3861-3886.

3. Mysak, E. R.; Wilson, K. R.; Jimenez-Cruz, M.; Ahmed, M.; Baer, T. Synchrotron Radiation Based Aerosol Time-of-Flight Mass Spectrometry for Organic Constituents. *Anal. Chem.* **2005,** *77*, 5953-5960.

4. Jayne, J. T.; Leard, D. C.; Zhang, X.; Davidovits, P.; Smith, K. A.; Kolb, C. E.; Worsnop, D. R. Development of an aerosol mass spectrometer for size and composition analysis of submicron particles. *Aerosol Sci. Technol.* **2000,** *33*, 49-70.

5. Tobias, H. J.; Ziemann, P. J. Compound identification in organic aerosols using temperature programmed thermal desorption particle beam mass spectrometry. *Anal. Chem.* **1999,** *71*, 3428-3435.

6. Woods III, E.; Miller, R. E.; Baer, T. The internal energy of neutral ethylene glycol molecules created in the laser vaporization of aerosol particles. *J. Phys. Chem. A* **2003,** *107*, 2119-2125.

7. Sykes, C.; Woods III, E.; Smith, G. D.; Baer, T.; Miller, R. E. Thermal Vaporization – Vacuum Ultraviolet Laser Ionization Time of Flight Mass Spectrometry of Single Aerosol Particles. *Anal. Chem.* **2001,** *73*, 2048-2052.

8. Abramoff, M. D.; Magelhaes, P. J.; Ram, S. J. Image Processing with ImageJ. *Biophotonics International,* **2004,** pp 36-42.

9. Jaoui, M.; Kamens, R. M. Mass balance of gaseous and particulate products analysis from alpha-pinene/NOx/air in the presence of natural sunlight. *Journal of Geophysical Research-Atmospheres* **2001,** *106* (D12), 12541-12558.

10. Woods III, E.; Smith, G. D.; Dessiaterik, Y.; Baer, T.; Miller, R. E. Quantitative detection of aromatic compounds in single aerosol particle mass spectrometry. *Anal. Chem.* **2001,** *73*, 2317-2322.

11. Woods III, E.; Smith, G. D.; Miller, R. E.; Baer, T. Depth-profiling of heterogeneously mixed aerosol particles using single particle mass spectrometry. *Anal. Chem.* **2002,** *74*, 1642-1649.

12. Stein, S. E. Infrared Spectra. In *NIST Chemistry WebBook, NIST Standard Reference Database Number 69*, Linstrom, P. J., Mallard, W. G., Eds.; National Institute

of Standards and Technology: Gaithersburg MD, 20899, 2005.

13. Katrib, Y.; Martin, S. T.; Hung, H. M.; Rudich, Y.; Zhang, H.; Slowik, J. G.; Davidovits, P.; Jayne, J. T.; Worsnop, D. R. Products and Mechanisms of Ozone Reactions with Oleic Acid for Aerosol Particles Having Core-Shell Morphologies. *J. Phys. Chem. A* **2004,** *108*, 6686-6695.

14. Hinds, W. C. *Aerosol Technology: Properties, Behavior, and Measurement of Airborne Particles;* 2nd ed.; Wiley-Interscience: New York, 1999.

15. Zelenyuk, A.; Cai, Y.; Imre, D. From Agglomerates of Spheres to Irregularly Shaped Particles: Determination of Dynamic Shape Factors from Measurements of Mobility and Vacuum Aerodynamic Diameters. *Aerosol Sci. Technol.* **2006,** *40*, 197-217.

16. DeCarlo, P. F.; Slowik, J. G.; Worsnop, D. R.; Davidovits, P.; Jimenez, J. L. Particle Morphology and Density Characterization by Combined Mobility and Aerodynamic Diameter Measurements. Part 1: Theory. *Aerosol Sci. Technol.* **2004,** *38*, 1185-1205.

17. Langmuir, I. The shapes of group molecules forming the surfaces of molecules. *Proc. Nat. Acad. Sci.* **1917,** *3*, 251-257.

18. Garland, E. R.; Rosen, E. P.; Clarke, L. I.; Baer, T. Structure of submonolayer oleic acid coverages on inorganic aerosol particles: evidence of island formation. *Phys. Chem. Chem. Phys.* **2008,** *10* (21), 3156-3161.

19. Pankow, J. F. Review and Comparative Analysis of the Theories on Partitioning Between the Gas and Aerosol Particulate Phases in the Atmosphere. *Atmos. Environ.* **1987,** *21* (11), 2275-2283.

20. Jang, M.; Kamens, R. M. A Predictive Model for Adsorptive Gas Partitioning of SOCs on Fine Atmospheric Inorganic Dust Particles. *Environ. Sci. Technol.* **1999,** *33*, 1825-1831.

21. Davidovits, P.; Kolb, C. E.; Williams, L. R.; Jayne, J. T.; Worsnop, D. R. Mass accommodation and chemical reactions at gas-liquid interfaces. *Chem. Rev.* **2006,** *106* (4), 1323-1354.

22. Maxwell-Meier, K.; Weber, R.; Song, C.; Orsini, D.; Ma, Y.; Carmichael, G. R.; Streets, D. G. Inorganic composition of fine particles in mixed mineral dust-pollution plumes observed from airborne measurements during ACE-Asia. *Journal of Geophysical Research-Atmospheres* **2004,** *109* (D19).

23. Iwahashi, M.; Kasahara, Y.; Matsuzawa, H.; Yagi, K.; Nomura, K.; Terauchi, H.; Ozaki, Y.; Suzuki, M. Self-Diffusion, Dynamical Molecular Conformation, and Liquid Structures of n-Saturated and Unsaturated Fatty Acids. *J. Phys.*

Chem. B **2000,** *104*, 6186-6194.

24. Hearn, J. D.; Lovett, A. J.; Smith, G. D. Ozonolysis of Oleic Acid Particles: Evidence for a Surface Reaction and Secondary Reactions Involving Criegee Intermediates. *Phys. Chem. Chem. Phys.* **2005,** *7* (3), 501-511.

25. Blyholder, G.; Adhikar, C.; Proctor, A. Structure and Orientation of Oleic-Acid Adsorbed Onto Silica-Gel. *Colloids and Surfaces A-Physicochemical and Engineering Aspects* **1995,** *105* (1), 151-158.

26. Lee, D. H.; Condrate, R. A. FTIR spectral characterization of thin film coatings of oleic acid on glasses: I. Coatings on glasses from ethyl alcohol. *J. Mater. Sci.* **1999,** *34* (1), 139-146.

27. Gericke, A.; Huhnerfuss, H. Investigation of Z-Unsaturated and E-Unsaturated Fatty-Acids, Fatty-Acid Esters, and Fatty Alcohols at the Air-Water-Interface by Infrared-Spectroscopy. *Langmuir* **1995,** *11* (1), 225-230.

28. Levitt, N. P.; Zhang, R. Y.; Xue, H. X.; Chen, J. M. Heterogeneous chemistry of organic acids on soot surfaces. *J. Phys. Chem. A* **2007,** *111* (22), 4804-4814.

29. Kwon, S.; Pignatello, J. J. Effect of natural organic substances on the surface and adsorptive properties of environmental black carbon (char): Pseudo pore blockage by model lipid components and its implications for N-2-probed surface properties of natural sorbents. *Environmental Science & Technology* **2005,** *39* (20), 7932-7939.

30. Goss, K. U.; Schwarzenbach, R. P. Adsorption of a diverse set of organic vapors on quartz, $CaCO_3$, and α-Al_2O_3 at different relative humidities. *J. Colloid Interface Sci.* **2002,** *252* (1), 31-41.

CHAPTER 4

KINETICS STUDIES OF THE REACTION BETWEEN O_3 AND ADSORBED OLEIC ACID

4.1 Introduction

This chapter details experiments conducted to measure the rate of reaction between O_3 and oleic acid adsorbed to silica and PSL core particles. Mechanisms controlling the interaction between O_3 and the adsorbed organic will be discussed in terms of the physical and chemical properties of the reaction. The uptake coefficient of O_3 by adsorbed oleic acid is derived from these measurements, and based on this determination the relevance of the model system will be discussed within the context of atmospheric chemistry.

4.2 Experimental methods for kinetics studies

Reaction between particle-bound oleic acid and O_3 was controlled in a flow tube and monitored with the ATOFMS. The experimental set-up for these studies is shown in Figure 4.1. Details of the procedure have been presented elsewhere[1,2] and will be summarized here. All experiments were conducted at atmospheric pressure (1 atm) and room temperature (298K). The coated particle stream from the oven was introduced into a side port of a 2.54 cm i.d., 1 m long glass flow tube. The aerosol concentration in the

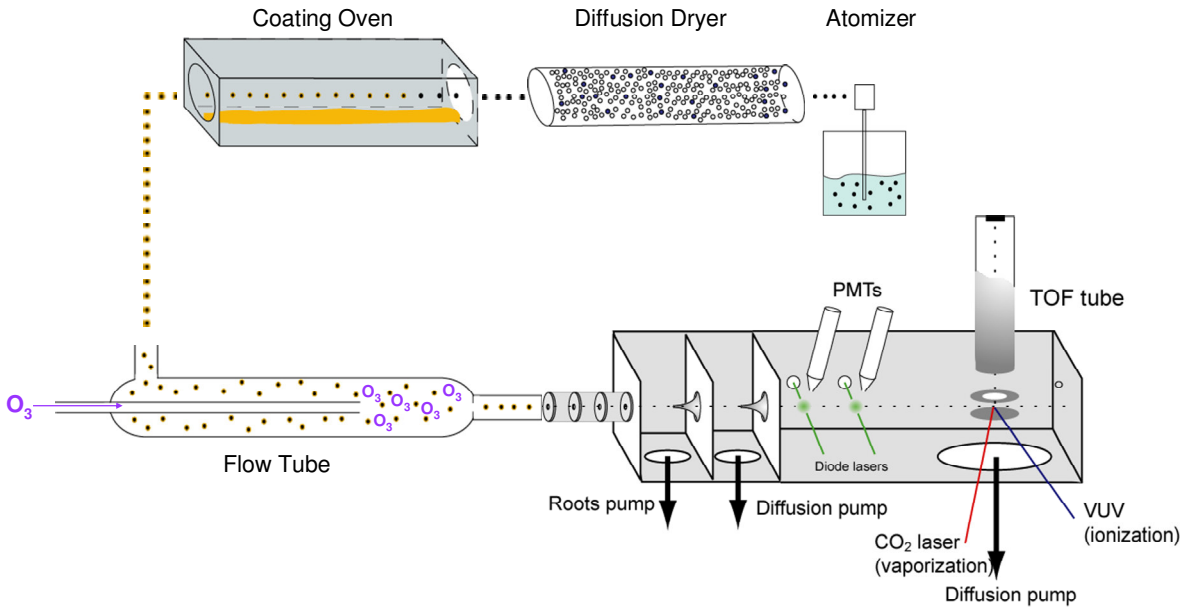

Figure 4.1. *Experimental set-up for kinetic studies: Particle generation and coating, flow tube reactor, and particle characterization by ATOFMS.*

flow tube was typically 10-100 particles cm^{-3} as measured by the APS. O_3, produced by flowing O_2 through an ozone generator (Pacific Ozone Technology, Model L11), was diluted by a factor of 45 with air before its concentration was determined by a 10 cm long home-built absorption cell monitoring the absorption of light at λ=254 nm.[2] The O_3 flow was introduced into the flow tube through a 0.44 cm i.d. glass injector that could be moved over the length of the flow tube to vary the interaction time between the O_3 and oleic acid. Velocity matching between the injected O_3 flow of 46 standard cubic centimeters per minute (sccm) and the aerosol flow ensured stable mixing and a laminar flow (Re = 18) through the flow tube. O_3 was held in excess of oleic acid by at least a factor of 35 such that its concentration was constant over the length of the flow tube and the bimolecular ozonolysis reaction can be considered pseudo-first-order. After traversing the flow tube, the particles entered the ATOFMS for mass analysis as described in Chapter 3.

4.3 Results of kinetics studies

4.3.1 Dependence on core type and coating coverage

Previous kinetic analyses of pure oleic acid ozonolysis indicate that the reaction takes place predominately at or near the surface of the particle.[2-5] By investigating a surfactant layer on a solid core with island thickness on the order of the estimated reacto-diffusive length of O_3 in oleic acid (10-20 nm), we isolated the reaction to the surface. Under this condition, the rate of loss of oleic acid can be expressed as:

$$\frac{d[Oleic]_{surf}}{dt} = -k_2^{surf}[O_3]_{surf}[Oleic]_{surf} \qquad (4.1)$$

where k_2^{surf} is the second order surface rate constant, and $[O_3]_{surf}$ and $[Oleic]_{surf}$ are the respective reactant surface concentrations. The reaction rate of adsorbed oleic acid with ozone was calculated by monitoring the change in the $M^{+\cdot}$ signal as a function of ozone exposure, which is the product of the ozone concentration in the flow tube and the time of interaction between the ozone and aerosol. Figure 4.2 illustrates how the $M^{+\cdot}$ signal of adsorbed oleic acid decays upon exposure to O_3.

A series of experiments investigating the effect of oleic acid surface coverage on the observed kinetics was performed on PSL and silica particles of both 1.6 μm and 3 μm sizes. O_3 in the flow tube was held at 2.1±0.3 x 10^{14} molecules cm^{-3} (8.4 ppm), in excess of oleic acid by at least a factor of 35, such that the ozonolysis reaction can be considered pseudo-first-order. This condition is demonstrated by the results of a typical loss of relative oleic acid signal upon exposure to O_3 ($P_{O_3} t$) as shown in Figure 4.3. An exponential decay describes the data well and yields a pseudo-first-order rate constant, k_1' ($atm^{-1}s^{-1}$), for the reaction of oleic acid and ozone on each inorganic core. Figure 4.4 shows a summary of pseudo-first-order rate constants measured for oleic acid ozonolysis on PSLs and silica aerosol particles. Between 3 – 7 experiments were performed at each oleic acid vapor pressure, and each data point and error bar represents the mean and standard deviation (±1σ) of the measurements. The average values for k_1' on PSLs are 2.17±0.06 x 10^4 $atm^{-1}s^{-1}$ and 2.25±0.20 x 10^4 $atm^{-1}s^{-1}$ for 1.6μm and 3μm diameter particles, respectively. The average values for k_1' on silica are 1.51±0.13 x 10^4 $atm^{-1}s^{-1}$ and 1.52±0.12 x 10^4 $atm^{-1}s^{-1}$ for non-porous 1.6μm and porous 3μm diameter particles, respectively.

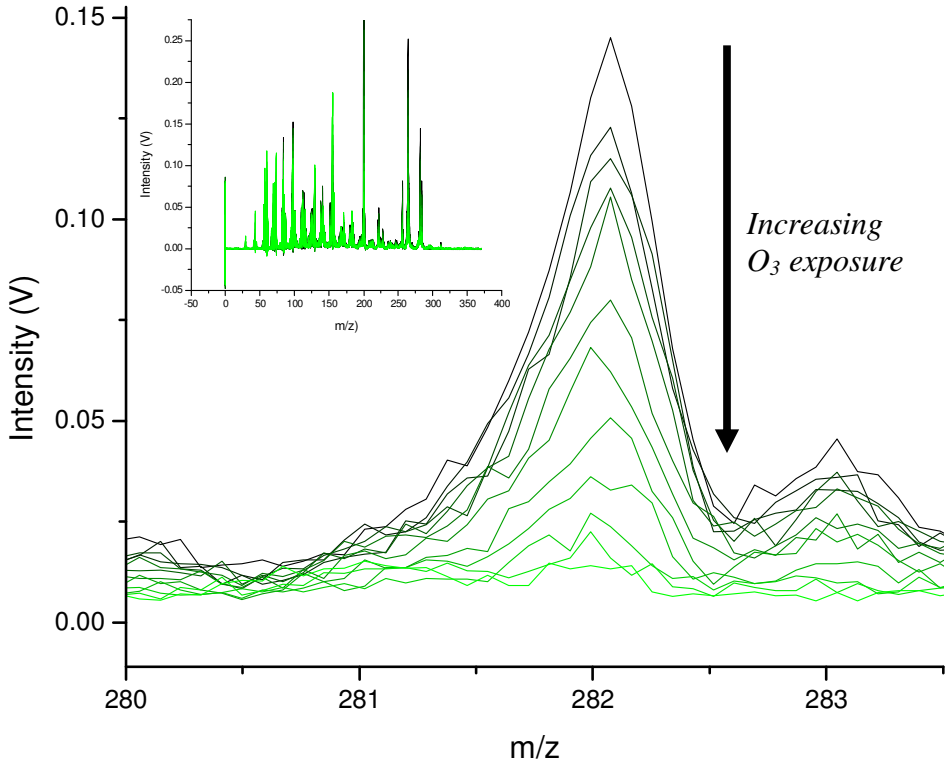

Figure 4.2. *Decay of the $M^{+\cdot}$ signal intensity (m/z = 282) upon exposure to O_3.* The inset shows the entire mass spectrum recorded with the ATOFMS at each injector position and also shows the growth of reaction products with increased O_3 exposure.

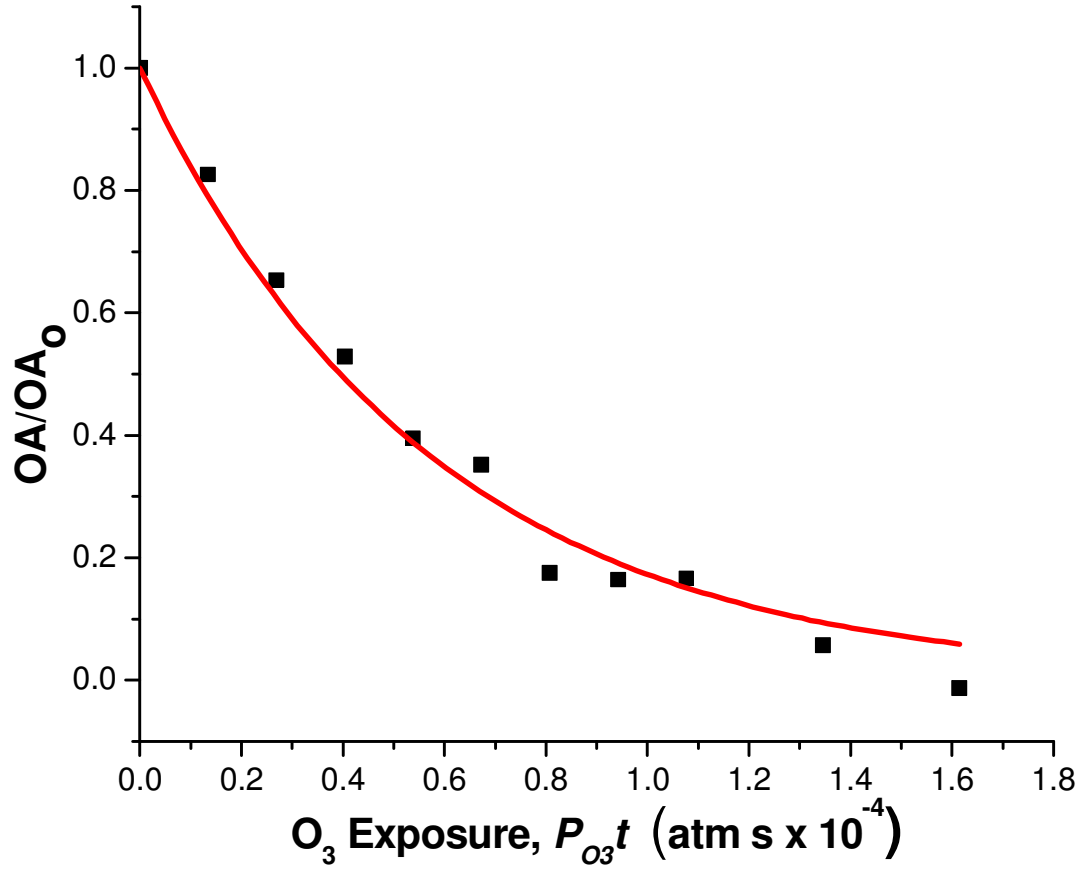

Figure 4.3. *Typical decay of the relative adsorbed oleic acid signal upon exposure to O_3.* The solid line represents a best-fit exponential decay to the data from which the rate constant k_1' is determined.

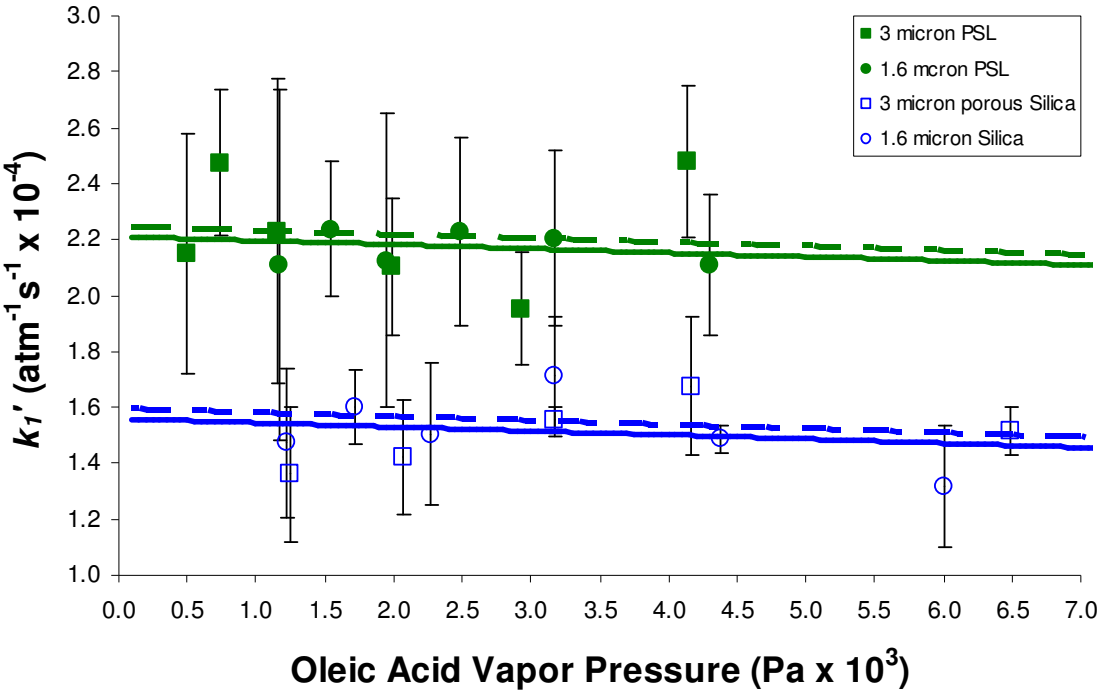

Figure 4.4. *Summary of observed rate constants for ozonolysis of adsorbed oleic acid as a function of oleic acid vapor pressure in the coating oven.* Solid (1.6µm diameter core particles) and dashed (3µm diameter core particles) lines represent the results of a random-effects meta regression analysis. The difference in the rate constants between the two core types is statistically significant ($p<0.001$). No association was found between the particle size or oleic acid vapor pressure and the rate constants ($p\geq0.5$ for each).

A random-effects meta-regression analysis was conducted with the pseudo-first order rate constant as the dependent variable and both oleic acid vapor pressure and core type as independent variables, using restricted maximum likelihood to estimate across-experiment variance. The meta-regression for each particle type is shown in Figure 4.4. Stata software (StataCorp., College Station, Texas), version 9.2, was used to conduct all meta-analyses. The results of the analysis are reported in terms of the p-value, which is the probability, given that the null hypothesis is true, that we would observe a difference as or more extreme as the one that we observed.

The key findings of these experiments are that: 1) oleic acid vapor pressure did not have a statistically significant association with kinetic rate; 2) core particle size did not have a statistically significant association with kinetic rate; and 3) at a given particle size and oleic acid vapor pressure, the kinetic rate for reaction on PSL particles was $0.65 \pm 0.18 \times 10^4$ $atm^{-1}s^{-1}$,or 43%, faster than that for silica particles.

4.3.2 Dependence of the observed rate constant on O_3 concentration

Surface reactions involving oxidation of sub-monolayer organic coatings by O_3 have frequently been shown to proceed through a surface-mediated Langmuir-Hinshelwood mechanism rather than a direct bimolecular Eley-Rideal mechanism.[6-10] Under a surface-mediated reaction, O_3 becomes bound to available surface sites prior to reaction and the observed first order kinetics exhibit a distinctly nonlinear relationship with increasing $[O_3]$ as the surface becomes saturated. A Langmuir isotherm can be used to model O_3 adsorption to a surface, and the resulting Langmuir-Hinshelwood expression

for the apparent first-order rate constant, k_1 (s^{-1}), is:

$$k_1 = \frac{k_{1,\max} K_{O_3}[O_3]}{1 + K_{O_3}[O_3]} \tag{4.2}$$

where $k_{1,max}$ is the product of the second order rate constant, k_2, and the number of available surface sites for adsorption [SS]; and K_{O_3} is the equilibrium partition constant for O_3 between gas and condensed phases. The composition of the substrate to which an organic surfactant is adsorbed has been shown to influence the observed Langmuir-Hinshelwood kinetics between O_3 and a surfactant layer.[8,9]

Flow tube experiments on both 1.6 μm PSL and 1.6 μm silica particles were performed over a range of O_3 concentrations for a coating $P_{vap} = 4.3 \times 10^{-3}$ Pa to evaluate whether O_3 interaction with the bare core particle surface participates in the oxidation mechanism of adsorbed oleic acid. The apparent first-order rate constant was evaluated directly from the relationship between the relative oleic acid signal loss and the reaction time rather than ozone exposure in order to determine an explicit [O_3] dependence. A summary of experimental values for k_1 is shown in Figure 4.5. The trend for oleic acid ozonolysis on PSL particles is clearly nonlinear, indicating that the particle surface is reaching saturation with O_3. The weighted nonlinear least-squares fit of Equation 4.2 to the PSL data is shown in Figure 4.5 along with the ±1σ confidence intervals. The Langmuir-Hinshelwood parameters derived from this fit are $k_{1,max} = 0.64 \pm 0.10$ s^{-1} and $K_{O_3} = 2.14(\pm 0.57) \times 10^{-15}$ cm^3 $molec^{-1}$. The observed rate constant for the reaction on silica particles is systematically slower than the corresponding value on PSL particles below [O_3] = 5×10^{14} molecules cm^{-3}, but appears to become faster than the reaction on

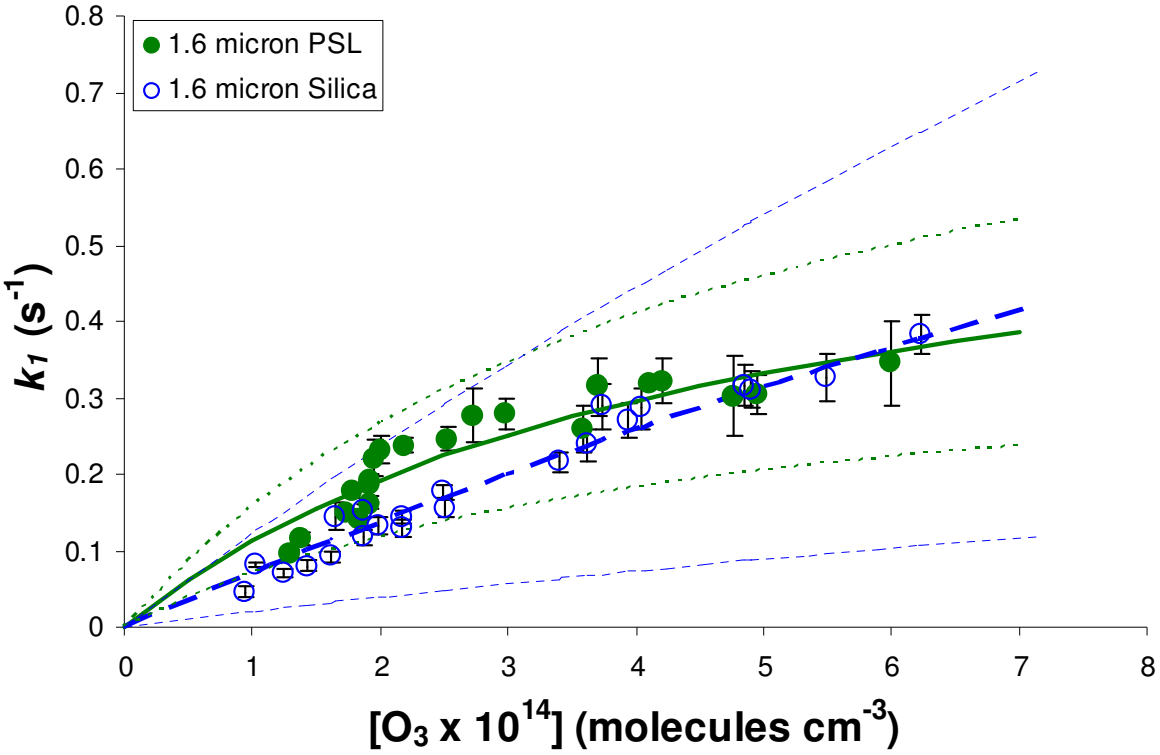

Figure 4.5. *[O_3] dependence of the pseudo-first-order rate constant for ozonolysis of adsorbed oleic acid on 1.6μm core particles of PSL and silica*. Oleic acid P_{vap} = 4.3 x 10^{-3} Pa. A Langmuir-Hinshelwood curve (solid line) for the PSL data and for the (long-dashed line) silica data are also included along with the corresponding 1σ confidence intervals for each fit (short-dashed lines).

PSL particles at the highest [O_3] explored. Although the first order kinetics on silica do not exhibit obvious curvature over the range of [O_3] investigated in this study, a nonlinear least-squares fit of Equation 4.2 to the silica data can still be performed under the assumption that saturation will occur at higher [O_3]. The resulting Langmuir-Hinshelwood parameters derived from the fit of Equation 2 to the silica data are $k_{1,max}$ = 2.2±1.1 s^{-1} and K_{O_3} = 3.59(±2.13) x 10^{-16} $cm^3 molec^{-1}$. Differences in the PSL and silica fit parameters will be discussed below.

4.3.3 Determination of Uptake Coefficients

Because values for rate constants are influenced by experimental conditions, inter-study comparisons are facilitated by expressing results of aerosol kinetic studies in terms of a reaction probability, or uptake coefficient, γ. The parameter γ represents the ratio of the number of collisions between two reactants that result in a chemical transformation to the total number of collisions that occur. When considering heterogeneous reactions between a gas phase oxidant and a surface bound organic, the magnitude of γ is influenced by the choice of which reactant to use as a frame of reference. For example, the reaction probability for oxidation of liquid aerosols such as pure oleic acid or multi-component mixtures of oleic acid is typically taken from the perspective of O_3 whereby γ represents the net rate of loss of the gas-phase species normalized to the gas-particle collision rate. Under the assumption that interaction between O_3 and oleic acid provides the sole loss mechanism for both species, the reaction probability from the perspective of O_3 is expressed as:

$$\gamma_{O_3} = \frac{4k_1 n_{oleic}}{\bar{c}_{O_3}[O_3]SA} \tag{4.3}$$

where n_{oleic} is the total number of oleic acid molecules available for reaction, $\bar{c}_{O_3}$ is the mean kinetic speed of O_3, and SA is the surface area of the particle. Typical values for γ_{O_3} for pure oleic acid are approximately 10^{-3}, representing one reaction per thousand collisions.[3,5,11] However, applying this formulation to the case where the surfactant layer does not uniformly cover the substrate presents some challenges in defining the reactive surface area. As a result, analysis of kinetics of surface and, more specifically, sub-monolayer reactions, have typically made use of a different parameterization of the uptake coefficient with the surfactant as a frame of reference whereby γ for the present study is defined as the number of oleic acid molecules at the surface lost relative to the ozone-surface organic collision frequency and can be expressed according to:[12]

$$\gamma_{oleic} = \frac{4k_1}{\bar{c}_{O_3}\sigma_{oleic}[O_3]} \tag{4.4}$$

where σ_{oleic} is the molecular cross-section of oleic acid. Since the reaction between O_3 and oleic acid has been monitored by observation of the loss of oleic acid rather than loss of O_3, the latter formulation appears to be more appropriate for the current system. Employing γ_{oleic} assumes that each oleic acid molecule on the surface is equally accessible to reaction by O_3, but given that the geometry of the island is similar to the reacto-diffusive length for O_3 in oleic acid this seems reasonable and a discussion of how the resulting values for γ_{oleic} may differ from γ_{O_3} is addressed below. Figure 4.6 shows the calculated values for γ_{oleic} based on the experimental data from Figure 4.5 as well as the

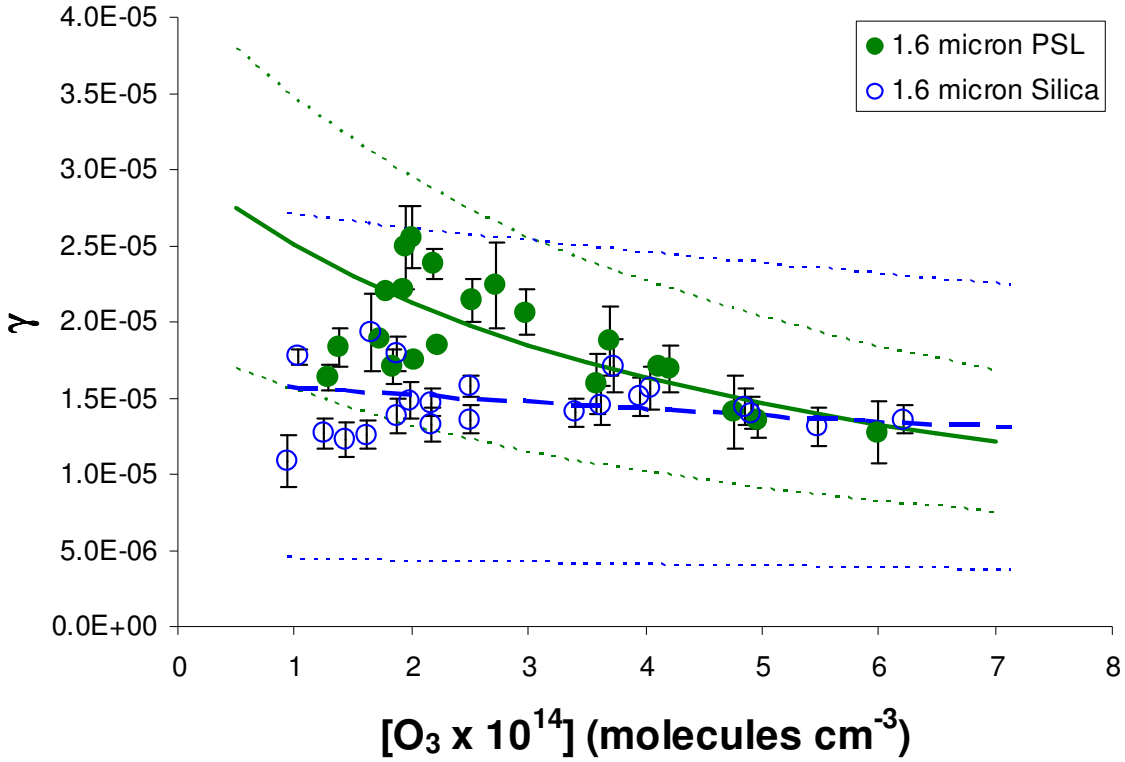

Figure 4.6. *[O_3] dependence of the uptake coefficient, γ, for ozonolysis of adsorbed oleic acid on 1.6μm core particles of PSL and silica*. Oleic acid $P_{vap} = 4.3 \times 10^{-3}$ Pa. 1σ confidence intervals for each fit (short-dashed lines) are reported.

approximation to the PSL (solid line) and silica (dashed line) data based on the Langmuir-Hinshelwood fitting parameters. Values for γ_{oleic} for reaction of oleic acid on PSLs decrease from 2.7 x 10^{-5} to 1.2 x 10^{-5} with increasing [O_3], overlapping at high [O_3] with the estimated value of γ_{oleic} for silica, which decreases from 1.6 x 10^{-5} to 1.3 x 10^{-5}. At lower O_3 concentrations γ_{oleic} is higher on PSL than silica, suggesting that the estimated lifetime of oleic acid adsorbed to different inorganic particle types in the atmosphere may depend both on the nature of the inorganic substrate and on the local O_3 concentration.

4.4 Discussion

4.4.1 Influence of island morphology on kinetics

While previous laboratory studies have reported ozonolysis kinetics of sub-monolayer surfactants[6,9,10], this study is the first to our knowledge to observe the ozonolysis kinetics of multilayer surfactant islands on coated aerosol particles. Such a morphology may have atmospheric relevance since microscopy and spectromicroscopy of ambient particles have shown that organic coatings are often internally mixed with inorganic particles such as dust and that the fraction of the total particle surface covered by organic material is highly variable.[13,14]

The observed oxidation kinetics sensitively depend on the morphology of the multilayer islands and on how the islands grow with increasing oleic acid deposition. The islands of oleic acid formed during vapor deposition onto 1.6 μm PSL and 1.6 μm silica core particles do not appear to change in size as the total coverage of oleic acid on the

core particle surface increases, and the resulting invariance in the surface to volume ratio of oleic acid encountered by O_3 explains the observed constant kinetics with increasing oleic acid surface coverage. In this sense, the multilayer islands of oleic acid react similarly with O_3 to sub-monolayer coatings of organic surfactant layers. Previous sub-monolayer studies also noted invariant pseudo-first-order kinetics of O_3 uptake by benzo-a-pyrene on sub-micron aerosols[6,8] or by oleic acid on suspended water droplets[15]. However, surfactant coatings above one monolayer, where the coating occurs evenly on the surface so that the underlying substrate is not exposed, have exhibited a significant decrease in the observed rate constants.[6,8,16] A recent study by Katrib *et al.* also investigated the ozonolysis of oleic acid adsorbed to PSL particles, though much smaller (100 nm) than used in this study, and were able to measure oleic acid coating thicknesses between 2-30 nm by measurement of the aerosol mobility diameter.[17] These coatings would represent multilayer adsorption of oleic acid to the PSL core assuming a uniform coating and, although kinetic information was not published, it was confirmed through private correspondence that no difference in the ozonolysis kinetics was observed between the oleic acid coating thicknesses investigated by Katrib *et al.*[18] This suggests that oleic acid islands were also likely to have been formed in the Katrib *et al*. study.

4.4.2 Influence of core particle size and porosity on kinetics

Although the geometry of oleic acid islands on 3 μm solid PSL and porous silica core particles was not measured by SEM and AFM analysis, the fact that the ozonolysis reaction rate is not statistically different than the rate measured on the respective 1.6 μm core particles indicates that the arrangement of oleic acid on the surface of the larger

particles must be similar to their smaller counterparts. There is also no evidence for hindrance of the reaction by pore confinement. This finding is perhaps the most surprising aspect of this study. The prior expectation was that oleic acid trapped inside the porous particle would have reacted more slowly due to diffusion of O_3 into the pores or physical constraints on oleic acid due to confinement in the pores. However, the surface analysis suggests that either the oleic acid never penetrated inside the porous silica particle so that the porosity had no effect on the kinetics or that oleic acid trapped in the pores was not efficiently desorbed by the CO_2 laser. Thus, the question of how efficiently ozone attacks trapped oleic acid inside particles remains an open question.

4.4.3 Influence of core particle type on kinetics

Two separate phenomena are responsible for the difference in the ozonolysis rate due to the nature of the core illustrated in Figures 4.4 and 4.5. The higher reactivity of oleic acid on the PSL spheres is the result of more efficient partitioning of O_3 to the PSL surface than to the silica surface, and the faster reaction on the silica particles at high O_3 concentrations may be due to differences in the ability of O_3 to attack the oleic acid double bond associated with the orientation or packing of oleic acid on the two surfaces. Both phenomena can be addressed in terms of the Langmuir-Hinshelwood parameters K_{O_3} and $k_{1,max}$ derived for reaction on PSL and silica, and will now be discussed at greater length.

The equilibrium constant defining the partitioning of O_3 between surface adsorption onto the core particle and the gas phase, K_{O_3}, is a factor of six times greater

for the PSL surface than for the silica surface indicating that O_3 is bound more strongly to the less polar PSL surface. This preference is consistent with the trend in K_{O_3} values for substrates of different polarities summarized by Kwamena et al.[9], and indicates that an O_3 molecule has a longer residence time on the surface of the PSL particles. With a longer residence time comes more opportunities to encounter an oleic acid double bond, which explains why the reaction between oleic acid and O_3 is faster on the PSL surface.

While the trend in K_{O_3} values for PSL and silica measured in this study is consistent with previous measurements for K_{O_3}, the magnitude of the values are not in obvious agreement. Although pure polystyrene is nonpolar, the value for K_{O_3} on PSL core particles is significantly smaller than measured for strongly nonpolar surfaces such as soot[6] and more closely resembles the K_{O_3} of the oxygenated surface of azelaic acid[9]. This is likely to be a result in part of the presence of water co-adsorbed to the PSL surface. The K_{O_3} value for silica is much lower than most values reported K_{O_3}, even below the value for partitioning to the surface of water (4.66×10^{-16} cm^3molec^{-1})[7], and indicates that O_3 is bound very loosely if at all to the surface of the silica particles. A linear dependence between k_I and O_3, indicative of an Eley-Rideal mechanism, has been measured previously for ozone oxidation of a surface-active organic, benzo-a-pyrene, sorbed to silica [16,19] and may be due in part to reaction between ozone and exposed silica surfaces [20], which can be competitive with chemical reaction on surfaces with sub-monolayer surfactant coverage[21].

The larger value of $k_{1,max}$ for the reaction on the silica particles indicates that even though O_3 has a longer residence time on the PSL surface, the reaction between oleic acid and O_3 is ultimately more efficient on the silica surface. This implies that, although the measured island geometries for oleic acid on the two core types are similar, the core composition may also alter the orientation or packing of the oleic acid on the two surfaces. Numerical simulations suggest that the orientation of long chain unsaturated molecules affects their reactivity with ozone[22], and the different polarities between the hydrophilic silica and hydrophobic polystyrene may result in different strengths and geometries of the oleic acid/substrate interaction on the two surfaces. The "quasi-smectic" self-coordination between oleic acid molecules observed in bulk solutions[23] has been hypothesized to influence its reactivity with ozone[5], and anything that disrupts this interaction could change the accessibility of the double bond to attack by O_3.

The orientation of the oleic acid in the multilayer islands on both surfaces may be different than for a uniform sub-monolayer coating of oleic acid. A recent study by McNeill *et al.*, for the ozonolysis of aqueous salt particles covered with ~0.9 monolayers of sodium oleate measured a $k_{1,max}$ of 0.05 s^{-1}, over an order of magnitude difference from the values in this study.[10] However, the resulting $\gamma_{oleic} \approx 10^{-5}$ reported by McNeill *et al.* is in good agreement with the results reported in Figure 3.6. Both of these results stand in contrast to the probability of reaction between O_3 and oleic acid on a suspended water droplet, $\gamma_{O_3} = 2.6 \times 10^{-6}$, reported recently[15]. This discrepancy may be due to differences in packing of oleic acid in the different studies. Gonzalez-Labrada *et al.* injected oleic acid onto the surface of a suspended water droplet and then removed volume from the

water droplet to create a monolayer of oleic acid at the surface of the drop. Compressing the insoluble monolayer of oleic acid is likely to alter its packing geometry as well as the molecular cross-section of an oleic acid molecule.

When comparing uptake coefficients among various experiments, it is important to establish a common perspective which defines γ. In order to calculate γ_{O_3} for the present morphology, a decision about how to define the reactive surface area of the particle is required. If, for example, O_3 was assumed to react exclusively with oleic acid and the surface area of the islands alone was used to define *SA,* the resulting values for γ_{O_3} for the reaction on silica would range from 1.2×10^{-4} to 9.8×10^{-5} over the range of $[O_3]$ investigated, which is over an order of magnitude higher than the values of $\gamma_{oleic.}$ Yet, how the reactive surface area is defined should probably depend on the partitioning coefficient, K_{O_3}, which determines how long the ozone stays on the surface before desorbing. Scaling the number of collisions O_3 makes with the uncoated surface of the core particle by the factor $K_{O_3}[O_3]$ to account for desorption, the resulting values for γ_{O_3} would range from 7.1×10^{-5} to 1.9×10^{-5} over the range of $[O_3]$ investigated. Finally, if the total surface area of the particle was used to define SA_{oleic}, the resulting value for γ_{O_3} would be 5.3×10^{-6}, which is similar to the value reported by Gonzalez-Labrada *et al.*[15] It becomes clear that although the uptake coefficient was intended to be a parameter that can be compared directly across experiments, one must pay close attention to how γ has been parameterized. Under all scenarios, however, the resulting uptake coefficient for the reaction involving adsorbed oleic acid is lower than the values reported for pure oleic

acid, indicating that the matrix effects are slowing the reaction.

4.5 Conclusions and atmospheric implications

The rate of the surface reaction between surface-adsorbed oleic acid and O_3 has been shown for the first time to be influenced by the composition of the aerosol substrate. The reaction is ultimately more efficient on the silica surface, but proceeds faster on the less polar PSL core at lower [O_3] due to the increased residence time of O_3 on the PSL surface. Invariant geometry of the adsorbed islands on both core types resulted in no kinetic dependence on oleic acid coverage or core particle surface area. As with so many kinetic studies of aerosols, these observations could be the result of multiple variables that were not effectively isolated. As such, this study raises many questions that it cannot answer, which will be discussed in Chapter 5. Nevertheless, these results indicate that the estimated lifetime of surface-adsorbed oleic acid, and likely similar unsaturated organics, by O_3 in the atmosphere will be affected by core composition and will be longer than the lifetime of a comparable amount of pure oleic acid. The different chemical aging experienced by adsorbed oleic acid is another example of the important role that particle morphology has in controlling aerosol reactivity and may help to explain the current discrepancy between laboratory and field measurements.[24]

References

1. Nash, D. G.; Tolocka, M. P.; Baer, T. The uptake of O_3 by myristic acid-oleic acid mixed particles: evidence for solid surface layers. *Phys. Chem. Chem. Phys.* **2006,** *8*, 4468-4475.

2. Smith, G. D.; Woods III, E.; Hauser, C.; Miller, R. E.; Baer, T. Reactive uptake of ozone by oleic acid aerosol particles: Application of single particle mass spectrometry to heterogeneous reaction kinetics. *J. Phys. Chem. A* **2002,** *106*, 8085-8095.

3. Morris, J. W.; Davidovits, P.; Jayne, J. T.; Shi, Q.; Kolb, C. E.; Worsnop, D. R.; Barney, W. S.; Jimenez, J.; Cass, G. R. Kinetics of submicron oleic acid aerosols with ozone; a novel aerosol mass spectrometric technique. *Geophys. Res. Lett.* **2002,** *29*, 71-1-71/4.

4. Moise, T.; Rudich, Y. Reactive uptake of ozone by proxies for organic aerosols: Surface versus bulk processes. *J. Geophys. Res.* **2000,** *105*, 14667-14676.

5. Hearn, J. D.; Lovett, A. J.; Smith, G. D. Ozonolysis of Oleic Acid Particles: Evidence for a Surface Reaction and Secondary Reactions Involving Criegee Intermediates. *Phys. Chem. Chem. Phys.* **2005,** *7* (3), 501-511.

6. Poschl, U.; Letzel, T.; Schauer, C.; Niessner, R. Interaction of ozone and water vapor with spark discharge soot aerosol particles coated with benzo[a]pyrene: O_3 and H_2O adsorption, benzo[a]pyrene degradation, and atmospheric implications. *J. Phys. Chem. A* **2001,** *105* (16), 4029-4041.

7. Mmereki, B. T.; Donaldson, D. J. Direct observation of the kinetics of an atmospherically important reaction at the air-aqueous interface. *J. Phys. Chem. A* **2003,** *107*, 11038-11042.

8. Kwamena, N. O. A.; Thornton, J. A.; Abbatt, J. P. D. Kinetics of surface-bound benzo[a]pyrene and ozone on solid organic and salt aerosols. *J. Phys. Chem. A* **2004,** *108* (52), 11626-11634.

9. Kwamena, N. O. A.; Staikova, M. G.; Donaldson, D. J.; George, I. J.; Abbatt, J. P. D. Role of the aerosol substrate in the heterogeneous ozonation reactions of surface-bound PAHs. *J. Phys. Chem. A* **2007,** *111* (43), 11050-11058.

10. McNeill, V. F.; Wolfe, G. M.; Thornton, J. A. The Oxidation of Oleate in Submicron Aqueous Salt Aerosols: Evidence of a Surface Process. *J. Phys. Chem. A* **2007,** *111(6),* 1073-1083.

11. Moise, T.; Rudich, Y. Reactive Uptake of Ozone by Aerosol-Associated Unsaturated Fatty Acids: Kinetics, Mechanism, and Products. *J. Phys. Chem. A* **2002,** *106*,

6469-6476.

12. Ammann, M.; Poschl, U.; Rudich, Y. Effects of reversible adsorption and Langmuir-Hinshelwood surface reactions on gas uptake by atmospheric particles. *Physical Chemistry Chemical Physics* **2003,** *5* (2), 351-356.

13. Russell, L. M.; Maria, S. F.; Myneni, S. C. B. Mapping organic coatings on atmospheric particles. *Geophys. Res. Lett.* **2002,** *29* (16).

14. Falkovich, A. H.; Schkolnik, G.; Ganor, E.; Rudich, Y. Adsorption of organic compounds pertinent to urban environments onto mineral dust particles. *Journal of Geophysical Research-Atmospheres* **2004,** *109* (D2).

15. Gonzalez-Labrada, E.; Schmidt, R.; Dewolf, C. E. Kinetic analysis of the ozone processing of an unsaturated organic monolayer as a model of an aerosol surface. *Physical Chemistry Chemical Physics* **2007,** *9* (43), 5814-5821.

16. Alebic-Juretic, A.; Cvitas, T.; Klasinc, L. Heterogeneous polycyclic aromatic hydrocarbon degradation with ozone on silica gel carrier. *Environ. Sci. Technol.* **1990,** *24* (1), 62-66.

17. Katrib, Y.; Martin, S. T.; Hung, H. M.; Rudich, Y.; Zhang, H.; Slowik, J. G.; Davidovits, P.; Jayne, J. T.; Worsnop, D. R. Products and Mechanisms of Ozone Reactions with Oleic Acid for Aerosol Particles Having Core-Shell Morphologies. *J. Phys. Chem. A* **2004,** *108*, 6686-6695.

18. Martin, S. T. personal communication. 2008.

19. Wu, C. H.; Salmeen, I.; Niki, H. Fluorescence Spectroscopic Study of Reactions Between Gaseous Ozone and Surface-Adsorbed Polycyclic Aromatic-Hydrocarbons. *Environmental Science & Technology* **1984,** *18* (8), 603-607.

20. Michel, A. E.; Usher, C. R.; Grassian, V. H. Reactive uptake of ozone on mineral oxides and mineral dusts. *Atmos. Environ.* **2003,** *37* (23), 3201-3211.

21. Usher, C. R.; Michel, A. E.; Stec, D.; Grassian, V. H. Laboratory studies of ozone uptake on processed mineral dust. *Atmos. Environ.* **2003,** *37* (38), 5337-5347.

22. Vieceli, J.; Ma, O. L.; Tobias, D. J. Uptake and collision dynamics of gas phase ozone at unsaturated organic interfaces. *J. Phys. Chem. A* **2004,** *108* (27), 5806-5814.

23. Iwahashi, M.; Kasahara, Y.; Matsuzawa, H.; Yagi, K.; Nomura, K.; Terauchi, H.; Ozaki, Y.; Suzuki, M. Self-Diffusion, Dynamical Molecular Conformation, and Liquid Structures of n-Saturated and Unsaturated Fatty Acids. *J. Phys. Chem. B* **2000,** *104*, 6186-6194.

24. Rudich, Y.; Donahue, N. M.; Mentel, T. F. Aging of organic aerosol: Bridging the

gap between laboratory and field studies. *Ann. Rev. Phys. Chem.* **2007,** *58*, 321-352.

CHAPTER 5

CONCLUSION

The compositional and morphological complexities of ambient organic aerosol particles present an enormous challenge to experimentalists in the field of atmospheric chemistry. Mimicking atmospheric processing of oleic acid has become a proving ground for simplified laboratory models of organic aerosol composition and morphology. Models composed of pure oleic acid and multi-component mixtures of organics have been unable to capture the behavior of real oleic-acid-bearing particles in the atmosphere. The experimental effort described in this work represents an attempt to explore a different, and atmospherically relevant, particle morphology for a model oleic acid aerosol: an adsorbed surfactant layer of oleic acid on a solid core particle. The influence of the core particle composition was explored by comparing the well-characterized reaction between oleic acid and O_3 on two distinct types of core particles. Silica, serving as an analog to mineral dust, represented a hydrophilic surface. Polystyrene latex represented an idealized hydrophobic surface similar to soot.

The creation of internally mixed particles involving an adsorbed layer of oleic acid necessitated the design and construction of a new condensation oven, which was characterized by a computational fluid dynamics model. The resulting coated particles

were analyzed by on-line and off-line techniques in order to characterize the composition and morphology of the core particles after passing through the coating oven. Combined information gathered by a number of analysis methods indicated that rather than coat the core particle surface uniformly, the adsorbed oleic acid associated into discrete islands. By forming islands, the adsorbed oleic acid left large areas of the core particle surface exposed. Kinetics experiments revealed that the reaction between O_3 and oleic acid was influenced differently based on the composition of the exposed surface. The experiments indicated that the rate of reaction was also influenced by arrangement or orientation of oleic acid within the islands on the two core particles that were investigated. These results were the first experimental observations of an effect of a core particle on the reaction between O_3 and oleic acid. Importantly, the measured values of the uptake coefficient for the reaction on both types of surfaces are significantly slower than what has been measured for pure oleic acid particles and are closer to estimates of the rate of oleic acid destruction based on atmospheric observations.

Two critical areas for future research related to this work lie in better characterizing the formation and growth of surface islands as well as further exploring the effect of core particle composition on heterogeneous reactions. Experiments are currently under way to investigate how oleic acid islands grow and coalesce on flat substrates. In addition to monitoring changes in island geometry, it would be invaluable to measure spectroscopically the molecular level arrangement of adsorbed oleic acid molecules within islands on different substrate surfaces to determine how the orientation of oleic acid molecules within the islands compares to oleic acid in a monolayer or bulk

liquid and whether this arrangement alters the accessibility of double bonds for attack by O_3. Multivalent metal ions, for example, which are prevalent in more complex mineral species and can be present in aqueous water droplets, have been shown to significantly alter surface measurements of oleic acid films[1] and may change the kinetics of the ozonolysis reaction even more than what has been reported here. Understanding the full extent to which the composition of the surface influences chemical reactivity of adsorbed organics will require kinetic investigations of other core types. The role that surface adsorbed water plays in the arrangement of oleic acid in the surface islands should also be determined. Additionally, further exploration of the potential for pore entrapment of an organic could be performed with synthetic particles possessing pores of different sizes.

These experiments also raise more general questions for the field of atmospheric chemistry. As discussed in Chapter 3, detection of the adsorbed surfactant layer was not possible by gentle thermal desorption using a cartridge heater. Considering that this method of particle desorption is most commonly employed in field deployed aerosol instruments, sub-monolayer organic coatings on refractory particles likely go largely undetected during field campaigns making their prevalence in the atmosphere difficult to assess. Such coatings also present a significant challenge for a uniform definition of the uptake coefficient, a parameter that serves as critical input to global climate models.

References

1. Linden, M.; Rosenholm, J. B. Influence of Multivalent Metal-Ions on the Monolayer and Multilayer Properties of Some Unsaturated Fatty-Acids. *Langmuir* **1995,** *11* (11), 4499-4504.